April 1990

EVALUATION OF THE REGIONAL OXIDANT MODEL (VERSION 2.1) USING AMBIENT AND DIAGNOSTIC SIMULATIONS

by

Thomas E. Pierce
Kenneth L. Schere
Atmospheric Sciences Modeling Division
Atmospheric Research and Exposure Assessment Laboratory
U.S. Environmental Protection Agency
Research Triangle Park, NC 27711

Dennis C. Doll
Technical Support Division
Office of Air Quality Planning and Standards
U.S. Environmental Protection Agency
Research Triangle Park, NC 27711

Warren E. Heilman
Computer Sciences Corporation
Research Triangle Park, NC 27709

Project Officer

Kenneth L. Schere
Atmospheric Sciences Modeling Division
Atmospheric Research and Exposure Assessment Laboratory
U.S. Environmental Protection Agency
Research Triangle Park, NC 27711

ATMOSPHERIC RESEARCH AND EXPOSURE ASSESSMENT LABORATORY
OFFICE OF RESEARCH AND DEVELOPMENT
U.S. ENVIRONMENTAL PROTECTION AGENCY
RESEARCH TRIANGLE PARK, NC 27711

April 1990

EVALUATION OF THE REGIONAL OXIDANT MODEL (VERSION 2.1) USING AMBIENT AND DIAGNOSTIC SIMULATIONS

by

Thomas E. Pierce
Kenneth L. Schere
Atmospheric Sciences Modeling Division
Atmospheric Research and Exposure Assessment Laboratory
U.S. Environmental Protection Agency
Research Triangle Park, NC 27711

Dennis C. Doll
Technical Support Division
Office of Air Quality Planning and Standards
U.S. Environmental Protection Agency
Research Triangle Park, NC 27711

Warren E. Heilman
Computer Sciences Corporation
Research Triangle Park, NC 27709

Project Officer

Kenneth L. Schere
Atmospheric Sciences Modeling Division
Atmospheric Research and Exposure Assessment Laboratory
U.S. Environmental Protection Agency
Research Triangle Park, NC 27711

ATMOSPHERIC RESEARCH AND EXPOSURE ASSESSMENT LABORATORY
OFFICE OF RESEARCH AND DEVELOPMENT
U.S. ENVIRONMENTAL PROTECTION AGENCY
RESEARCH TRIANGLE PARK, NC 27711

NOTICE

The information in this document has been subject to the United States Environmental Protection Agency's peer and administrative review and has been approved for publication as an EPA document. Mention of trade names or commercial products does not constitute endorsement or recommendation for use.

AFFILIATIONS

Messrs. Pierce, Schere, and Doll are on assignment to the U.S. Environmental Protection Agency from the National Oceanic and Atmospheric Administration, U.S. Department of Commerce. Dr. Heilman is currently with the U.S. Forest Service in East Lansing, Michigan.

ABSTRACT

This report discusses an evaluation of the latest version of EPA's Regional Oxidant Model, ROM2.1. In the ambient evaluation, model estimates were compared with ambient measurements of hourly surface ozone collected on 26 days during the summer of 1985 in the Northeastern United States. Observed and modeled maximum daytime concentrations agreed, on average, to within 2 ppb or 1.4% (79 ppb versus 77 ppb). The model tended to underestimate at the higher extremes of the frequency distribution. The 95th-percentile value was underestimated by 8 ppb or 6.6% (127 ppb versus 119 ppb), and the overall maximum value was underestimated by 50 ppb or 22.7% (219 ppb versus 169 ppb). Underestimates at the upper percentiles tended to be more prevalent in the southern and western portions of the model domain. Concentrations at the lower end of the frequency distribution were slightly overestimated. Estimated and observed spatial patterns of three day maximum ozone generally showed good agreement. ROM2.1 improved noticeably over ROM2.0 with regard to the orientation of the high-ozone plumes in the Northeast Corridor and the depiction of high concentrations along the coast of Maine. Similar to ROM2.0, a tendency to underestimate peak concentrations near Washington, DC was again evident with ROM2.1. A unique aspect of the ambient evaluation was an assessment of the model's ability to estimate boundary conditions for the Urban Airshed Model. Near the New York City metropolitan area, estimated and observed boundary conditions agreed to within 4 ppb or 7.6% (57 ppb versus 61 ppb). Model performance was degraded, however, during some situations with dynamic mesoscale wind flow conditions.

ROM2.1 also underwent a series of diagnostic tests to investigate the accuracy of its numerical solution algorithms. When the model was subjected to extremely steep concentration gradients (steeper than those observed in the ambient atmosphere), the model did not conserve mass during a 48 h simulation, deviating by as much as 18% from the initialized value. With more realistic concentration gradient tests, however, the model conserved mass.

ROM2.1 will be undergoing a series of improvements based largely on the findings of this evaluation. The next version of the model will include refinement of vertical layer specifications and turbulence parameters, and a correction to the mass imbalance problem. Later versions of the model will likely include a dynamic meteorological processor that will simulate nonsteady-state flows.

CONTENTS

Abstract iii
Figures vi
Tables viii
Acknowledgements x

1 Introduction 1

2 Episode Selection for the Ambient Evaluation 4

3 Data Base Development for the Ambient Evaluation 8

4 Ambient Evaluation 14

5 Diagnostic Evaluation 55

6 Summary and Recommendations 90

References 96

Appendix: Statistical Summaries for the August 1985 Episode 98

FIGURES

Number		Page
1	Daily exceedances of ozone in the Northeastern United States	7
2	The ROMNET modeling domain	11
3	ROM grid points overlaying the UAM OMNYMAP domain	11
4	Ozone monitoring sites divided into five geographical groups	12
5	OMNYMAP region monitoring sites used for developing boundary conditions	12
6	Quantile-quantile plots of daytime hourly ozone for the July 1985 episode	26
7	Comparison of observed and modeled daily maxima for the July 1985 episode	32
8	Surface weather maps for July 9-11, 1985	35
9	Spatial patterns of maximum ozone for July 9-11, 1985	36
10	Surface weather maps for July 13-15, 1985	37
11	Spatial patterns of maximum ozone for July 13-15, 1985	38
12	Surface weather maps for July 18-20, 1985	39
13	Spatial patterns of maximum ozone for July 18-20, 1985	40
14	Surface weather maps for August 13-15, 1985	41
15	Spatial patterns of maximum ozone for August 13-15, 1985	42
16	Mean residuals versus wind persistence for the UAM boundary	45
17	Mean residuals versus daily average wind direction for the UAM boundary	45
18	Division of the OMNYMAP boundary into eight groups	46
19	Mean daytime ozone concentrations by UAM group for the UAM boundary	46

FIGURES (continued)

Number		Page
20	Mean residuals for each UAM group experiencing incoming flow	47
21	Ozone concentrations for July 10, 1985 (0800 EST)	48
22	Ozone concentrations for July 10, 1985 (1000 EST)	49
23	Ozone concentrations for July 10, 1985 (1200 EST)	50
24	Ozone concentrations for July 10, 1985 (1400 EST)	51
25	Ozone concentrations for July 10, 1985 (1600 EST)	52
26	Hourly cloud cover and solar fluxes for grid cell (45,21)	53
27	Hourly layer thicknesses for grid cell (45,21)	53
28	Hourly wind speeds for grid cell (45,21)	54
29	Anticyclonic rotational flow used in test cases 1A, 1B, and 1C	68
30	Initial species concentration field in ROM layer 1 for test case 1A	69
31	Time series of normalized mass ration within the entire ROM domain for test case 1A	70
32	Three-dimensional schematic of height of top of ROM layer 1 for test case 1B	71
33	Three-dimensional schematic of height of top of ROM layer 2 for test case 1B	72
34	Time series of normalized mass ratio within the entire ROM domain for test case 1B	73
35	Time series of normalized mass ratio within the entire ROM domain for test case 1C	74
36	Purely divergent wind field used in test case 2	75
37	Three-dimensional schematic of height of top of ROM layer 1 for test case 2	76
38	Three-dimensional schematic of height of top of ROM layer 2 for test case 2	77

FIGURES (concluded)

Number		Page
39	Three-dimensional schematic of height of top of ROM layer 3 for test case 2	78
40	Initial species concentration field in ROM layer 1 for test case 2	79
41	Time series of normalized mass ratio within the entire ROM domain for test case 2	80
42	Quasi-constant wind field used in test cases 0, OA, and OB	81
43	Initial species concentration field in ROM layer 1 for test case 0	82
44	Time series of normalized mass ratio within the entire ROM domain for test case 0	83
45	Initial species concentration field in ROM layer 1 for test case OA	84
46	Time series of normalized mass ratio within the entire ROM domain for test case OA	85
47	Time series of normalized mass ratio within the entire ROM domain for test case OB	86
48	Frequency distribution of paired grid O_3 concentration differences	87
49	Frequency distribution of paired grid NO_x concentration differences	88
50	Frequency distribution of paired grid ROG concentration differences	89
A-1	Quantile-quantile plots of hourly ozone from the August 1985 episode	100
A-2	Comparison of observed and modeled ozone maxima from the August 1985 episode	103

TABLES

Number		Page
1	Ozone monitoring sites used for developing UAM boundary conditions	13
2	Summary statistics for all hourly and maximum ozone concentrations	26
3	Comparison of the July and August 1985 episodes	27
4	Statistical summary by geographical group for the July 1985 episode	28
5	Summary statistics for UAM boundary conditions	43
6	Daily statistics of UAM boundary condtions	44
7	Maximum percentage changes in total mass during a simulation	95
A-1	Summary statistics of hourly daytime ozone for the August 1985 episode	99
A-2	Summary statistics of daily ozone maxima for the August 1985 episode	99

ACKNOWLEDGMENTS

The authors gratefully acknowledge the contributions made by Trudy Boehm, Carlie Coats, Jeanne Eichinger, Susan Hallyburton, Sundar Jambunathan, Dianne Jordan, Don Olerud, Chet Wayland, and Jeff Young of Computer Sciences Corporation under contract number 68-01-7365.

SECTION 1

INTRODUCTION

After realizing that summertime episodes of photochemical smog were a regional and not a localized urban phenomenon, EPA embarked on a research program in the middle 1970's to develop a regional-scale computer model for simulating the transport and fate of ozone (O_3) and its precursors. Research efforts included extensive field studies (Vaughan, 1985) and model development (Lamb, 1983). This work eventually resulted in the creation of the first operational version of the EPA Regional Oxidant Model (ROM1) (described by Lamb, 1983 and 1984; and Lamb and Laniak, 1985). Testing of ROM1 and the analysis of field data prompted additional improvements, including the ability to model biogenic emissions, horizontally-varying layer thicknesses, and improved deposition relationships. After a period of development, the first application version of the ROM (Version 2.0) was made in 1986. It has since been used for several studies in the Northeast and the Gulf Coast region of the U.S., and it has undergone an intensive evaluation by Schere and Wayland (1989) using field data collected in 1980.

Additional needs by the northeastern states and the emergence of new model improvements prompted the development of ROM2.1 as reported by Young et al. (1989). Improvements to ROM2.1 over ROM2.0 included an expanded modeling domain, an updated methodology for computing biogenic emissions of hydrocarbons, revisions in the objective wind field interpolator to remove known biases in the low-level wind flow, and a more sophisticated anthropogenic emissions processor.

Creation of ROM2.1 was primarily motivated by the needs of the Regional Ozone Modeling for Northeast Transport (ROMNET) project (EPA, 1988a). In general, the objective of ROMNET is to investigate interurban transport of ozone and its precursor emissions in the Northeast to support state air pollution control agencies in the development of State Implementation Plans

to achieve the National Ambient Air Quality Standard (NAAQS) for O_3. In this regard, ROM is being used to estimate regional O_3 concentrations and to examine the effectiveness of a variety of hydrocarbon (VOC) and nitrogen oxides (NO_x) emissions control strategies for reducing O_3. Another major objective of the ROMNET project is to use ROM calculations for deriving boundary conditions for urban-scale applications with the Urban Airshed Model (UAM) (Godowitch and Schere, 1989). Because of ROM's importance for comparing the estimated effectiveness of emission control strategies and for estimating boundary conditions, representatives of the ROMNET project asked EPA's Office of Research and Development to evaluate the performance of ROM2.1. This report summarizes the evaluation.

The approach we took complements the work of Schere and Wayland (1989), who evaluated the previous version of ROM, Version 2.0. The primary difference between the two evaluations is that Schere and Wayland used a special field-study data set from 1980, while our evaluation used routinely-collected data from 1985. These data include the anthropogenic emissions inventory, which was adapted from the 1985 National Acid Precipitation Assessment Program (NAPAP) inventory (EPA, 1988b). Our evaluation, unfortunately, could not be as comprehensive as that of Schere and Wayland (1989). They had access to extensive field measurement data for ozone, hydrocarbons, and nitrogen oxides as well as aircraft transects; we were able to use only routine data stored in EPA's Aerometric and Information Retrieval System (AIRS). After surveying AIRS, it was concluded that nitrogen oxide and hydrocarbon measurements were too coarse for a rigorous model evaluation. Therefore, we limited the evaluation of ROM2.1 to hourly observations of surface ozone from state and local agency monitoring sites.

In this report, we compare observed and modeled ozone concentrations for selected periods of high ozone observed during the summer of 1985. Periods from 1985 were chosen because they correspond to the base year emissions inventory. The objectives of the ambient evaluation were (1) to examine overall evaluation statistics to determine whether a general bias exists in the model calculations, (2) to look at spatial patterns of maximum concentration to determine whether a spatial bias exists, and (3) to examine

the model's applicability for determining UAM boundary conditions.

In addition to the ambient evaluation, we performed a series of "stressful" diagnostic tests on the model. In the original development of the first generation ROM (ROM1), a number of diagnostic tests were performed to probe the accuracy of the numerical algorithms used to solve the equations that simulated physical and chemical processes (Lamb and Laniak, 1985). These tests were designed in a hierarchial fashion beginning with a chemistry-only simulation. Transport was then added to the chemical simulation, then vertical mixing, and finally source emissions. These tests represented the next step after independent (external to the ROM framework) tests of the model's numerical algorithms (Lamb, 1983). Results from this original set of diagnostic tests demonstrated that the model faithfully represented solutions to the relevant equations.

Since the time of ROM1, numerous changes have been made to the entire ROM modeling system culminating in the most recent version of the second-generation ROM model (ROM2.1). Although there were significant changes to the chemical and physical processes simulated within the ROM, few changes were made to the basic numerical algorithms employed to solve these processes. Nevertheless, a new round of diagnostic testing was proposed for ROM2.1 that would complement the earlier work done with ROM1. We performed these diagnostic tests on the production version of ROM2.1 used for the ambient evaluation exercises described earlier. In the diagnostic evaluation section, the accuracy of the numerical algorithms will be assessed by evaluating the model's ability to conserve mass for these diagnostic tests.

SECTION 2

EPISODE SELECTION FOR THE AMBIENT EVALUATION

Because we wanted the model simulations to correspond to the base year of the 1985 NAPAP emissions inventory, we examined ozone monitoring data from 1985 for candidate episodes. Daily exceedances (hourly concentrations greater than 120 ppb) of observed ozone in the northeastern U.S. during 1985 are shown in Figure 1. Two clusters of episodes were apparent: middle July and early August. We examined these episodes further for possible starting and ending dates for model simulations, recognizing that the ROM is designed for three-day segments starting at noon and that the first segment should be initialized with "clean" (low ozone/precursor concentrations) conditions. The episodes we selected for modeling for this evaluation were July 7-22 and August 7-16. Brief descriptions of meteorological conditions and observed ozone concentrations are given below.

THE 7-22 JULY 1985 EPISODE

Two rather distinct synoptic patterns characterized this period, occurring on July 7-15 and July 16-22. From the 7th to the 15th, surface troughs and frontal boundaries predominated in the modeling domain. From the 8th to the 10th, a surface trough persisted along the coast from southern New England to the Delmarva area and then westward to a front along the Ohio Valley. From the 11th to the 13th, an east-to-west frontal boundary was located along the Virginia/North Carolina border westward to the Ohio Valley. Weak high pressure was located over New York with a weak ridge extending from New England to Pennsylvania. On the 14th, a frontal boundary approaching the east coast from the west set up weak southwesterly flow along the Northeast Corridor. Cloudiness was widespread throughout the domain from the 9th to the 14th, and showers were occasionally observed in the western portion of the domain.

Southwesterly flow and hot temperatures predominated during the second portion of this episode. On the 16th, a cold front was located along the east coast but moved offshore by the 17th. High pressure over the Great Lakes produced a light northwesterly flow along the Northeast Corridor. The high progressed southeastward on the 18th and gradually weakened as it moved into Virginia and North Carolina on the 19th and 20th. Weak southwesterly flow was observed along the Corridor on the 19th and 20th with relatively hot daily maximum temperatures (upper 80's and low 90's [°F]). By the 21st, a surface trough was located along the east coast while a cold front approached from the west. Maximum temperatures near 90°F were again observed along the East Coast on the 21st. The cold front swept through the Northeast Corridor on the 22nd.

Exceedances of ozone were observed along the Corridor on the 9th, 13th, 19th, and the 20th. Peak hourly concentrations were 165 ppb in central New Jersey on the 9th; 218 ppb in New York City on the 13th; 163 ppb in northern New Jersey on the 19th; and 152 ppb in southern Connecticut on the 20th. Isolated exceedances were observed in the New York City metropolitan area on the 10th and 21st and near Philadelphia on the 16th.

THE 7-16 AUGUST 1985 EPISODE

The 7th to the 10th was characterized by a high pressure ridge that extended from New England through central Pennsylvania into western Virginia and West Virginia. Weak northerly and northeasterly flow occurred along the Corridor. Showers were observed along the Corridor on the 8th. A cold front moved through the Corridor on the 11th and was located offshore on the 12th. High pressure moved southeastward from north of the Great Lakes on the 12th, setting up a ridge along the east coast on the 13th. Relatively high temperatures were observed in the Baltimore/Washington area on the 13th (low 90's). On the 14th and 15th, high pressure extended from off the East Coast into the southeastern U.S. Weak but relatively well-defined southwesterly flow developed along the east coast and high temperatures were observed from New England to Washington, DC (upper 80's to low 90's). A cold front approached the East Coast on the 15th and moved offshore on the 16th.

Widespread exceedances of ozone were first observed on the 9th, extending from Wilmington, DE, to New York City. Exceedances were observed from New York City to Washington, DC, on the 13th and throughout the Corridor on the 14th and 15th. On other days, only scattered exceedances were observed along the Corridor.

On the 9th, peak concentrations ranged from 160 ppb in Wilmington to 164 ppb in New York City. On the 13th, a peak concentration of 201 ppb was observed near New Brunswick, NJ, with values greater than 150 ppb in Baltimore, Trenton, and New York City. Peak concentrations on the 14th included 187 ppb in Baltimore, 184 ppb in New York City, and 169 ppb near Portland, ME. On the 15th, peak values ranged from 188 ppb to 219 ppb in southern and central Connecticut, and concentrations along the Maine coast were above 150 ppb.

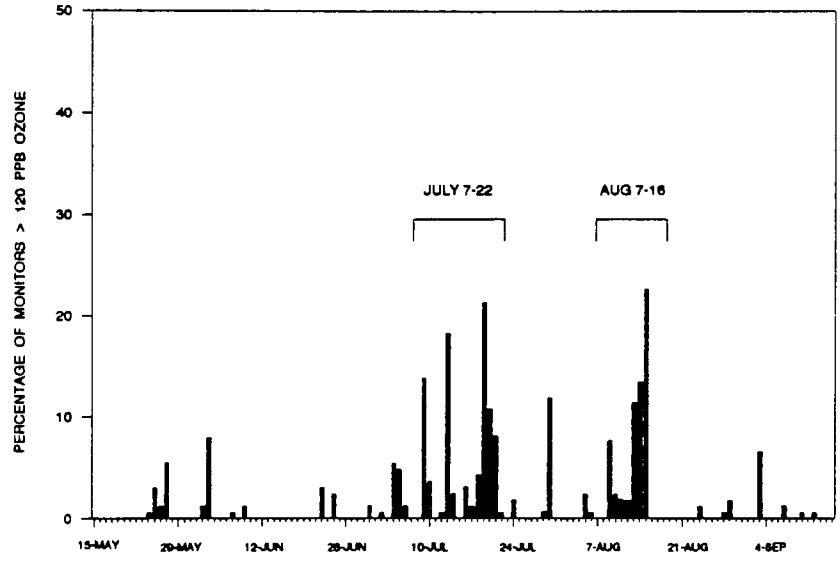

Figure 1. Daily exceedances of ozone in the northeastern U.S. during 1985. An exceedance consists of an hourly concentration greater than 120 ppb.

SECTION 3

DATA BASE DEVELOPMENT FOR THE AMBIENT EVALUATION

Basically, two types of databases were needed for the ambient evaluation: hourly concentrations of ozone from (1) model estimates and (2) observations. Development of these two data bases is described below.

MODEL ESTIMATES

To produce the modeled database, we executed the ROM for the two episodes discussed in Section 2. Model inputs included National Weather Service surface and upper-air meteorological data, observed ozone concentrations for estimating boundary conditions, and hydrocarbon and nitrogen oxide emissions (both anthropogenic and biogenic). More details on model input requirements are given by Young et al. (1989).

The ROM is a three-layer Eulerian grid-scale model that estimates hourly photochemical species concentrations for a 64 by 52 grid as shown in Figure 2. Each grid cell is $1/6^{\circ}$ latitude by $1/4^{\circ}$ longitude, or approximately 19 km by 19 km. For this study, we evaluated only hourly ozone concentrations from layer 1; concentrations from this layer most closely represent surface ozone observations. In layer 1, an individual grid cell is typically ~100 m in vertical extent at night, and 200-500 m deep during the day.

We developed three different model databases for the evaluation. (1) **Point estimates from gridded data:** For the portion of the evaluation concerned with general statistics, we interpolated gridded estimated ozone values to actual monitoring locations using a biquintic interpolation scheme (Lamb, 1985) that is consistent with the methodology used in the model. (2) **Contoured values of gridded data:** For analyzing spatial patterns, we used an objective contouring algorithm to produce computer graphics depicting concentration fields based on the gridded ROM data. (3) **Interpolated values**

derived using the ROM/UAM interface methodology: For the portion of the evaluation concerned with boundary conditions, we employed a fairly elaborate interpolation scheme, described below, that is consistent with the ROM/UAM interface developed for the ROMNET program (Godowitch and Schere, 1989).

1. A band of three ROM grid cells surrounding the UAM New York Metropolitan area domain (Rao, 1987) was defined (see Figure 3).
2. Three-hour running averages, centered on the hour, were calculated for each hour for each ROM grid cell noted in the three-cell band.
3. Using the hourly concentration averages from step 2, an hourly spatial average was taken of each three-cell set normal to the UAM outer boundary and the result noted on the UAM boundary.
4. These concentrations were then spatially interpolated (using linear averages) to the UAM grid cell centers along the boundary.

This procedure allowed us to transform boundary conditions from a 19-km grid size to the grid size of the UAM domain, typically 4 to 10 km.

OBSERVATIONS

We developed the following three observation databases, which are analogous to the three model databases: (1) a set of observations used for developing overall statistics; (2) a set of observations used for creating contour plots; and (3) a set of observations used for developing UAM boundary conditions. We obtained ozone concentrations from monitoring data archived in EPA's Aerometric Information and Retrieval System (AIRS) (EPA, 1989), which contains a national database of hourly ozone (O_3) concentrations and information on monitoring sites. Hourly O_3 concentrations were selected for sites located in the U.S. portion of the ROMNET domain for the two episodes that we modeled with ROM. (Canadian O_3 monitoring data are not included on AIRS and were not readily available for this analysis.) An extensive review and screening of the data was performed. We included only daytime values (0800 h LST to 1900 h LST) in the evaluation because nighttime observations

are influenced by localized processes that often include scavenging of O_3 by NO_x emissions and therefore do not reflect vertically-integrated O_3 concentrations in layer 1 of the ROM (Schere and Wayland, 1989). Furthermore, we excluded a site's data on days missing more than 25% of their observations. We also examined the data for extremely high or low values. Several sites, such as Poughkeepsie (NY), were eliminated because mean daytime O_3 concentrations were consistently below 50 ppb and may have reflected local NO_x scavenging. Of the more than 200 sites in the original database, 187 of these were used in computing general statistics. For portions of the analysis, the data were divided into five geographical groups (Figure 4).

For the spatial plots, little effort was made to eliminate sites because only maximum concentrations were considered. As a result, the plots showed a few locations with extremely low values (due either to poor data recovery or local NO_x scavenging). We ignored these sites when manually contouring the data.

The monitoring data used for developing the UAM boundary condition database were given special consideration. The approach we followed is consistent with the guidance given by Rao (1987). Because so few monitoring sites were available for developing boundary concentrations, we distributed the monitored data among six locations along the UAM boundary: south, southwest corner, west, northwest corner, north, and east (Table 1). The assignment of particular sites to a boundary location depended on the prevailing wind direction for that day. If more than one site was available for a location, the hourly concentrations were averaged. Monitors used in our analysis of boundary conditions are shown in Figure 5. After averaging at the six locations, concentrations were spatially interpolated (using linear avearaging) along the UAM boundary. To be consistent with the ROM/UAM interface methodology, we then used the hourly concentrations to create three-hour running averages as described earlier.

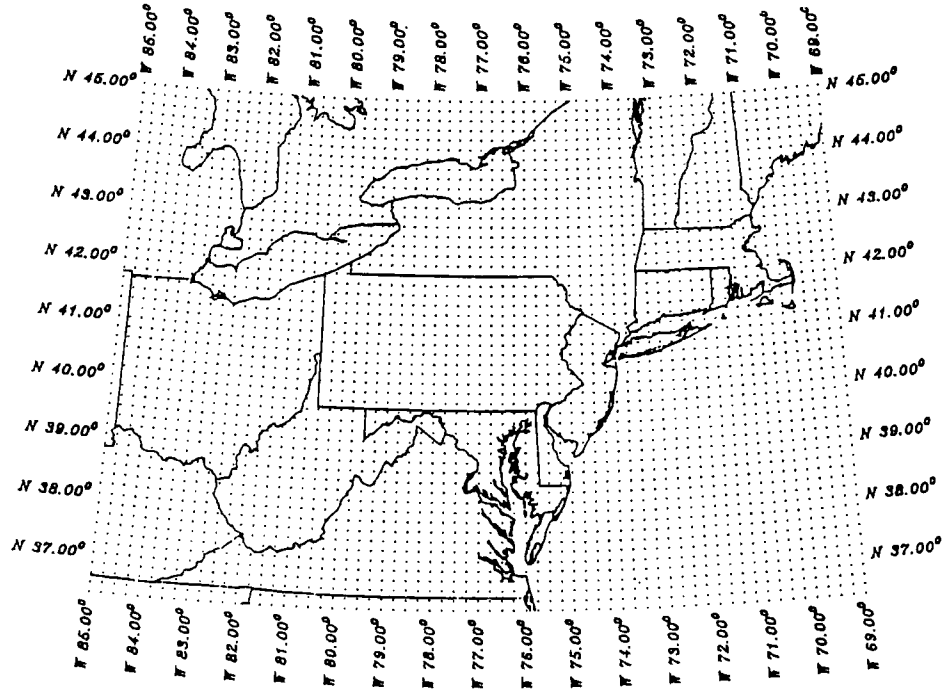

Figure 2. The ROMNET modeling domain. Dots represent model grid cell centers

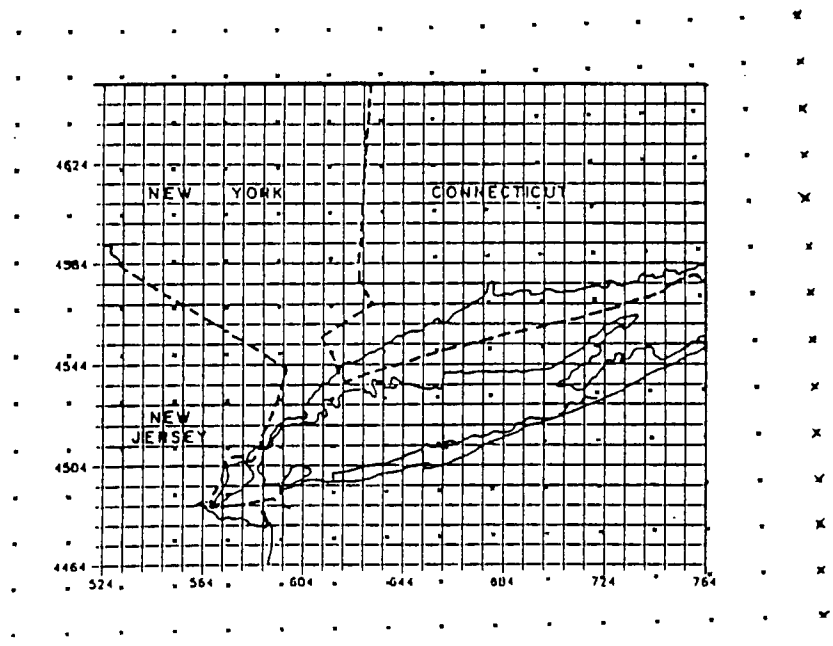

Figure 3. ROM grid points overlaying the UAM domain for the New York City metropolitan area (also referred to as the OMNYMAP domain).

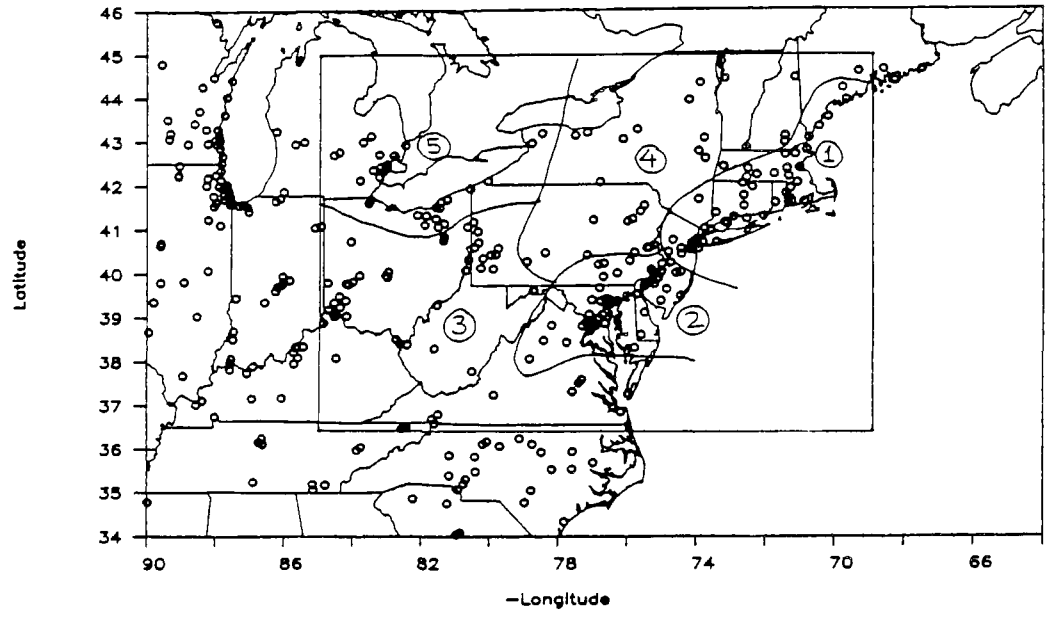

Figure 4. AIRS ozone monitoring sites divided into five geographical groups.

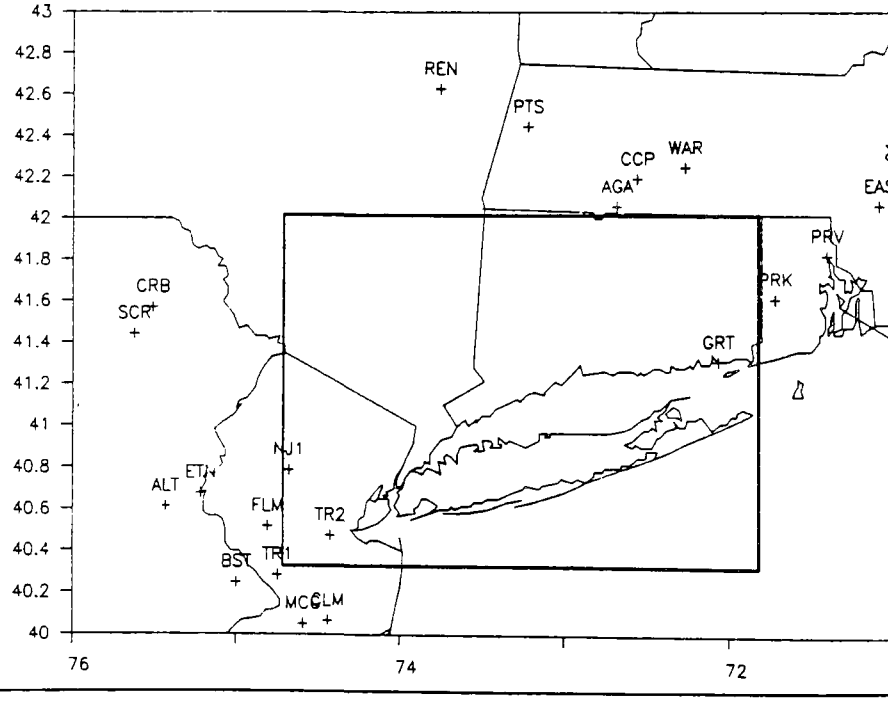

Figure 5. The monitoring sites used for developing boundary conditions for the OMNYMAP domain.

Table 1. Ozone monitoring sites used for developing UAM boundary conditions along the OMNYMAP domain. The arrows indicate which sites are used on each day of the episode; the direction of the arrow indicates the location(s) along the boundary that the data are used (↑ = south, ↗ = southwest corner, → = west, ↘ = northwest corner, ↓ = north, and ← = east).

		July															
Monitoring site	ID	07	08	09	10	11	12	13	14	15	16	17	18	19	20	21	22
Ocean Co, NJ	CLM							↑									
McGuire AFB, NJ	MCG			↑			↑	↗	↑	↑				↑		↑	
Trenton, NJ	TR2	↑	↑	↑	↑	↑	↑	↑		↑	↑	↑	↑		↑	↗↑	↑
Trenton, NJ	TR1		↗↑	↑	↗↑		↗↑	↗	↑	↗↑	↑		↑	↗↑		↗↑	
Flemington, NJ	FLM	↑	→	↗→	↗→	↑	→	→	→	→	↗→	→	→	→	↗→	→	↗→
Bristol, PA	BST		↗	↗	↗		↗		↗	↗	↗			↗		↗	
Morris Co, NJ	NJ1							→				→	→			→	
Allentown, PA	ALT		→	→	→	→	→		→	→	→			→	→	→	→
Easton, PA	ETN	→	→	→		→	→		→	→	→			→	→		→
Scranton, PA	SCR	→	→	→	→	→			↘	↘	→			↘	→	↘	→
Carbondale, PA	CRB	→				→			↘	↘				↘		↘	
Rensselaer, NY	REN	↓				↓									↓		↓
Agawam, MA	AGA	↓	↓	↓	↓	↓	↓	↓	↓	↓	↓	↓	↓	↓	↓	↓	↓
Pittsfield, MA	PTS	↓				↓						↓	↓		↓		↓
Chicopee, MA	CCP											↓	↓				
Ware, MA	WAR											↓	↓				
Groton, CT	GRT	←	←	←	←	←	←	←	←	←	←	←	←	←	←	←	←
Kent Co, RI	PRK			←								←	←				
Providence, RI	PRV											←	←				

		August									
Monitoring site	ID	07	08	09	10	11	12	13	14	15	16
Ocean Co, NJ	CLM					↑		↑			
McGuire AFB, NJ	MCG	↑	↑			↑		↑	↑		
Trenton, NJ	TR2	↑	↑	↑	↗↑	↑	↑	↑	↑	↑	↑
Trenton, NJ	TR1	↗↑	↗↑		↗	↑	↑	↑	↑	↑	
Flemington, NJ	FLM	→	→	→	→	→	↗→	↗→	→	→	↗→
Bristol, PA	BST	↗	↗			↗	↗	↗	↗	↗	
Morris Co, NJ	NJ1			→	→						
Allentown, PA	ALT	→	→			→	→	→	→	→	→
Easton, PA	ETN	→	→			→	→	→	→	→	→
Scranton, PA	SCR	↘				↘	→		↘	↘	→
Carbondale, PA	CRB	↘				↘			↘	↘	
Rensselaer, NY	REN										↓
Agawam, MA	AGA	↓	↓	↓	↓	↓	↓	↓	↓	↓	↓
Pittsfield, MA	PTS								↓		↓
Chicopee, MA	CCP			↓		↓	↓	↓			
Ware, MA	WAR			↓		↓	↓	↓			
Groton, CT	GRT	←	←	←	←	←	←	←	←	←	←
Kent Co, RI	PRK			←							
Providence, RI	PRV										

SECTION 4
AMBIENT EVALUATION

To emphasize different aspects of model performance, we broke the ambient evaluation of ROM2.1 into three parts: overall statistics, spatial patterns, and UAM boundary conditions.

OVERALL STATISTICS

Using the modeled and observed databases of hourly ozone concentrations, descriptive statistics were computed using SAS (1985) procedures. From these general statistics, we attempted to assess the overall temporal and spatial performance. The intent here was not to evaluate ROM in a deterministic manner--that is, by comparing closely paired observations and estimates. We believe that using ROM in a strictly deterministic manner is inappropriate because (1) ROM's grid cells are of significant size (19 km by 19 km), (2) stochastic variations in atmospheric flow cannot be resolved using the current network of meteorological observing sites, and (3) the degree of spatial variability of actual O_3 concentrations cannot be detected by the current monitoring network. In fact, Schere and Wayland (1989) and Lamb and Hati (1987) also recommend against the deterministic use of models such as the ROM.

Summary statistics for all modeled and observed daytime hourly concentrations for the combined July and August episodes are shown in Table 2, together with statistics for daily maxima at all sites. The observed and modeled data sets were treated separately in calculating the statistics. The mean observed and modeled values agree fairly closely; the hourly means agree to within 10 ppb and the daily maximum means agree to within 1 ppb (which is not significant at the 99% confidence level). Although the model overestimated the mean hourly value, it tended to underestimate the hourly and daily maximum values in the upper extremes of the frequency distributions. The 95th-percentile hourly value was underestimated by 1 ppb, and the maximum was underestimated by 50 ppb; the daily maximum values show a

similar tendency.

Statistics for the individual July and August episodes are shown in Tables 3a and 3b; they are similar to those for the combined episodes. Because results for the two episodes are similar to each other, we limit our discussions in the rest of this report primarily to the July episode. A complete list of statistics for the August episode is available in the appendix.

To examine spatial trends in the data, we separated the monitoring sites into five geographical groups (Figure 4) as follows: (1) Northern Corridor, (2) Southern Corridor, (3) Ohio Valley-Middle Atlantic, (4) Interior Northeast, and (5) Great Lakes. Statistics for each group are summarized in Tables 4a and 4b. Depending on the statistic, model performance was better in some groups than in others. The statistic we preferred to examine was the 95th-percentile value from the daily maximum concentrations, because it is robust and can be related to NAAQS assessment. As shown in Table 4b, all concentrations at the 95th percentile were underestimated except for group 1, which was overestimated by 5%. It is encouraging to note that, except for group 3 which was underestimated by 19%, all estimated and observed concentrations at the 95th percentile agreed to within 10%.

A valuable tool for assessing model performance is a quantile- quantile plot, which can be used to compare the frequency distributions of sorted observed and sorted estimated concentrations. The concentrations are sorted from highest to lowest and then plotted on an *x-y* plot. The *x*-axis depicts observed data, and the *y*-axis depicts estimated data.

Quantile-quantile (hereafter refered to as QQ) plots of hourly daytime concentrations for each of the five geographical groups during the July episode are shown in Figures 6a-6e. In each of these plots, the solid line denotes a perfect fit, and the dashed lines show a ten percent deviation from this line. The findings from the QQ plots are consistent with overall statistics shown previously. Model estimates from groups 2, 3, and 4 tended to be lower than observations in the higher quantiles; underestimates were

evident in the top 30 percent of group 2, top 50 percent of group 3, top 20 percent of group 4. Group 1 showed general overestimates in the upper quantiles (except for the top 1%), and group 5 ranged from good agreement to overestimates at the upper values. Overestimates were evident at the lower ends of the frequency distribution for all five groups. Median values in general agreed quite well. In groups 1 and 5, median values were overestimated by about 20% (around 10 ppb); in groups 2, 3, and 4, the median was overestimated by 10% or less. In the Northeast Corridor, differences between the northern portion of the Corridor (group 1) and the southern portion (group 2) were evident. Group 2's estimates agreed much better with observations than did group 1's. Similar to what Schere and Wayland (1989) noted in their evaluation of ROM2.0, estimates in the southern part of the Corridor tended to be lower than the observations at the upper end of the frequency distribution, although estimates were within 10% of observations except for the maximum value. The tendency to underestimate peak concentrations in group 2 will be discussed below in the spatial analysis section. The region showing the greatest underestimate in the upper values was group 3, an area removed from the extensive metropolitan area along the Northeast Corridor. In groups 4 and 5, agreement was quite good.

In an effort to understand how well the ROM tracked daily maximum concentrations, we computed frequency distributions of maximum (observed and estimated) ozone concentrations from the data in each group for each day. Figures 7a-7e compare box plots of modeled and observed daily maximum concentrations for all but the first two days of the July episode. The first two days are not shown because the model is strongly influenced by initial conditions and tends to underestimate ozone concentrations during this "start-up" period. The box plots denote the maximum, 75th percentile, 50th percentile (or median), 25th percentile, and minimum value. These plots show similar results to those noted in the QQ plots for hourly concentrations; however, they also provide temporal information.

On a daily basis, the model tended to track the observations fairly well. For all of the regions combined, there were about equal numbers of days with underestimates and overestimates. As discussed for the QQ plots,

group 1 tended to experience the most overestimates (12 out of 14 daily medians were overestimated) while group 3 tended to experience the most underestimates (medians for 12 out of 14 days were underestimated). The daily maximum plots also show that as one moves away from the Corridor (groups 1 and 2), median daily maximum concentrations tended to approach background values.

One of the ROM's most important uses is to simulate days having ozone exceedances (hourly concentrations greater than 120 ppb). In group 1, eight exceedance days were observed while ten exceedance days were estimated, thus indicating that the ROM tends to slightly overestimate in the northern portion of the Corridor. Further to the south in group 2, however, ten exceedance days were observed but only six were estimated. In group 3, six exceedance days were observed but none were estimated. The monitors reporting these six exceedances were in smaller urban areas such as Richmond, Norfolk, and Charleston (WV) than those found in the Northeast Corridor. This suggests that the coarse grid resolution (19 km) of the ROM may be insufficient to adequately resolve smaller urban plumes. Also, naturally-occuring hydrocarbon and NO_x emissions are probably more important in these areas because of the relatively lower anthropogenic emission densities; so, uncertainties in estimating naturally-occurring emissions may have contributed to poor performance in group 3. Despite the relatively poor model performance in the southern portion of the domain, performance in the Great Lakes, Interior Northeast, and the Northern Corridor groups seems quite good.

SPATIAL PATTERNS

For this portion of the evaluation, we examined spatial patterns of maximum hourly ozone for four distinct three-day episodes that represent a range of meteorological conditions and model performance.

The 9-11 July Episode

This was a period of unsettled weather with weak pressure gradients.

For much of the episode, a weak surface trough was draped from Long Island to Virginia to northeastern Ohio to Illinois (Figure 8). By the 10th, southwesterly flow became better defined in advance of a cold front moving eastward through the Great Lakes. Of special interest on this day was a mesoscale high pressure area associated with a line of thunderstorms in central Pennsylvania, which eventually moved through the southern part of the corridor and significantly reduced ozone concentrations. This feature will be discussed below in the section on background concentrations. By the morning of the 11th, less humid conditions and northwesterly flow prevailed as the cold front had pushed off the East Coast.

During this period, monitors picked up ozone plumes above 120 ppb from Wilmington, DE, to Boston (Figure 9). Observed and estimated maximum hourly concentrations greater than 160 ppb were observed near central New Jersey and coastal Connecticut. Agreement over southern Connecticut was good, although the modeled plume appears to be shifted slightly east and south of observed values. The model also shifted the high concentrations just off the coast of New Jersey near Atlantic City. Simulating small-scale features during this episode was particularly difficult because of the weak wind flow, the occurrence of the mesoscale high, and the persistence of a coastal trough. Overall, however, estimates of maximum ozone for this episode agreed fairly well with observed data.

The 13-15 July Episode

Figure 10 shows a meteorological scenario typically associated with elevated ozone concentrations in the Northeast. A weak cool high pressure system centered over New York on the 13th gave way to a warm front on the 14th. By the 15th, southwesterly flow was fully established. Unsettled conditions prevailed in the western portion of the model domain. Showers were reported on the 14th and the 15th in western New York and Pennsylvania in advance of a slow moving cold front.

During this episode, two separate areas of high ozone values were observed (Figure 11). A modest area of exceedances (maximum of 132 ppb) was

noted from Boston to the southern coast of Maine. High concentrations were also noted in distinct "blobs" near Philadelphia and New York City. Concentrations greater than 200 ppb were observed near Wilmington, DE, (211 ppb) and Bayonne, NJ (218 ppb). Although an area of observed exceedances stretched from Washington, DC, to central Long Island, no well-defined plume downwind of New York City was apparent.

Except north of New York City, estimated ozone concentrations were lower than those observed during this episode. However, Figure 11 shows that the intermittent nature of the high ozone concentration areas was well represented. Near Boston, the modeled and observed concentrations agreed closely as noted by the placement of the 140 ppb contour on both plots. Unfortunately downwind of Wilmington, DE, the model underestimated the peak observed concentration by about 80 ppb. Part of the poor performance may be due to a coastal trough that existed during this episode as shown in the synoptic analysis for July 15th (Figure 10). Pagnotti (1987) points out that small-scale features such as this tend to produce localized pockets of high ozone that would not be well-represented by a regional model such as the ROM.

The 18-20 July Episode

This period began with weather forecasters tracking Tropical Storm Ana, which moved harmlessly off the New England coast. Figure 12 shows that high pressure held firmly over the Northeast, gradually shifting southward and weakening. By the 19th, southerly flow had become fully established over the Corridor. On the 20th, a coastal trough was evident along the Atlantic Coast.

Under light wind conditions, high concentrations were once again positioned in small, distinct areas (Figure 13). Values above the standard stretched from the Delmarva peninsula to central Massachusetts. The highest concentration (164 ppb) was observed near Trenton, NJ. A small but impressive area of high concentrations (maximum of 152 ppb) was observed along the coast of Maine. With minor exceptions, the model showed reasonable agreement to the peak observed values during this period (Figure 13). A

plume over 120 ppb extended from near Baltimore northward to off the coast of Maine. Pockets over 160 ppb were estimated near New York, which agreed, in general, with the observed values. Except for missing the high concentrations over the Delmarva peninsula, ROM appears to do a good job predicting the magnitude and placement of the maximum ozone plume during this period.

The 13-15 August 1985 Episode

This episode was similar to the July 13-15 episode. Weak cool high pressure was positioned over the Northeast on the 13th (Figure 14). The system had moved eastward by the 14th allowing weak southwesterly flow to ensue. By the 15th, a cold front began moving through the western portion of the domain. Southwesterly flow strengthened, but a hint of a coastal trough was evident in the surface weather map.

Monitoring data revealed an extensive area of ozone exceedances that stretched from Wilmington, DE, to coastal Maine (Figure 15). Highest concentrations were observed near Hartford, CT (219 ppb). An isolated area of high concentration (maximum of 187 ppb) was observed just north of Baltimore.

The general orientation of the modeled ozone plume is excellent when compared to observations (Figure 15). The highest estimates, however, approached only 200 ppb, more than 20 ppb less than the highest observation. The model did simulate an area of high concentrations (greater than 180 ppb) off the coast of Maine, close to where relatively high concentrations were observed. While the model did not replicate the extreme peaks, it satisfactorily estimated the pattern and shape of the ozone plume near the Northeast Corridor.

BOUNDARY CONDITIONS

One of the intended uses of ROM is to estimate boundary conditions for the Urban Airshed Model (UAM). UAM modeling will be needed for resolving

small-scale gradients of ozone near urban areas and for determining the degree of nonattainment in the urban airshed relative to the NAAQS for O_3. The grid resolution of the UAM varies from 2 to 10 km, whereas the ROM has a grid resolution of about 19 km. For this evaluation, we compared ROM estimates of ozone boundary concentrations from layer 1 with boundary concentrations derived from monitoring data taken near the OMNYMAP domain; the development of the two databases was described in Section 3. This evaluation was limited to near-surface concentrations because measurements were available only from surface-based monitors. The 73 UAM grid points used in our analysis stretch from the coast of New Jersey clockwise to the coast of Connecticut. We excluded grid boundaries over the Atlantic Ocean because of an obvious lack of ozone monitoring data there.

We began the analysis by looking at the overall performance of the ROM in estimating daytime boundary conditions. Table 5 shows summary statistics for the 20,155 data points available; these data were taken from valid combinations of estimated and observed daytime (0800 LST to 1900 LST) hourly concentrations for 73 grid locations for 24 days of data. The model slightly overestimated the mean concentrations (by 5 ppb or 7.6%). At higher quantiles, however, the model tended to underpredict in a manner consistent with the statistics we presented earlier. In addition, the larger standard deviation of the observed concentrations shows that observations exhibited more variability than the model estimates.

Because there was no overwhelming bias apparent in the model, we examined the boundary condition calculations in further detail. Table 6 compares estimated and observed mean concentrations on a daily basis. While the mean values summed over all the days agreed to within 10%, there was some day to day variability. Percent differences for individual days ranged from -24% to +49%. However, estimated and observed mean values were within ±10 ppb on 14 of the 22 days. Other pertinent information on mean wind persistence, wind speed, and wind direction is also noted in Table 6.

Figure 16 displays model performance as a function of wind persistence. Surprisingly, the more persistent flow conditions were associated with

greater overestimates, as noted by the mean fractional errors which dropped from 23% percent during very persisent conditions to -18% during low persistence.

Next we looked for a relationship between model performance and daily average wind direction. Figure 17 shows, as expected, that southerly and southwesterly winds were most prevalent during the model simulations. In terms of model performance, model estimates and observations agreed more closely when southerly winds pervailed. With southerly winds, there were 10 days of overestimates and 8 days of underestimates, for an average error of 5%. With northerly winds, the model overestimated on all five days, and the average error was +26%.

We then geographically stratified the data set to look for spatial biases in the estimates. Figure 18 shows the eight groups of grid cells formed, with group 1 located in the south and group 8 located in the east. Mean observed and estimated concentrations for the eight groups are shown in Figure 19. The highest observations and estimates occurred in group 1, which is located in the center of the Northeast Corridor and would experience high ozone concentrations typical of southwesterly flow conditions. It is noteworthy that the observed and modeled patterns in Figure 19 resemble each other; both show a minimum along the northern boundary and a maximum for group 1. Best agreement occurred for groups 3 and 5.

The above statistics have included all grid points regardless of the wind direction. Next using the same eight grid cell groups, we examined model performance for individual groups experiencing incoming flow on a given day. For example, if southwesterly winds predominated, we then analyzed the daytime concentrations for group 2. Figure 20 shows the mean residuals for each group for days having upwind flow. As we saw in Table 6, residuals varied appreciably from day-to-day, ranging from -15% to +25%. However, 8 of 13 days experienced mean residuals less than 10%.

There were a few days when the model performance was admittedly disappointing. In particular, day 191 showed a 25% overestimate in group 2.

Although we lacked the resources to analyze every day in detail, we examined this day in order to gain some insight on model performance.

The 1200 GMT surface weather map for 10 July 1985 (Julian day 191) gave some indication as to why observed concentrations were lower than expected in eastern Pennsylvania and western New Jersey. This map (Figure 8) shows a mesoscale high over south central Pennsylvania which was apparently induced by a cluster of thunderstorms. A stationary front extending from a low over central Indiana stretched eastward to northern Virginia and merged into a surface trough that stretched northeastward along the Atlantic seaboard. The main weather feature was a combined cold and occluded front positioned along the St. Lawrence Valley southward through the Ohio Valley.

To examine why the daytime ozone observations were underestimated in group 2, we generated hourly plots from both the observations and the estimates. Figure 21 shows the observed and estimated concentration fields for 0800 EST (one hour after the 1200 GMT surface weather map). Two features are given on the observed plot: weather data reported at each National Weather Service surface observing site, and measured hourly ozone concentrations. The circled ozone measurements denote the sites used in generating the observed UAM boundary conditions for group 2. The 18 gridded model values used in defining group 2's boundary conditions are enclosed by a rectangle. At 0800 EST, estimates averaged more than 20 ppb higher than the observed values. The weather data indicate that the surface trough is still located along the Atlantic Seaboard. Ahead of this trough, winds were generally from the south; behind the trough, winds were generally from the west.

Moving to 1000 EST, estimates were still about 20 ppb higher than the observations (Figure 22). Observed concentrations in northeastern Pennsylvania were particularly low. This area was experiencing overcast skies, temperatures around 22°C, and high relative humidity. This suggests the likelihood of shower activity which may have caused lower ozone concentrations by allowing increased vertical transport and reduced photochemical production.

By 1200 EST, thunderstorm activity had begun (Figure 23) as indicated by the Wilmington (DE) observation. Overestimates by the model continued throughout group 2. Although overcast and relatively cool conditions predominated in eastern Pennsylvania, Atlantic City experienced hot, sunny conditions as indicated by their temperature of 34°C. The estimated concentration field shows a strong gradient across group 2, ranging from 79 ppb in the northwest to 102 ppb in the southeast. The observed concentrations, in contrast, range from 40 ppb to 69 ppb. Observed concentrations as high as 111 ppb were reported in central New Jersey but these were not prescribed for use in the UAM/ROM interface methodology. After investigating additional sources of meteorological data, we found that Philadelphia reported a wind gust of 45 miles per hour. This information, which was not available in the routine modeling data base, strongly suggests the nearby presence of organized convective activity such as a squall line.

Figure 24 shows that by 1400 EST, shower activity had moved into Atlantic City. The temperature in Atlantic City dropped over 5°C in two hours and observed ozone concentrations in the area dropped over 50 ppb. Easterly winds reported at both Philadelphia and Wilmington are probably indicative of outflow from thunderstorm activity in central New Jersey. Meanwhile over northeastern PA, skies are beginning to clear although ozone concentrations remain low. Predictions in group 2 seem less affected by the storm activity and are as high as 112 ppb.

By 1600 EST, (Figure 25) observed concentrations near Scranton had rebounded to near modeled values (65 ppb versus 75 ppb). In the area near Atlantic City, which was still experiencing shower activity, estimated concentrations were as high as 125 ppb but observed concentrations were only around 30 ppb.

The meteorological data we used in the ROM offer some clues as to why the ROM overestimated concentrations in group 2. Figures 26 through 28 show time series of selected meteorological parameters that were calculated for grid cell (45,21), the cell for which modeled concentrations were underlined

in each of the plots shown earlier. The simulated cloud cover and solar fluxes in Figure 26 did show some effect of the observed cloudy conditions but probably not enough. Cloud cover increased to more than 90% by 1300 EST but only slightly reduced the computed solar flux. The model layer heights (Figure 27) show some increase, with layer 3 growing to 1700 m by 1100 EST. However, the localized convective activity probably caused more vigorous vertical and horizontal mixing than was simulated in the model. Horizontal dilution in the model also was probably smaller than actual dilution as indicated by the relatively low modeled wind speeds in Figure 28. Apparently the small-scale (relative to the model) cluster of thunderstorms was not captured in the overall interpolation of meteorological data.

This case study was noteworthy because it highlighted some of the ROM's limitations. ROM is a regional-scale model that was designed for application in relatively benign, steady-state summertime conditions. The occurrence of a mesoscale surface trough and localized thunderstorm activity resulting in dynamic subgrid-scale atmospheric processes seems to have affected the ROM's ability to estimate boundary conditions along portions of the UAM domain on day 191. The results indicate that development of UAM boundary conditions from either observed or modeled data should include careful examination of the effects of mesoscale meteorological conditions, which as we have shown, can cause localized perturbations in ozone concentrations.

TABLE 2. SUMMARY STATISTICS FOR ALL DAYTIME HOURLY AND DAILY MAXIMUM OZONE CONCENTRATIONS (IN PPB) FOR THE ROMNET REGION (JULY AND AUGUST 1985 DATA MERGED)

Conc. type	n	Mean obs.	Mean model	Std. dev. obs.	Std. dev. model	95th Percentile obs.	95th Percentile model	Maximum obs.	Maximum model
Daytime hourly	40,534	55.2	64.5	26.8	19.2	102.0	101.1	219.0	169.2
Daily Maximum	3,707	78.6	77.5	26.7	22.2	127.0	118.7	219 0	169.2

TABLE 3A. COMPARISON OF THE JULY AND AUGUST 1985 EPISODES (DAYTIME HOURLY STATISTICS, IN PPB)

Episode	n	Mean obs.	Mean model	Std. dev. obs.	Std. dev. model	95th Percentile obs.	95th Percentile model	Maximum obs.	Maximum model
July 1985	25,129	56.8	66.6	26.0	19.3	102.0	103.2	218.0	169.2
August 1985	15,405	52.7	61.1	28.0	18.7	102.0	97.0	219.0	161.3

TABLE 3B. COMPARISON OF THE JULY AND AUGUST 1985 EPISODES (DAILY MAXIMUM STATISTICS, IN PPB)

Episode	n	Mean obs.	Mean model	Std. dev. obs.	Std. dev. model	95th Percentile obs.	95th Percentile model	Maximum obs.	Maximum model
July 1985	2,271	79.9	79.6	25.1	22.5	125.0	120.9	218.0	169.2
August 1985	1,436	76.6	74.1	29.0	21.3	131.0	114.1	219.0	161.3

TABLE 4A. STATISTICAL SUMMARY BY GEOGRAPHICAL GROUP FOR THE JULY 1985 EPISODE (DAYTIME HOURLY CONCENTRATIONS, PPB).

Group	n	Mean		Std. dev.		95th Percentile		Maximum	
		obs.	model	obs.	model	obs.	model	obs.	model
1	6206	60.2	78.4	27.8	21.9	111.0	118.7	218.0	169.2
2	6776	65.2	72.6	27.5	19.0	110.0	107.6	211.0	159.8
3	5902	54.3	57.3	23.7	11.8	95.0	79.4	155.0	103.5
4	3604	47.8	56.4	20.1	12.8	83.0	81.3	126.0	121.4
5	2641	45.2	57.9	19.5	11.3	80.0	78.5	108.0	108.0

TABLE 4B. STATISTICAL SUMMARY BY GEOGRAPHICAL GROUP FOR THE JULY 1985 EPISODE DAYTIME (DAILY MAXIMUM CONCENTRATIONS, PPB).

Group	n	Mean		Std. dev.		95th Percentile		Maximum	
		obs.	model	obs.	model	obs.	model	obs.	model
1	558	88.0	97.8	28.9	23.1	138.0	144.9	218.0	169.2
2	609	90.7	87.9	23.8	19.5	130.0	120.8	211.0	159.8
3	537	75.1	65.9	19.1	12.1	109.0	88.0	155.0	103.5
4	328	66.1	64.7	17.9	14.5	96.0	91.7	126.0	121.4
5	239	63.4	67.2	17.8	11.7	94.0	89.3	108.0	108.0

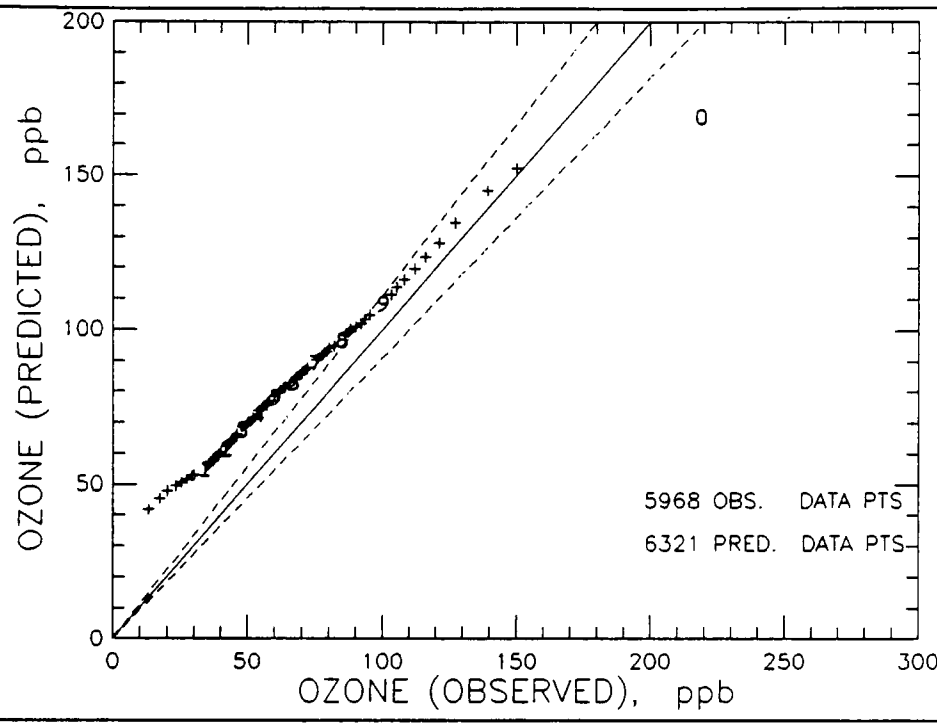

Figure 6a. Quantile-quantile plot of daytime hourly ozone for the July 1985 episode (Group 1, Northern Corridor).

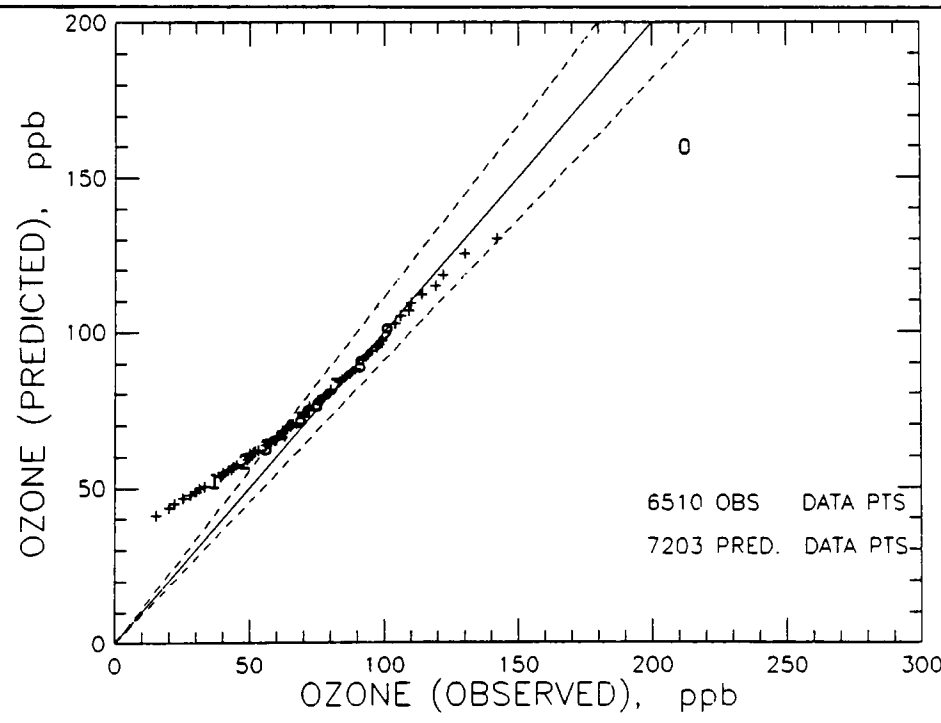

Figure 6b. Quantile-quantile plot of daytime hourly ozone for the July 1985 episode (Group 2, Southern Corridor).

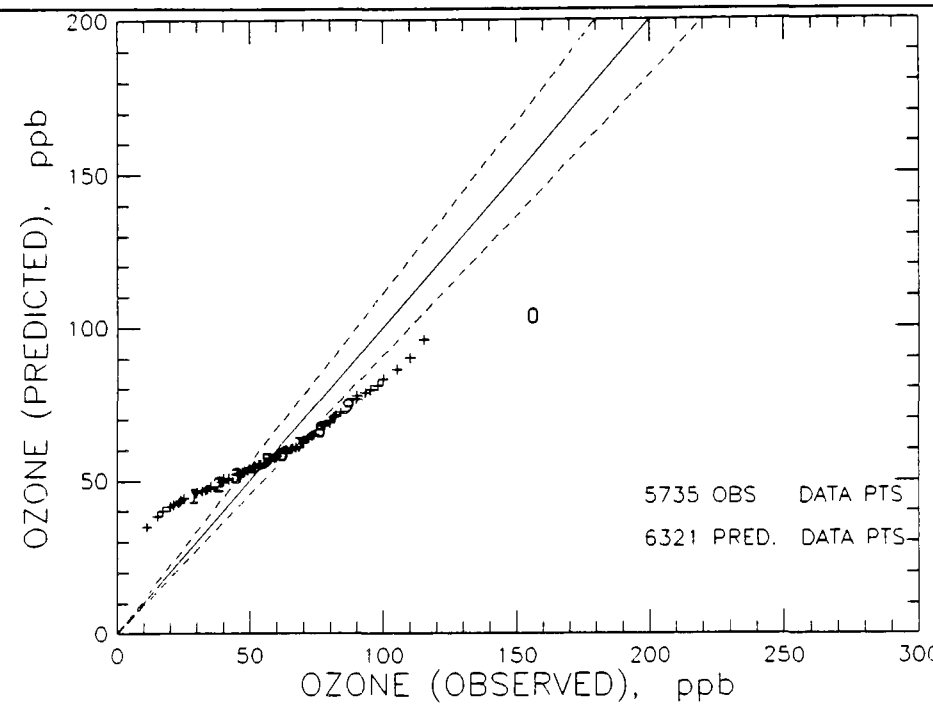

Figure 6c. Quantile-quantile plot of daytime hourly ozone for the July 1985 episode (Group 3, Ohio Valley-Middle Atlantic).

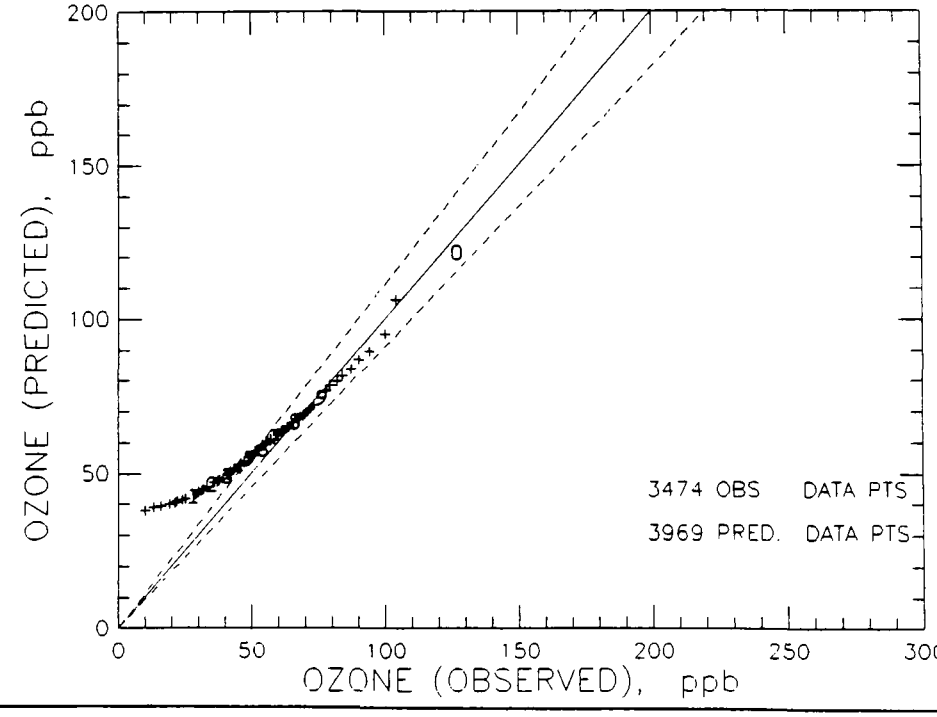

Figure 6d. Quantile-quantile plot of daytime hourly ozone for the July 1985 episode (Group 4, Interior Northeast).

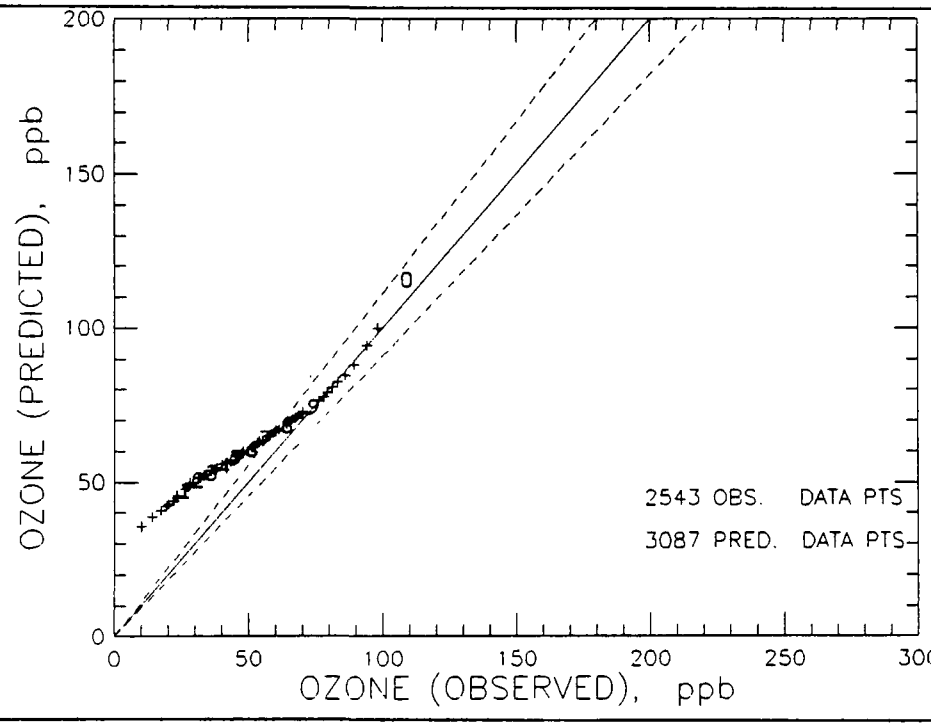

Figure 6e. Quantile-quantile plot of daytime hourly ozone for the July 1985 episode (Group 5, Great Lakes).

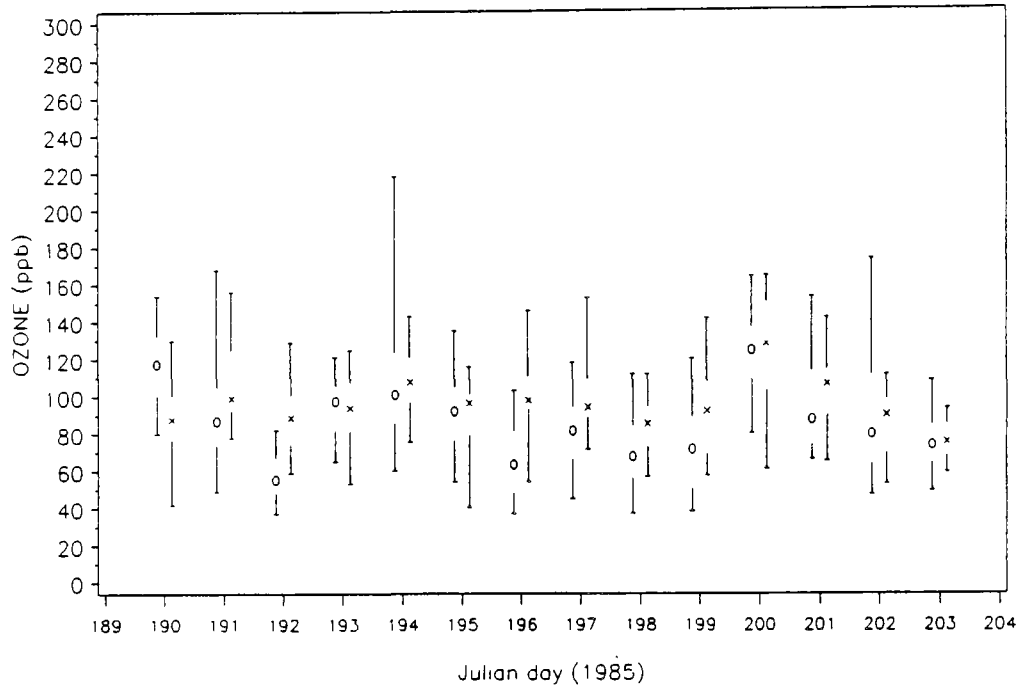

Figure 7a. Comparison of observed (*o*) and modeled (*x*) maximum ozone for the July 1985 episode (Group 1, Northern Corridor).

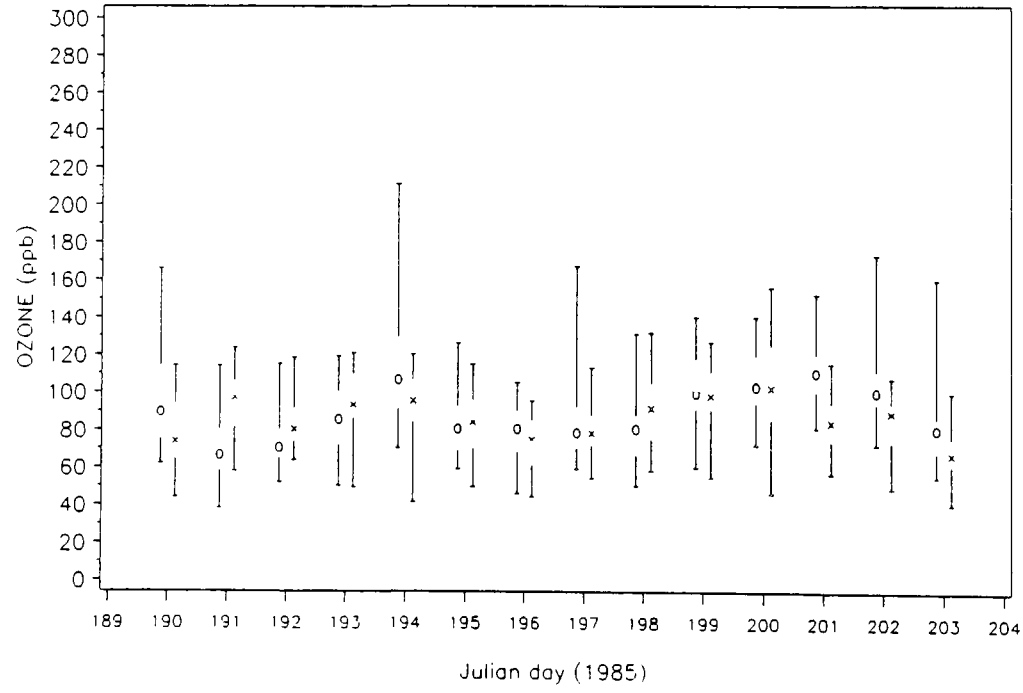

Figure 7b. Comparison of observed (*o*) and modeled (*x*) maximum ozone for the July 1985 episode (Group 2, Southern Corridor).

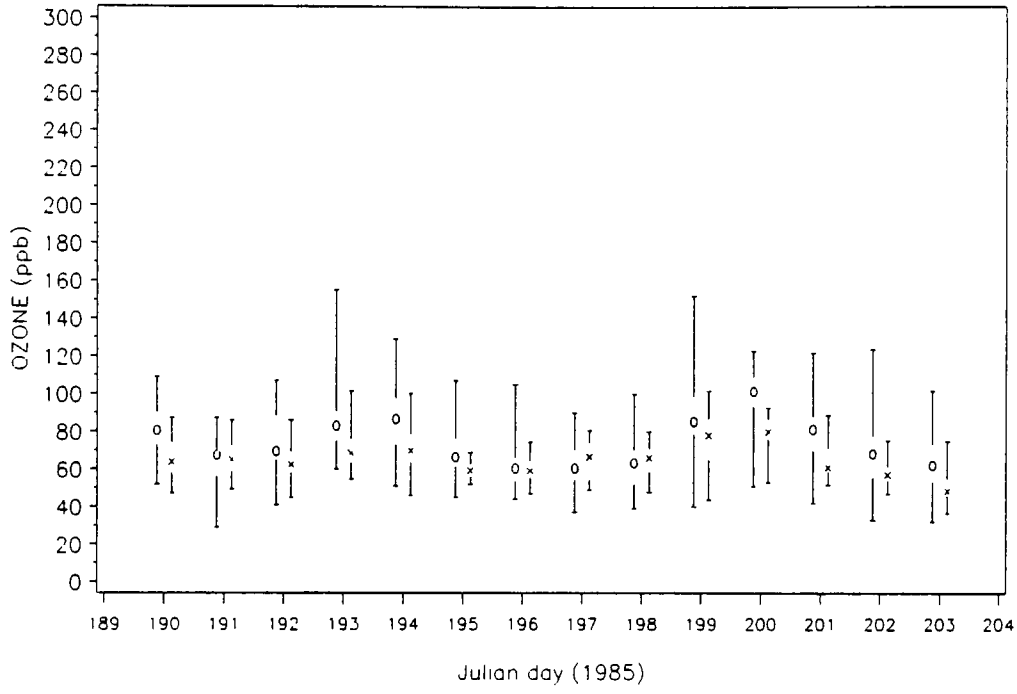

Figure 7c. Comparison of observed (*o*) and modeled (*x*) maximum ozone for the July 1985 episode (Group 3, Ohio Valley-Middle Atlantic).

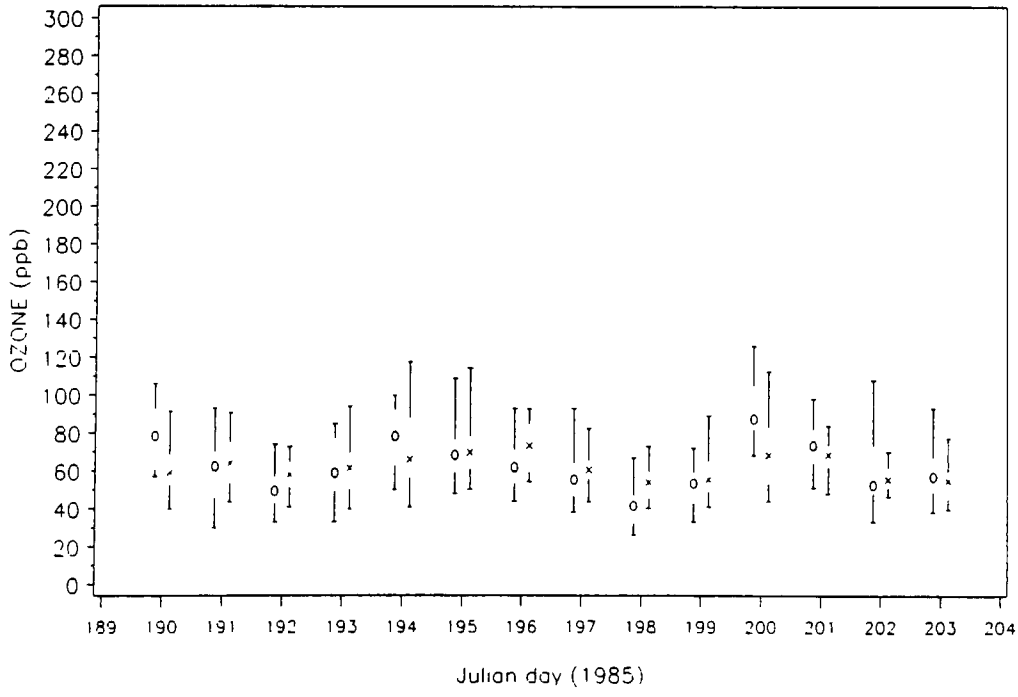

Figure 7d. Comparison of observed (*o*) and modeled (*x*) maximum ozone for the July 1985 episode (Group 4, Interior Northeast).

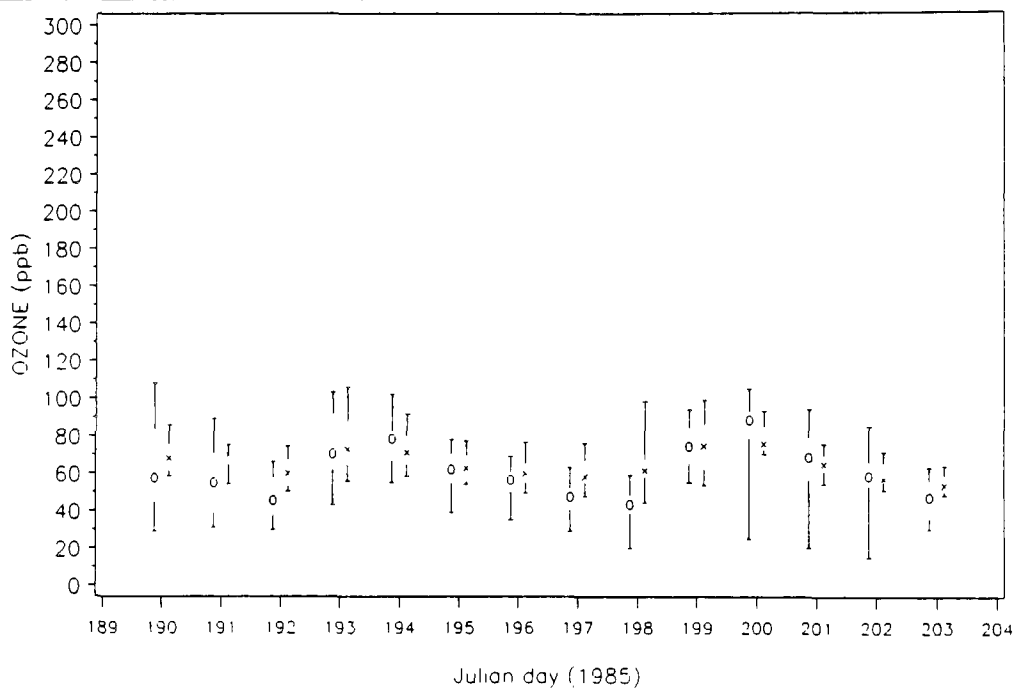

Figure 7e. Comparison of observed (*o*) and modeled (*x*) maximum ozone for the July 1985 episode (Group 5, Great Lakes).

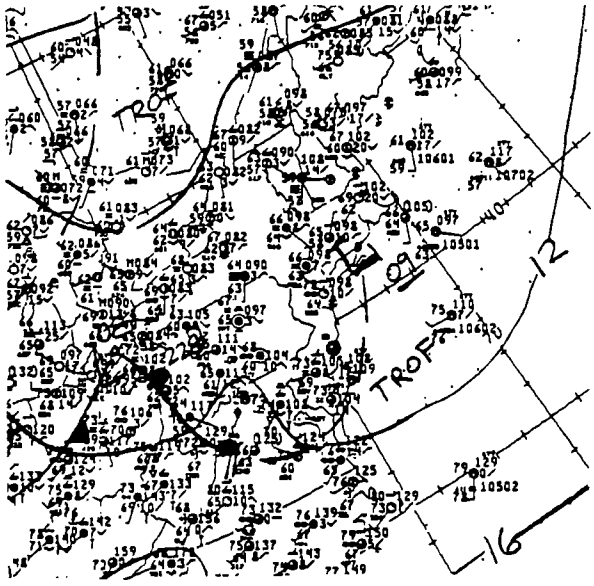

July 9

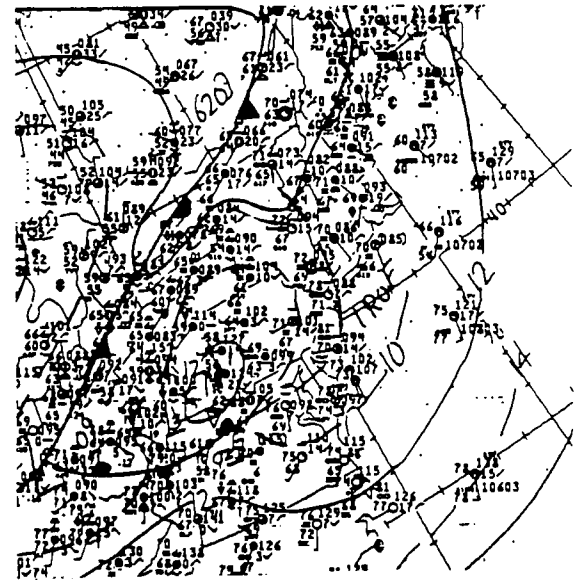

July 10

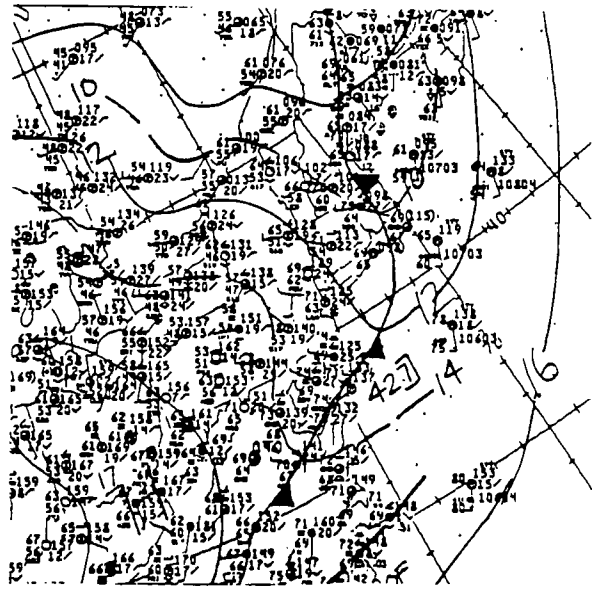

July 11

Figure 8. Surface weather maps for July 9-11, 1985.

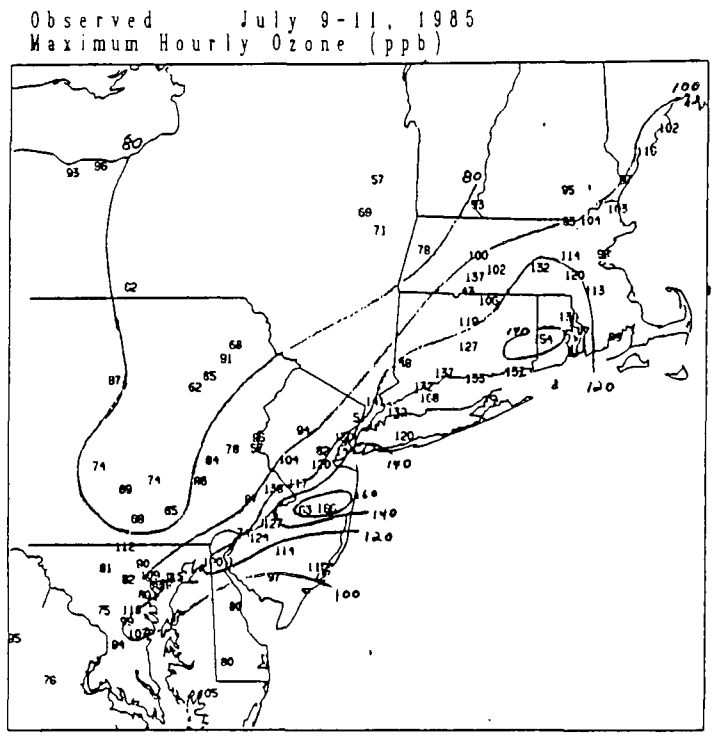

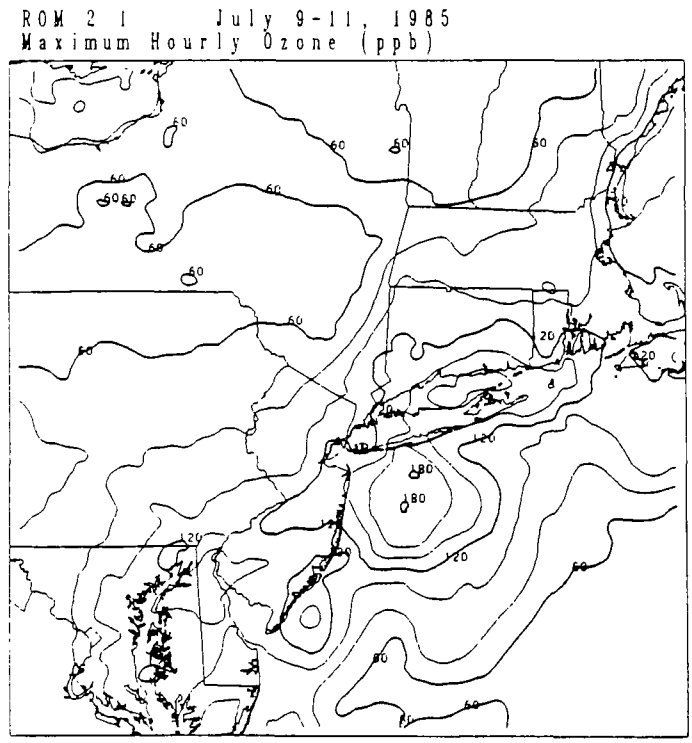

Figure 9. Spatial patterns of maximum ozone for July 9-11, 1985.

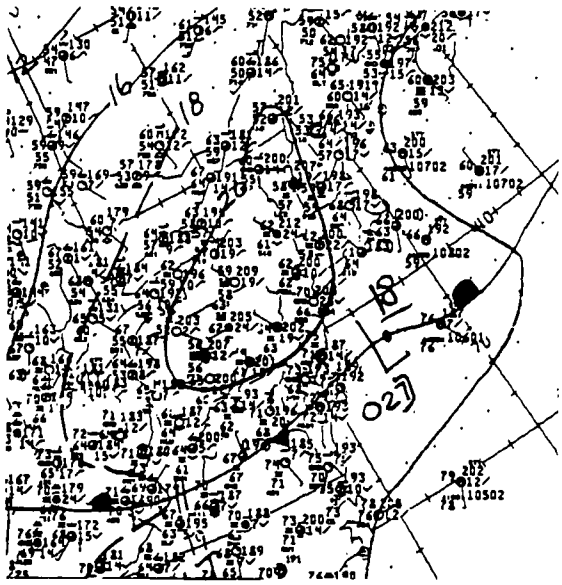

July 13

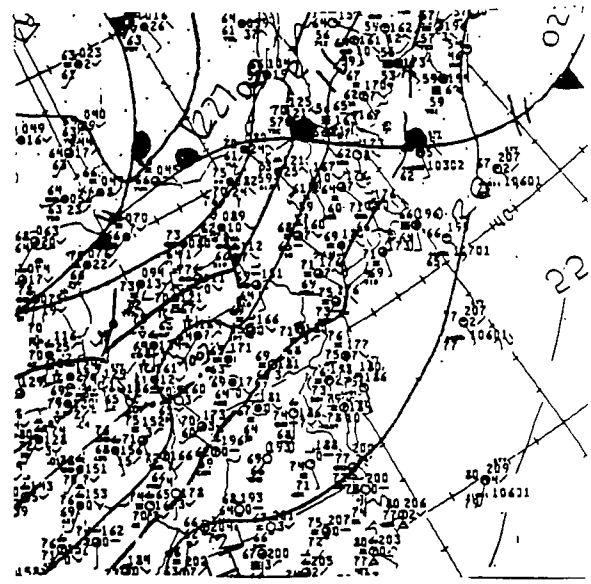

July 14

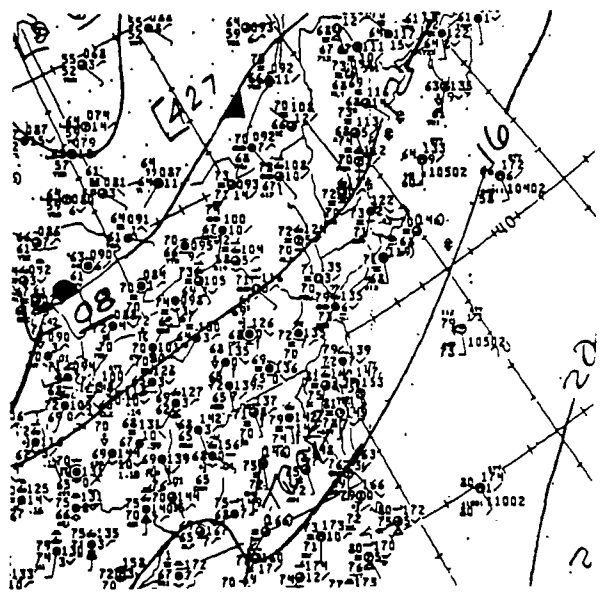

July 15

Figure 10. Surface weather maps for July 13-15, 1985.

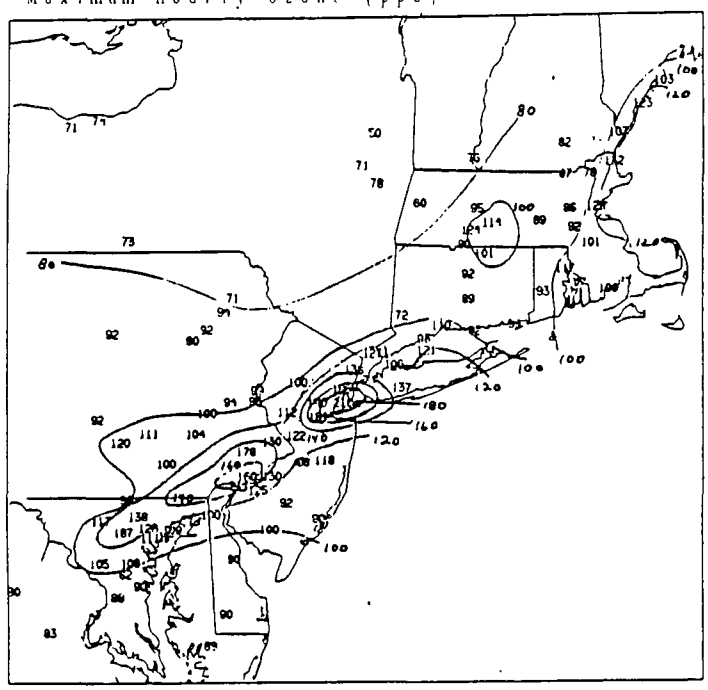

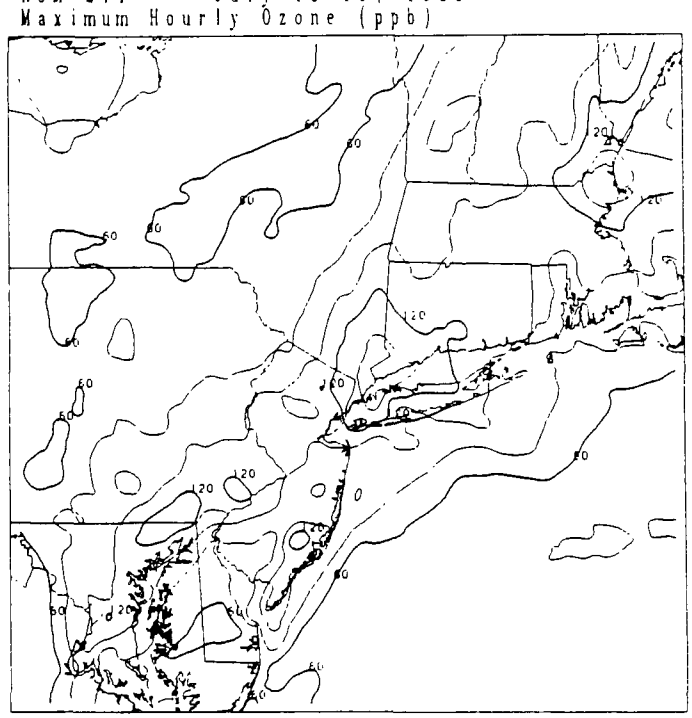

Figure 11. Spatial patterns of maximum ozone for July 13-15, 1985.

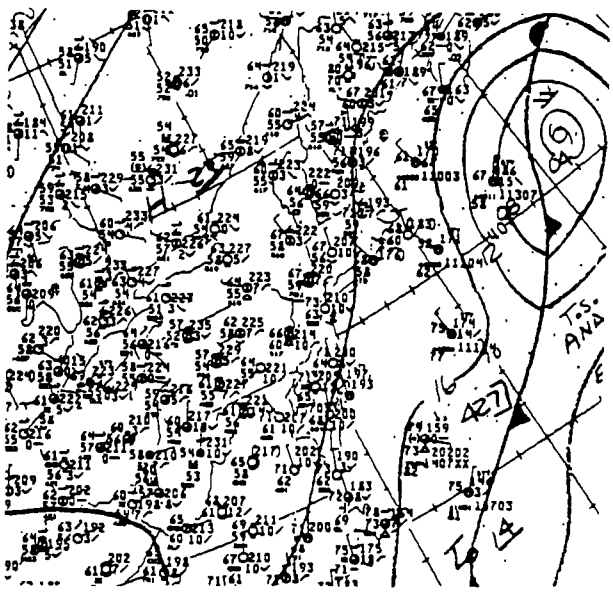

July 18

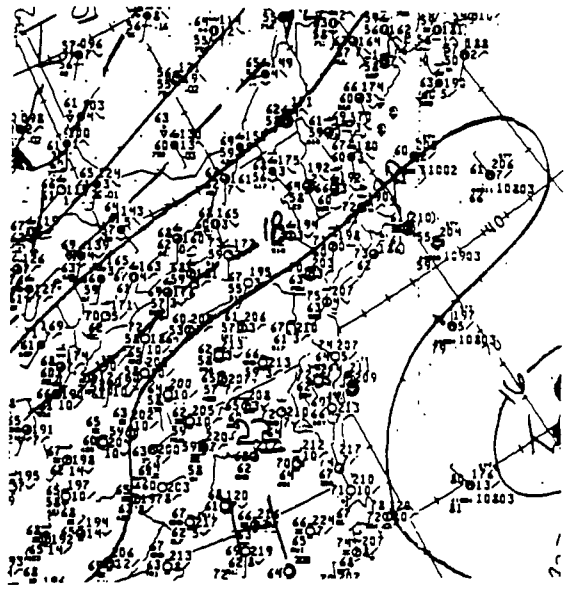

July 19

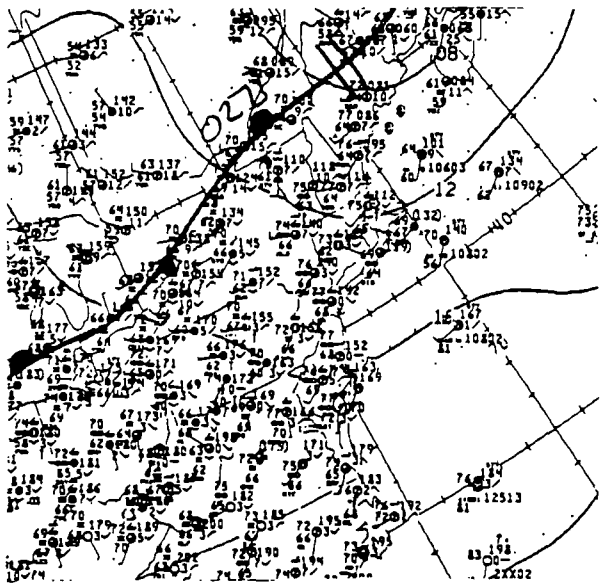

July 20

Figure 12. Surface weather maps for July 18-20, 1985.

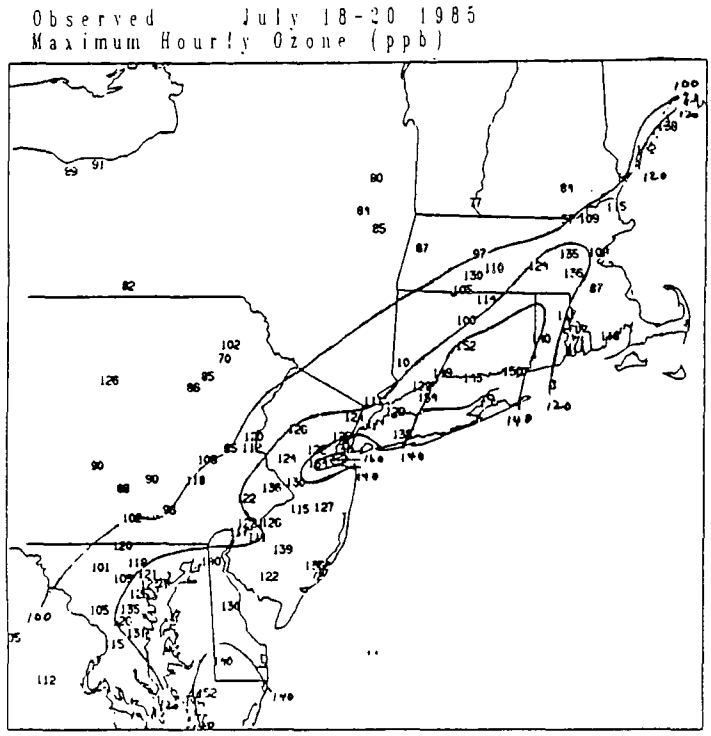

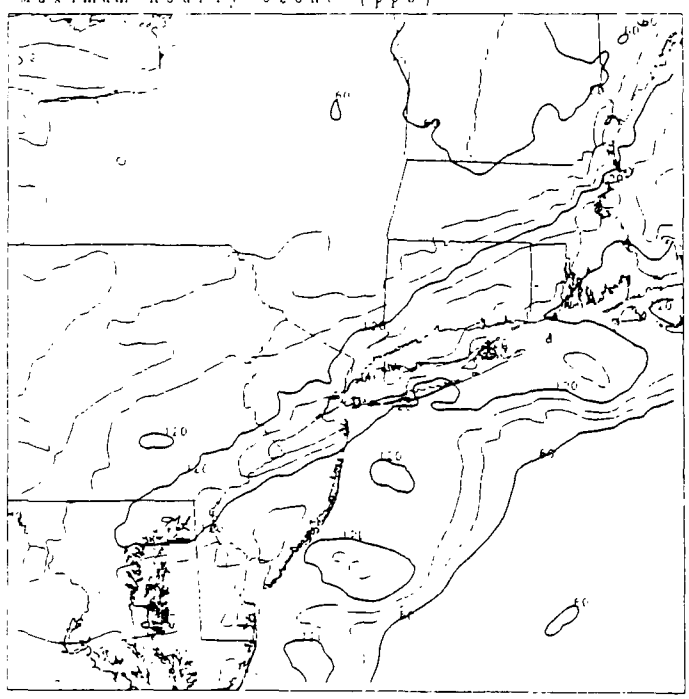

Figure 13. Spatial patterns of maximum ozone for July 18-20, 1985.

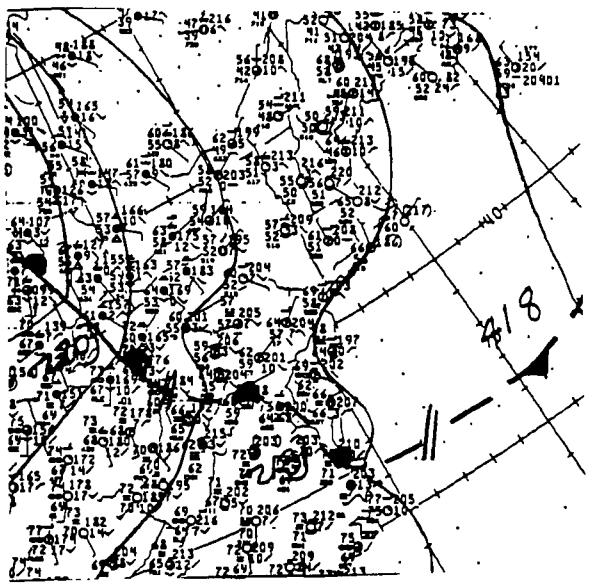

August 13

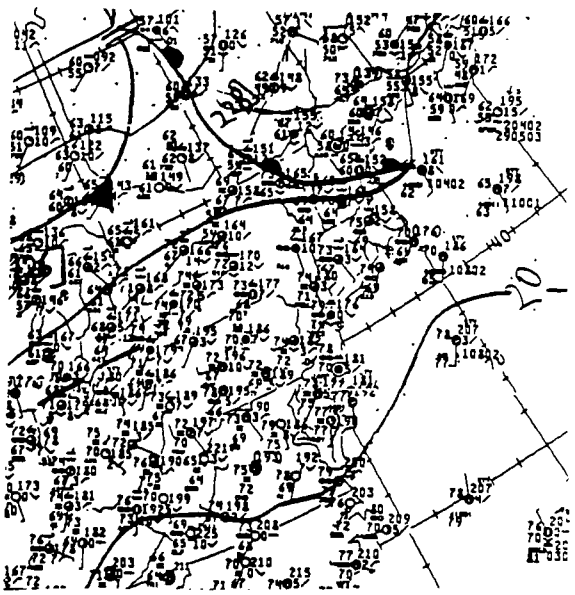

August 14

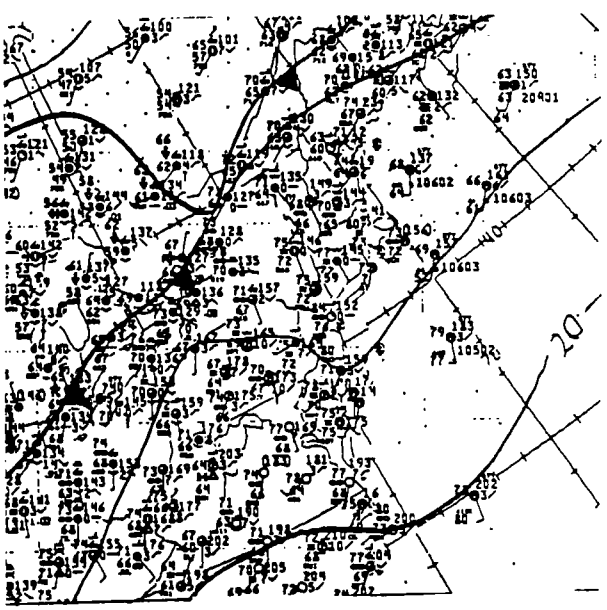

August 15

Figure 14. Surface weather maps for August 13-15, 1985.

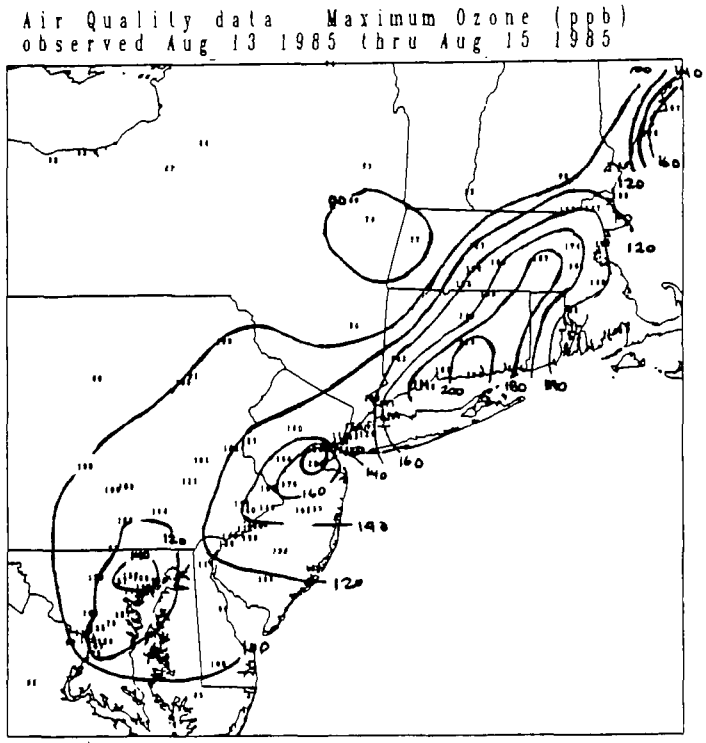

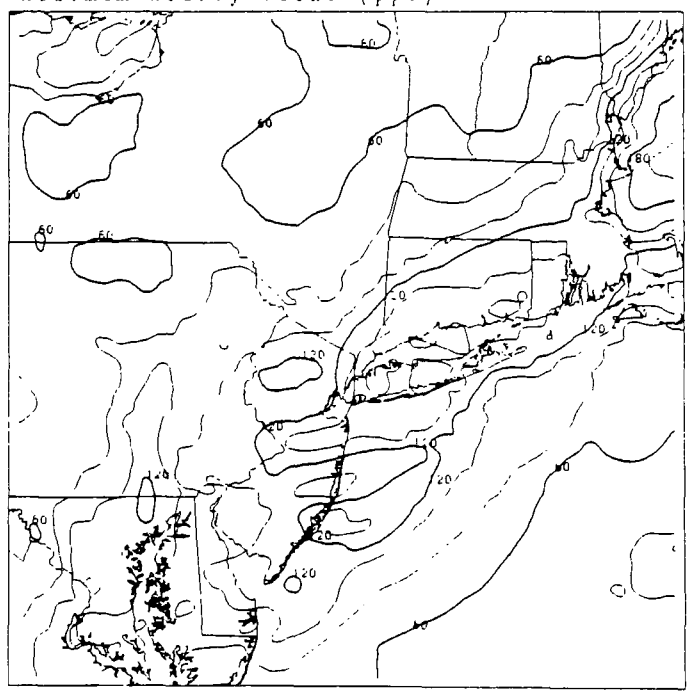

Figure 15. Spatial patterns of maximum ozone for August 13-15, 1985.

TABLE 5. SUMMARY STATISTICS FOR UAM BOUNDARY CONDITIONS (HOURLY DAYTIME OZONE, PPB, FOR THE JULY AND AUGUST 1985 EPISODES)

Statistic	Modeled	Observed	Percent Difference
n	20,155	20,155	
Mean	60.9	56.6	+7.6%
Std. deviation	17.7	25.2	-29.8%
95th Percentile	92.9	102.0	-8.9%
Maximum	146.7	179.3	-18.2%

TABLE 6. DAILY SUMMARIES OF UAM BOUNDARY CONDITIONS[1]

Date (1985)	Mean ozone (ppb) model	obs.	Percent difference	Direction (o)	Mean wind speed (ms^{-1})	Persistence[2]
July 8	46 4	35.1	+32.2%	250	5.2	0.89
July 9	59.3	70.1	-15.4%	171	3.8	0 72
July 10	66.8	57.1	+17.0%	233	4.6	0.80
July 11	63.5	45.5	+40.0%	320	4.7	0.91
July 12	61.0	56.5	+8.0%	165	4.6	0.80
July 13	72.6	70.0	+3.7%	187	3.1	0.52
July 14	64.5	58.9	+9.5%	215	5.9	0.89
July 15	67.0	44.9	+49.2%	200	5.2	0.94
July 16	61.7	51.1	+20.7%	169	3.0	0.73
July 17	57.8	46.1	+25.4%	35	4.4	0.83
July 18	56.2	48.9	+14.9%	70	3.7	0.22
July 19	74.2	79.6	-6.8%	222	5.9	0.94
July 20	70.8	74.1	-4.5%	265	4.4	0.85
July 21	53.8	60.2	10.6%	177	4.1	0.55
August 8	46.2	42.3	+9.2%	221	4.7	0.87
August 9	54.9	72.0	-23.8%	110	8.7	0.48
August 10	55.9	52.1	+7.3%	168	3.6	0.80
August 11	52.3	54.5	-4.0%	200	4.0	0.80
August 12	56.6	40.3	+40.4%	2	4.4	0 88
August 13	59.7	62.5	-4.5%	159	4.1	0.68
August 14	69.2	69.7	-0.7%	222	3.8	0.70
August 15	80.1	72.7	+10.2%	331	5.4	0.94

1. All land-based UAM boundry grid cells were used, for daytime hours only.

2. Persistence = (vector mean wind speed)/(scalar mean wind speed) Based upon all daytime hourly wind observations from National Weather Service stations near the OMNYMAP domain.

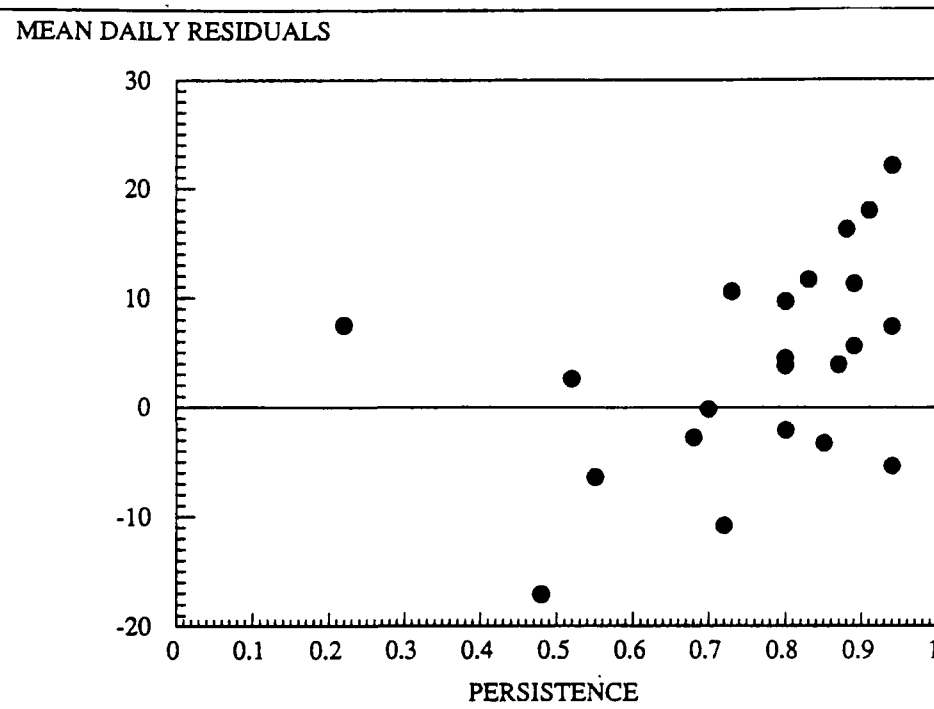

Figure 16. Mean residuals versus wind persistence for the UAM boundary.

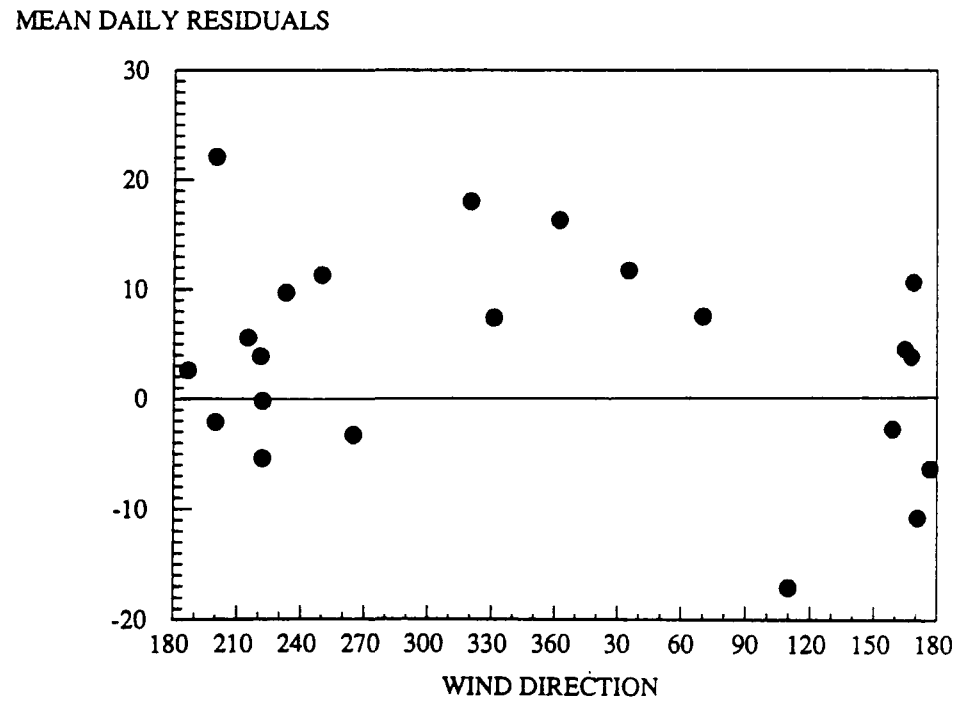

Figure 17. Mean residuals versus daily average wind direction for the UAM boundary.

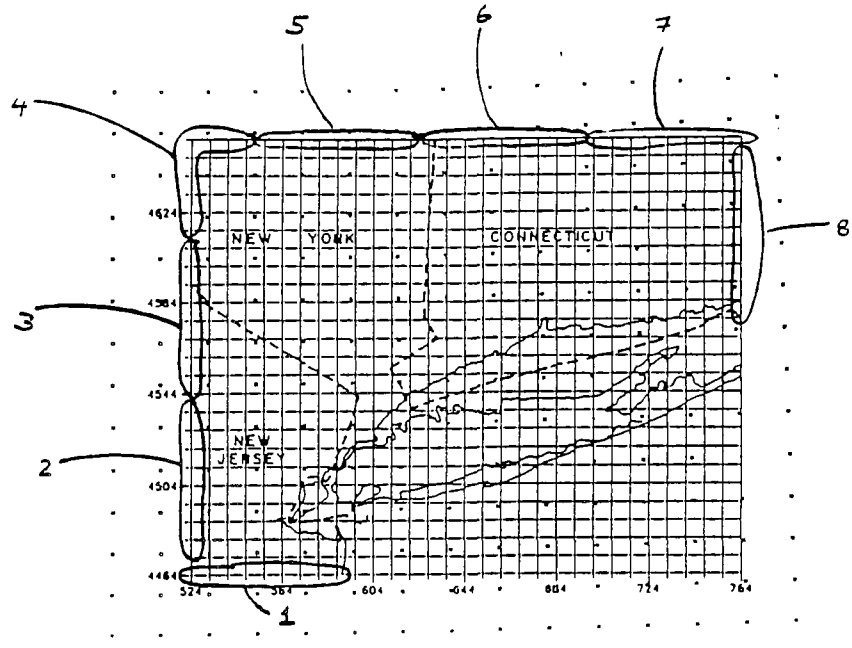

Figure 18. Division of the OMNYMAP boundary into eight groups.

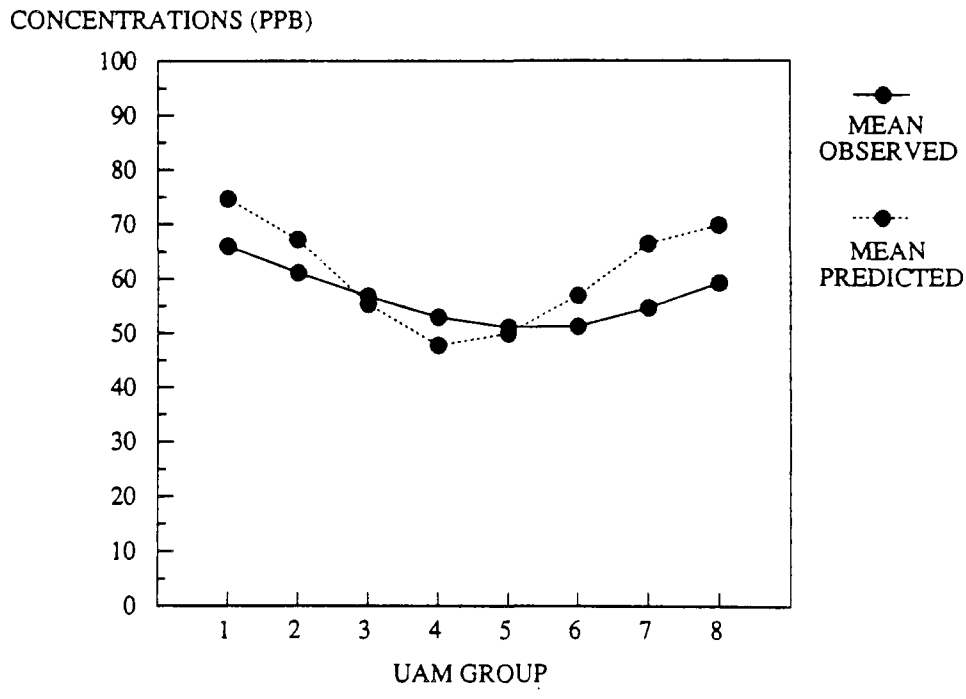

Figure 19. Mean daytime ozone concentrations by UAM group along the UAM boundary.

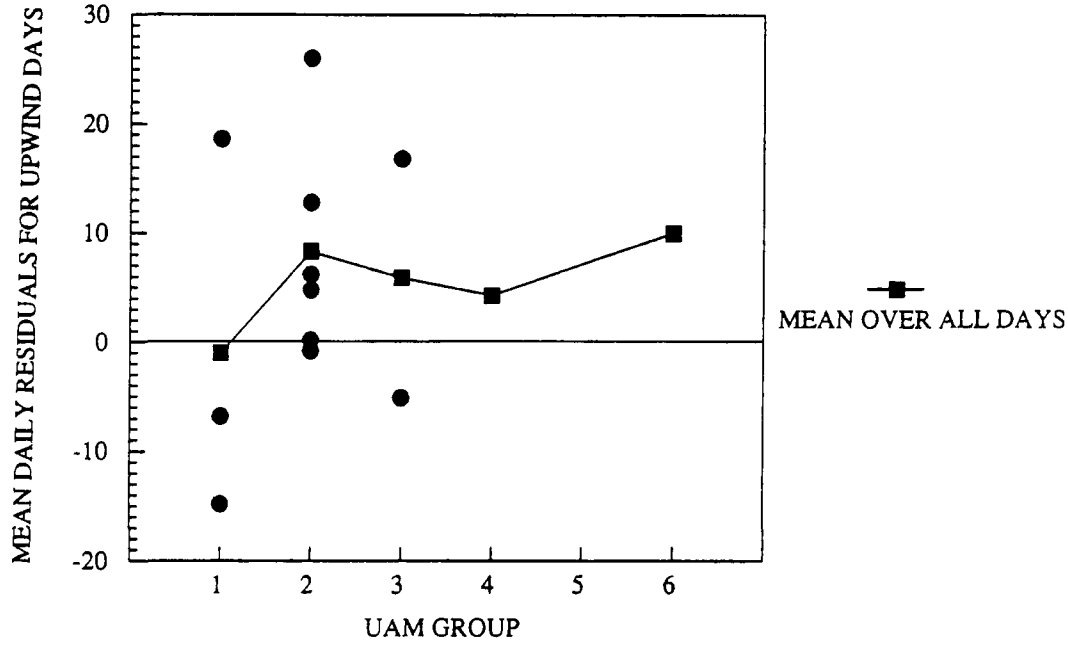

Figure 20. Mean residuals for each UAM group experiencing incoming flow.

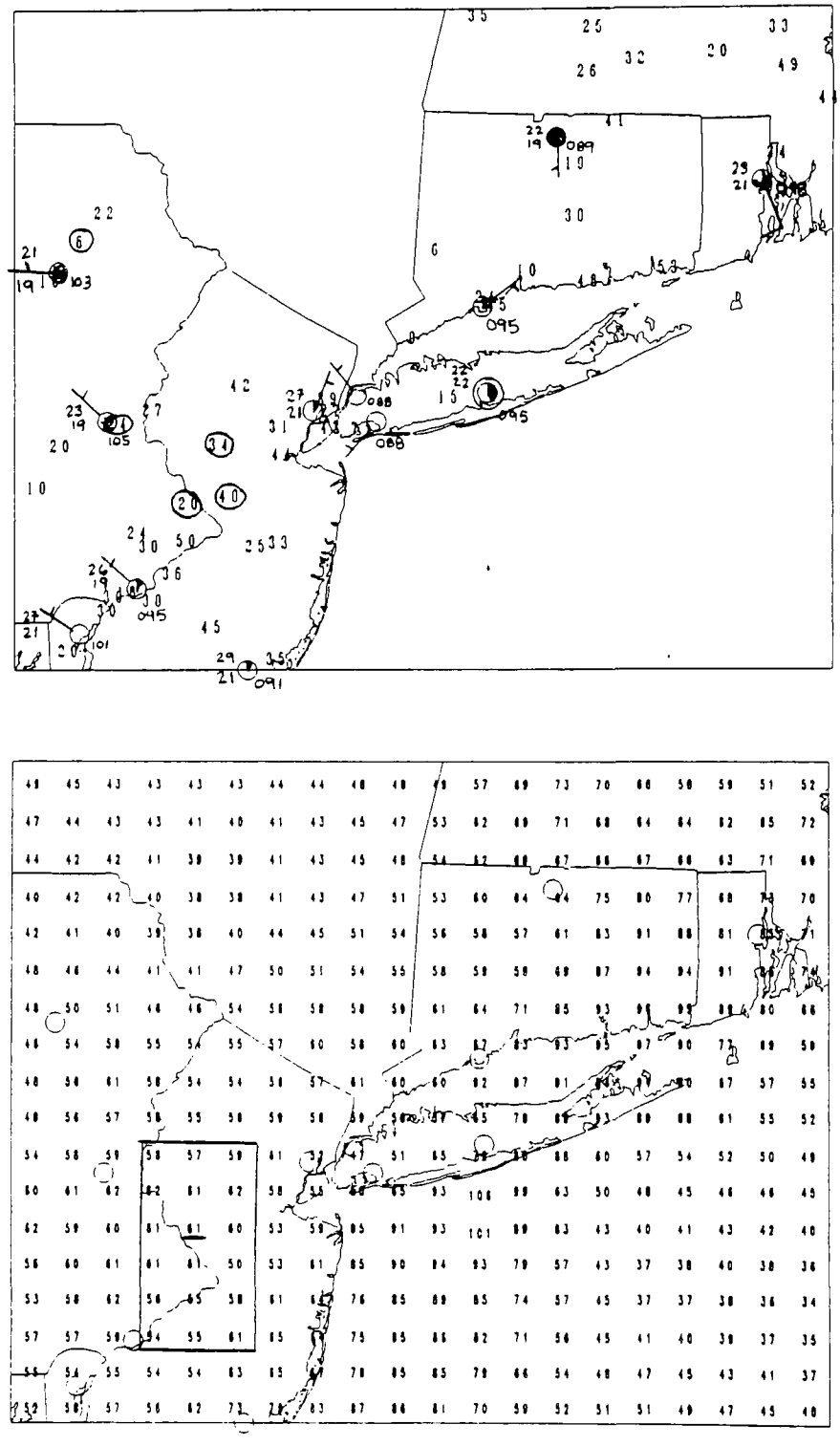

Figure 21. Ozone concentrations for July 10, 1985 (0800 EST). Observed data are in the top plot, and gridded model estimates are in the bottom plot.

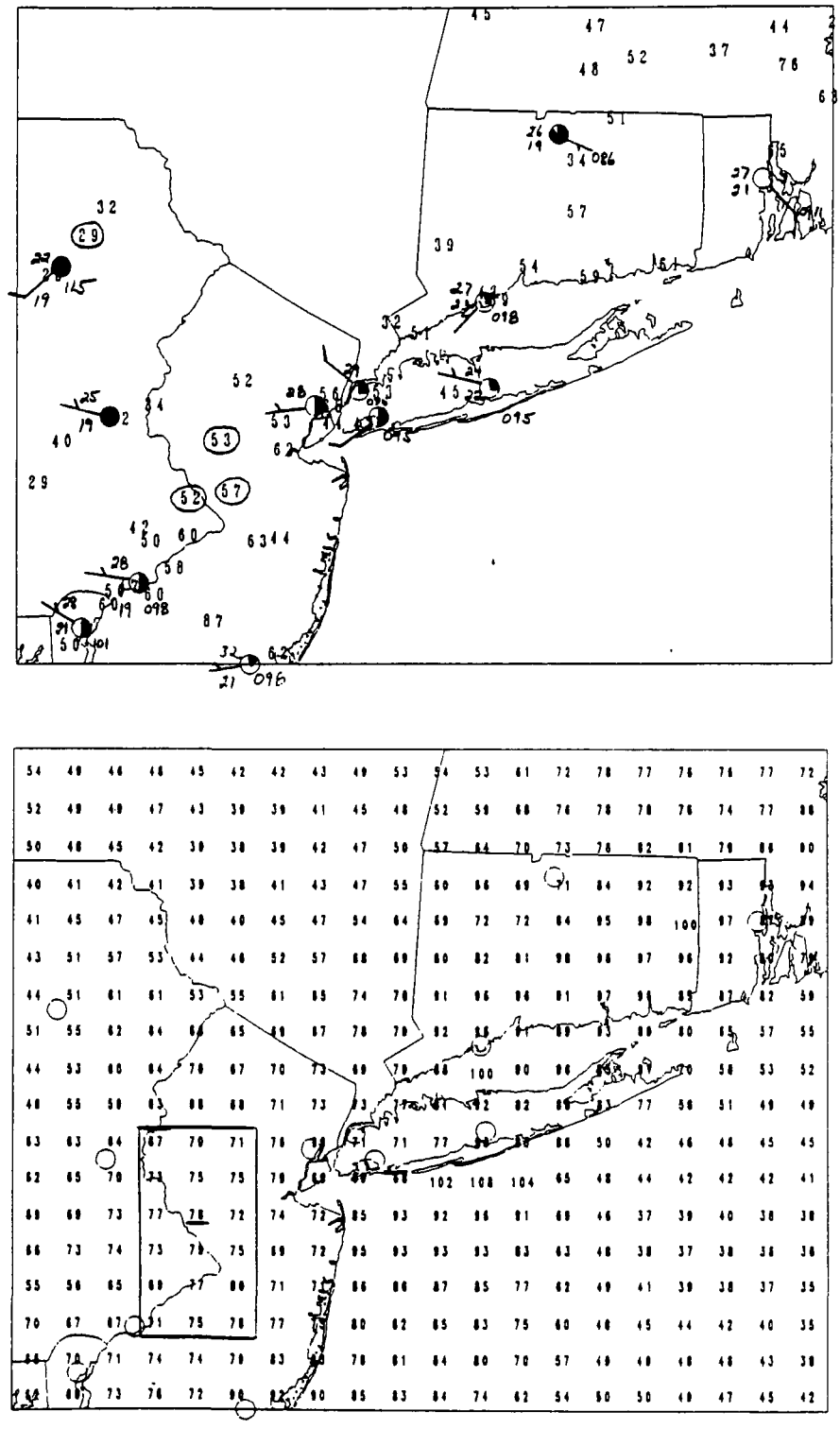

Figure 22. Ozone concentrations for July 10, 1985 (1000 EST). Observed data are in the top plot, and gridded model estimates are in the bottom plot.

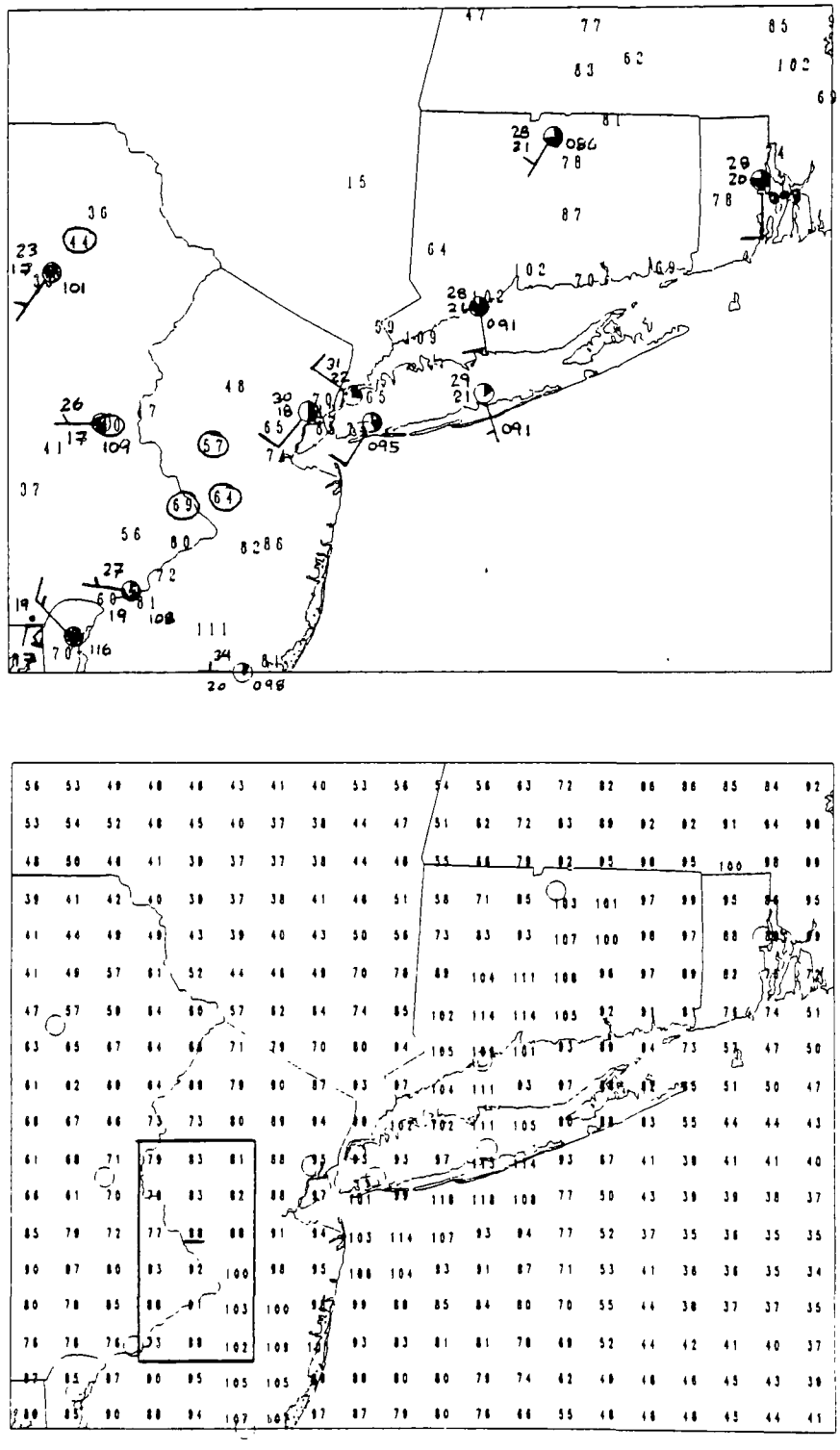

Figure 23. Ozone concentrations for July 10, 1985 (1200 EST). Observed data are in the top plot, and gridded model estimates are in the bottom plot.

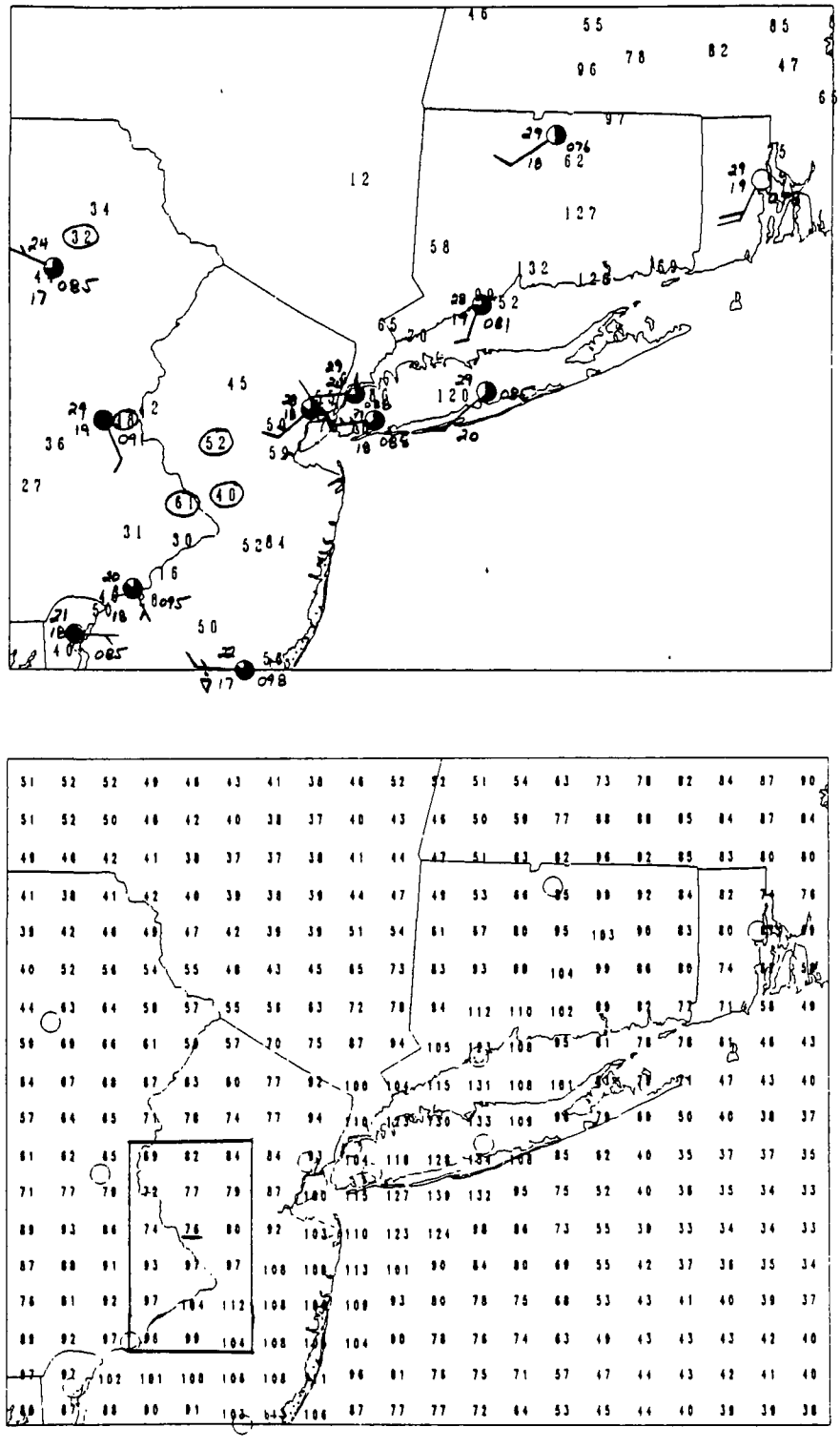

Figure 24. Ozone concentrations for July 10, 1985 (1400 EST). Observed data are in the top plot, and gridded model estimates are in the bottom plot.

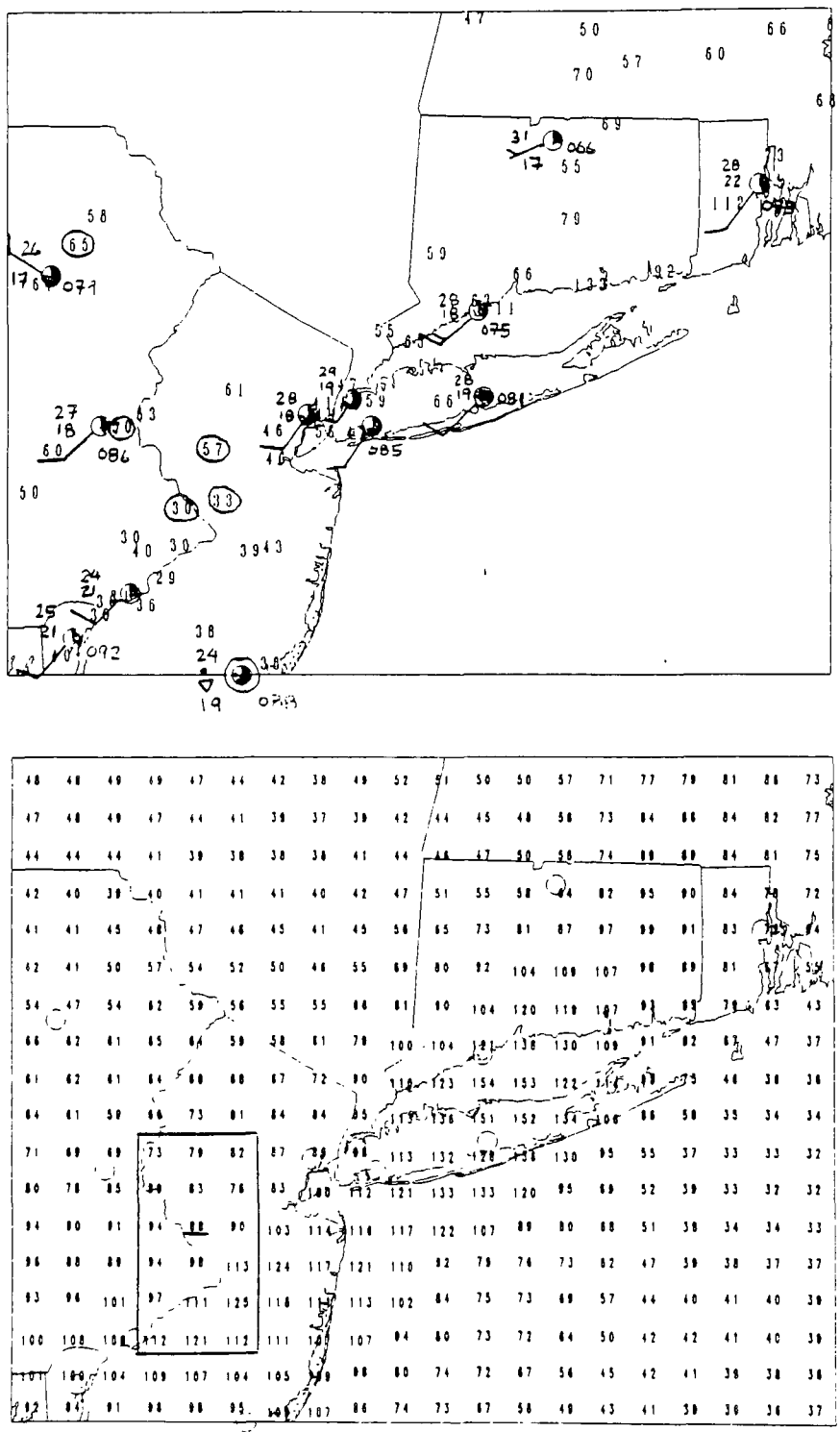

Figure 25. Ozone concentrations for July 10, 1985 (1600 EST). Observed data are in the top plot, and gridded model estimates are in the bottom plot.

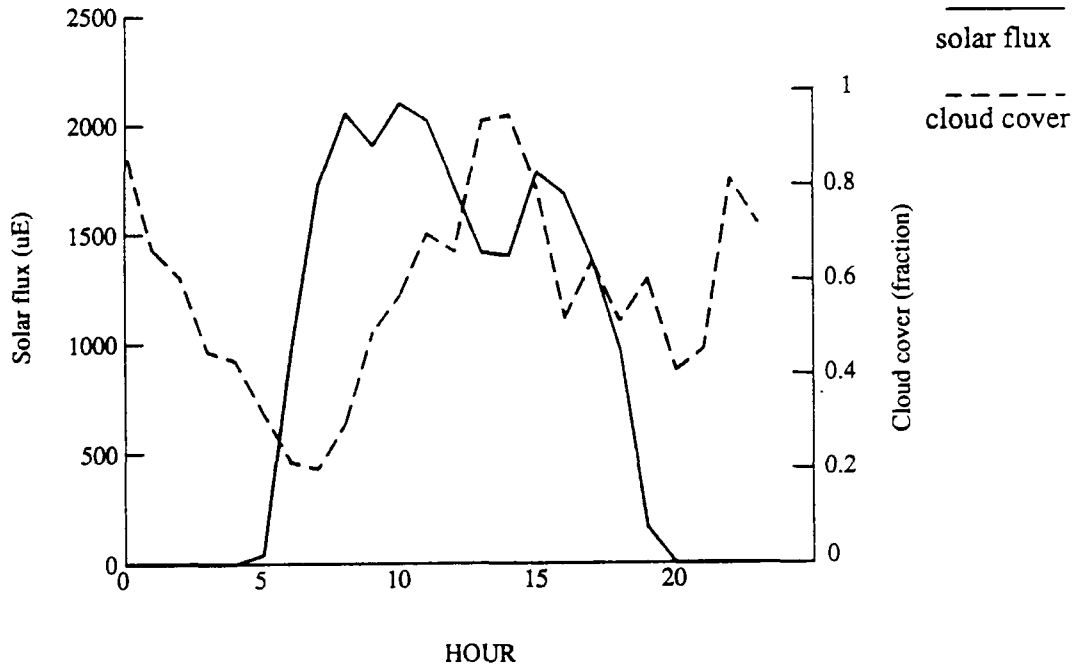

Figure 26. Hourly cloud cover and solar fluxes for grid cell (45,21).

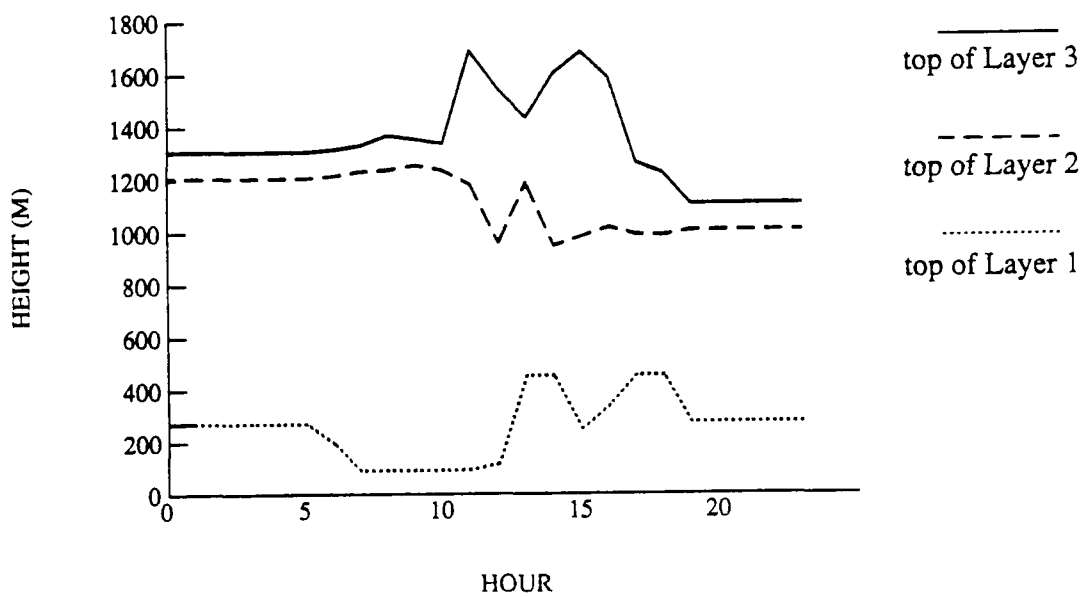

Figure 27. Hourly layer heights for grid cell (45,21).

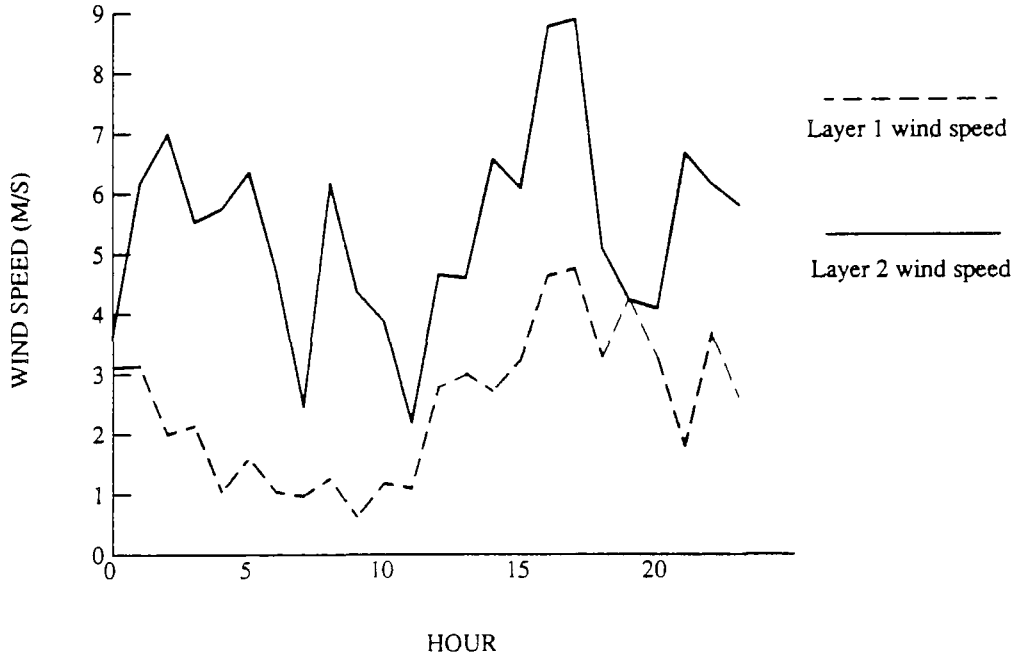

Figure 28. Hourly wind speeds for grid cell (45,21).

SECTION 5

DIAGNOSTIC TESTS

The earlier ROM diagnostic tests performed by Lamb and Laniak (1985) began with a chemistry-only simulation and added processes from that point. One of the problems with that hierarchy of tests is that the chemistry aspects of the ROM are, perhaps, the most complex and non-linear of all processes simulated. Testing those aspects first may well mask problems in numerical algorithms designed to test simpler processes, such as horizontal transport and vertical flux. The current series of diagnostic tests were designed with a reverse hierachical order from the original series of tests. That is, horizontal transport and vertical fluxes were tested first, and the chemistry was activated only in the last test. This hierarchy proceeds from the simpler to the more complex simulation processes.

The current series of tests were designated as Tests 1, 2, and 3, and were designed to test numerical procedures for transport and vertical flux, horizontal transport only, and transport and chemistry only, respectively. Test 1 was further subdivided into a number of subtests, all of which are described below. Later, an even simpler series of tests for horizontal transport (Tests 0) were added.

DESCRIPTION AND RESULTS OF TESTS

In order to perform diagnostic tests on ROM2.1 and its most critical processors under known atmospheric conditions, a specialized processor system, STG4, was developed to allow the specification of certain wind field and model layer patterns in an analytically defined atmosphere. By predetermining the wind field and model layer depth patterns in time and three-dimensional space, the capacity of the ROM and specific processors to obey various physical laws may be tested.

In the production version of the ROM processor network, sequential stages of the processors are executed toward the preparation of the complete ROM input file. Among the data types processed in the first four stages are included all of the meteorological parameters such as wind, temperature, density, cloud cover, etc. Also processed in these first four stages are the definitions for all three of the ROM layers. All of these physical variables and various others, as required by the ROM processors subsequent to stage four, are defined by STG4.

Particular wind flow and layer definition sets for each test case are defined in STG4. Routines there define the wind field and the vertical layer boundaries, each of which may be dependent on the various physical quantities that are analytically defined in STG4. Eight test cases have been defined and incorporated into STG4.

The analytically defined atmospheres in STG4 were developed from the ideal gas law and the atmospheric physical relationships defined by the hydrostatic and hypsometric equations. Horizontal diffusion due to turbulent eddies is set to zero for these tests. The temperature lapse rate is defined to be adiabatic, which is a good approximation for the actual atmospheric mixed layer where the ROM is designed to work. The only atmospheric definitions which do not approximate the real atmosphere are the neglect of the effect of water vapor on the specific gas constant for air and the assumption of no horizontal diffusion due to turbulent motion. The neglect of water vapor effects was necessary to achieve a tractable solution of the atmospheric definition equations.

Test Case 1A

This case is designed to test the horizontal transport and interlayer mass flux mechanisms in the model. For this test case, a circular anticyclonic wind field, shown in Figure 29, is specified identically for all three model layers. This wind field exhibits perfect solid body rotation on a

spherical earth. Therefore, the divergence in the horizontal plane is zero for all locations in the definition region. This aspect of the wind field guarantees that any vertical mass exchange will be the result of changes in the depth of the vertical layers, and not as the result of convergence or divergence of the horizontal winds.

A temporally oscillating pattern of ROM layer depths was used to provide the mechanism for vertical mass flux between ROM layers. The three layer tops are kept horizontally flat at all times, with the heights of the top of layer one and two oscillating up and down in time. The layer tops are defined by:

$$Z_1(I,J) = 500 + (300)[\ \sin[\ (2\pi / 60{,}000)\ t\ ]\ ]\ \ m$$
$$Z_2(I,J) = 1000 + (300)[\ \sin[\ (2\pi / 60{,}000)\ t\ ]\ ]\ \ m$$
$$Z_3(I,J) = 1500\ m$$

where t is the elapsed time, in seconds, from the beginning of the simulation. This layer top definition represents an up and down oscillation of layer two itself, with its thickness remaining constant in time (500 m). The depth of the full model domain is fixed over all space and time (1500 m).

For test case 1A, all chemical reactions are turned off in ROM2.1. Only one chemical species, used as a mass tracer, is given a spatially-dependent initial concentration that differs from the prescribed background concentration. This species is given the following initial concentration distribution:

$$C(I,J) = [\ C(I_0,J_0) - B\ ][1 - (R / 2.5)] + B \qquad R < 2.5$$
$$C(I,J) = B \qquad R > 2.5$$

where I and J are the grid column and row indices, respectively, $C(I_0,J_0)$ = 1 ppm is the initial species concentration at grid cell (I_0,J_0), B = 0.001 ppm is the background concentration, and R is the distance, in grid cell lengths, from the center of cell (I_0,J_0) to the center of cell (I,J). The background concentration, B, is also used as the concentration value at inflow boundary

cells.

The initial concentration distribution is applied to all three model layers, with I_0 and J_0, for each layer, given by:

$$\begin{aligned} &\text{Layer 1:} \quad I_0 = 18, \quad J_0 = 14 \\ &\text{Layer 2:} \quad I_0 = 30, \quad J_0 = 35 \\ &\text{Layer 3:} \quad I_0 = 42, \quad J_0 = 14 \ . \end{aligned}$$

The initial concentration distribution for Layer 1 is depicted in Figure 30 for test case 1A. It should be noted that the initial concentration magnitudes are completely arbitrary, because the chemical reactions are turned off for this test case. The gradients in the concentration field and the total mass are the significant factors in these tests. The concentrations can change only in response to the atmospheric dynamics or to any numerical errors associated with the ROM transport scheme. Concentration "clouds" identical to the one depicted in Figure 30 are also initialized in ROM layers 2 and 3, except that they are centered at different locations in the horizontal grid.

As an initial test of the adequacy of the numerical algorithms we will examine the mass conservation within the model domain through the simulation period for each of the tests. Ideally, total mass within the domain will remain the same throughout the time period, despite the advective and vertical flux processes occurring in Test 1A. The rate of angular rotation chosen for the wind field in this test causes the mass field to make one complete revolution in 100 time steps. Figure 31 presents a time history of the total mass in the model domain through slightly more than one complete revolution. The mass is represented as normalized mass; that is, the ratio of the mass in the domain at some time t_i compared to the initial mass field at t_0, $M(t_i)/M(t_0)$.

There is an oscillation evident in the mass field over time. The periodicity corresponds to that of the oscillation in the ROM layer depths for this test. Mass increases as much as 6% in the model domain during the first

third of the simulation. Later, a mass decrease of around 2% is evident. The overall trend in the mass field is toward a decrease over time. The degree of mass change is not particularly strong here, although the test does suggest that mass conservation errors may occur when the model layer interfaces change significantly over time.

Test Case 1B

Test case 1B is very similar to 1A, except that the layer heights vary over space instead of over time. This case is also designed to test the transport and numerical algorithms of the model. The wind field and the initial concentration fields for the three ROM layers are the same for test 1B as they were for 1A.

The heights of the layer one and layer two tops are specified as functions of the radial direction from the grid cell containing the wind field rotation axis (30,21) to the grid cell centers. Starting with the radial line to the north of the center of rotation, and moving clockwise, the top of layer one decreases in height by an amount proportional to the sine of the compass direction of the radial line. Thus, along a radial line pointing east from the wind field rotation axis, the height of the top of layer one reaches a minimum value. As the radial line sweeps around to the south, the height returns to the original value. For grid cell locations with column indices less than 30, the heights of the top of layer one are symmetrical with the layer one heights at grid cell locations with column indices greater than 30. A three-dimensional view of the cell heights in layer 1 is given in Figure 32.

The height of the top of layer two is defined in the opposite sense of layer one, and is symmetrical with layer 1 at all locations. Layer 2 heights are shown in Figure 33. The top of layer 3 is defined to be horizontally flat. All layer heights are held constant in time for test 1B. Analytic expressions for the layer 2 top heights are given by:

$$Z_1(I,J) = 500 - (300)[\ \sin\ [\ \pi/2 - \tan^{-1}(x/y\ )\ ]\ \mathrm{m}$$

$$Z_2(I,J) = 1000 + (300)[\ \sin[\ \pi/2 - \tan^{-1}(\ x/y\ )\ ]\ \text{m}$$
$$Z_3(I,J) = 1500\ \text{m}$$

where x is the distance from the grid cell longitude to the axis of rotation longitude, and y is the distance from the grid cell latitude to the axis of rotation latitude.

The normalized mass ratio for the entire model domain during the simulation of test 1B is shown in Figure 34. The mass total remains within close proximity of the original mass amount during the simulation. Maximum changes of about 4% from the original mass can be seen.

Test Case 1C

This test case is designed to examine the accuracy of the numerical transport scheme alone, without vertical fluxes occurring. The wind field and initial mass fields for each ROM layer used here are identical to those used for test case 1A. The layer top heights are horizontally flat and are constant in time for test 1C. This allows for an examination of the ability of the ROM to conserve mass during periods of rotational (non-divergent) flow with no vertical transport across the layer interfaces. The layer top heights are defined as follows:

$$Z_1 = 500\ \text{m}$$
$$Z_2 = 1000\ \text{m}$$
$$Z_3 = 1500\ \text{m}.$$

The layer top heights act as material surfaces, resulting in no transport of air across the layer boundaries.

The normalized mass ratio for test 1C is shown in Figure 35. We see here that the total mass within the domain grows by nearly 7% in the first third of the simulation, and then stabilizes later at a mass increase of approximately 8% over the initial mass. Considering that there are no

physical or chemical sources or sinks of mass in the model simulation, this is a significant mass increase.

Test Case 2

This case is a somewhat more complex test of the numerical transport algorithms in the ROM. For this test case, a purely divergent (convergent) flow field is used. The layer average wind fields for each of the model layers are identical, resulting in no vertical wind shear. A west-to-east zonal wind field is defined for each layer such that speed maxima exist along the western and eastern boundaries of the modeled region, and speed minima exist along the central longitude of the modeled region. The speed of this flow is defined for any grid cell location by the following equation:

$$U = U_w[0.75 + 0.25(\cos(2\pi x/D))]$$

where U_w is the latitude-dependent wind speed at the western edge of a particular grid cell row, x is the distance of a given grid cell center to the grid cell center along the western edge of the modeled region along a connecting latitude line, and D is the distance from the grid cell center on the western edge to the grid cell center on the eastern edge of the modeled region along a connecting latitude line. This definition results in speeds at the central longitude of exactly one-half the speeds at the western and eastern edges of every grid cell row. There exists, therefore, convergent flow in the western half of the model domain, and divergent flow in the eastern half. This windfield is depicted in Figure 36.

It was desired for test case 2 that the layer boundaries represent material surfaces, or surfaces across which there is no flux of material. Thus, the layer heights must be determined such that, given the layer average wind fields and the physical variables analytically defined in STG4, there is no transport of air across the layer boundaries. This stipulation requires that the layer heights be determined based on the defined wind field. The resulting field of spatially varying layer heights for model layers 1, 2, and

3 are shown in Figures 37, 38, and 39, respectively. Here, although there are spatial variations in the layer heights, there is no flux of material between layers.

The initial concentration field for test case 2, ROM layer 1, is shown in Figure 40. It is similar to that shown in Figure 30 for test case 1, with two exceptions. First, the cloud is centered at the east side of the grid to allow for westerly zonal wind flow. Second, the peak concentration along each row has been stretched from a width of 1 grid cell to 3 grid cells, resulting in quasi-elliptical concentration cross sections instead of circular ones. Identical mass clouds exist in layers 2 and 3, with their centers displaced southward from the layer 1 cloud by 10 grid cells for layer 2 and 20 cells for layer 3. Background concentrations outside the cloud mass are identical to those for test case 1A.

The mass conservation results for test case 2 are shown in Figure 41. As before, this plot presents a time history of the normalized mass $[M(t)/M(t_0)]$ in the entire model domain during the simulation. While the concentration cloud remains within the domain the normalized mass should always be equal to 1.0. The cloud mass traverses the model domain from west to east in 90 time steps. We see that during the first half of this simulation the total mass increases by nearly 18% within the grid. This corresponds to the region of convergent winds and increasingly deep layer heights. As the cloud mass enters the region of divergent winds and increasingly shallow layer heights the mass increases tend to level off and eventually the mass begins to decrease. This decrease, however, occurs at a much slower rate than the earlier mass increase, thus resulting in a net mass increase of approximately 13% at the end of the simulation.

Results of this test show some disturbing features. Mass conservation should be preserved in any numerical transport scheme. Results of test case 2 clearly show that mass is not being conserved here. Since the test formulation was such that the model layer interfaces act as material surfaces, there should be no vertical flux of mass. To attempt to isolate the mass

increase phenomenon further, a simpler test (Test 0) was proposed which would examine the numerical transport in a less divergent wind field.

Test Case 0

Test cases 1C and 2, described above, showed that the numerical transport scheme produced significant mass increases for simulations of 90-100 time steps for purely rotational and divergent flow fields, respectively. Since this was an unexpected and somewhat disturbing finding, we decided to proceed to a test 0 series, instead of the planned test 3 (transport, vertical flux, and chemistry). In the test 0 series we attempt to simplify the transport environment to isolate the cause of the mass increase.

The ROM layer heights for test case 0 were spatially and temporally constant over the model domain and were set at the values used in test case 1C. The wind field prescribed was "essentially" constant in space and time. The winds were zonal from west to east with a velocity corresponding to:

$$U = (5/6)\ D/t_c$$

where D is the distance from the western edge of the modeled region to the eastern edge of the modeled region along the particular latitude, and t_c is the time required for a parcel of air to travel the distance D (180,000 s). The north-south extent of the model domain varies from 38^0N to 45^0N, and the rms value of the wind speed over the domain is 5.6 m/sec, with very small variations in wind speed from row to row. The wind field used in test 0 is shown in Figure 42.

The initial concentration field for test 0 is the same as that specified for test case 1A, except that the locations of the cloud centers are as follows:

Layer 1: $I_0 = 5$, $J_0 = 30$
Layer 2: $I_0 = 5$, $J_0 = 20$

Layer 3: $I_0 = 5$, $J_0 = 10$.

The initial concentration field for ROM layer 1 is shown in Figure 43. Background and inflow boundary concentrations were again set to .001 ppb. The concentration cloud traverses the model domain in just over 100 time steps.

The mass conservation time history for the model domain in test case 0 is shown in Figure 44. This plot shows an initial mass increase of about 0.33% per time step, while at the end of the simulation, the increase was about 0.065% per time step. A total mass increase of about 10% was noted toward the end of this simulation. This result is significant because the test has isolated the numerical errors to the horizontal transport scheme, without the complicating effects of vertical redistribution of mass.

Test Case 0A

To determine the degree to which the noted mass increases from the numerical advection algorithms were a function of the magnitude of initial concentration gradients, a second test was performed in which the concentration gradient was diminished. The concentration distribution in each layer is given by:

$$C(I,J) = [\ C(I_0,J_0) - B\ ][\ 1 - (R / 9.5)\ ] + B \qquad R < 9.5$$
$$C(I,J) = B \qquad R > 9.5$$

Concentrations above the background value cover a much larger area within each layer than the concentrations in test case 0. In order to assure that no mass from the initial distribution within each layer is lost through the boundaries of the modeled region during the simulation period, an adjustment is made in positioning the initial cloud concentrations. The peak concentration locations are placed farther away from the region boundaries than in test case 0. The locations are given by:

Layer 1: $I_0 = 12$, $J_0 = 22$

Layer 2: $I_0 = 12$, $J_0 = 20$

Layer 3: $I_0 = 12$, $J_0 = 18$.

Figure 45 shows the initial concentration field in ROM layer 1 for test case 0A. The wind fields and layer heights for this test case are identical to those used in test case 0.

The time history of the normalized mass within the model domain for this simulation is shown in Figure 46. There are not as many time steps considered during the simulation as there were in test 0 because the larger size of the concentration cloud causes the mass to begin leaving through the outflow edge sooner in this test. Nevertheless, it is clearly evident from the figure that the mass is essentially conserved during the simulation, with a mass increase of only 0.6% at the end of the simulation. The contrast between the results of this test and test 0 demonstrate that the numerical artifact of the mass increase is a function of the magnitude in concentration gradient. This result is not surprising given the nature of finite difference approximations.

Test Case 0B

In the final test case presented here we investigate the effect of "clipping" negative concentration predictions from the model run. Many numerical transport schemes, including the one used in the ROM, produce small negative ripples of concentration near the edges of large concentration gradients when these gradients are advected (McRae et al., 1982). The negative concentrations are a result of the limitations of finite difference approximations to large sub-grid gradients. The negative values, in themselves, do not pose a problem for the advection routines. However, when the advection solution is passed to the chemistry portion of an air quality model there must be no negative concentrations since these are not defined in a chemical simulation. Typically, as here, the negative values produced by the numerical transport solution are "clipped", or set to either zero or a very small positive number. In our case they were set to 10^{-16}. Since we are not solving the chemical equations thus far in these analytical tests it is

possible to retain any negative concentrations resulting from the transport simulation. In test case 0B we have suppressed the negative clipping, and allow the propagation of any negative concentrations.

The layer depths are the same as those used in test case 0, constant in space and time. The wind field is also the same as in test case 0, simple zonal flow. The initial concentration field is the same as that used in test case 2, with sharp concentration gradients surrounding a flatter core. The mass conservation results for this test are shown in Figure 47. The normalized mass ratio indicates an initial increase of mass of about 0.5%, dropping back to about 0.4% for the remainder of the simulation. This value should be compared to the nearly 10% (and rising) normalized mass ratio at the end of the test 0 simulation. It is apparent that the clipping of negative concentrations has introduced a significant mass increase during the advection of sharp concentration gradients.

Now that the cause of the mass increase has been isolated, the next area of concern is the degree to which the mass imbalance affects actual ambient simulations with the ROM model. From the testing performed above it has been found that the degree of mass increase is a function of the concentration gradients within an advected field. The tests have generally employed very sharp gradients to stress the numerical algorithms. These gradients are larger than those found in the real atmosphere for regional trace gases The question we must answer is whether the mass increases effected by the concentration gradients and the attendant chemical responses in ambient simulations are serious enough to warrent consideration of a mass correction algorithm to the numerical transport scheme.

We have made a first attempt to answer this question. A two-day ambient ROM simulation has been performed for July 6-7, 1988, a particularly severe O_3 episode in the Northeast U.S. The model domain used is the ROMNET domain described in earlier sections. In addition to the base run, containing any mass imbalances caused by the "clipping" of negatives, a simulation was performed in which a first-order correction was made to the advected

concentration field to assure mass conservation. The algorithm used for the correction was based on a global assessment of "negative mass" clipped out of the domain during an advection step for a single chemical species and ROM level. This negative mass was then added back to the clipped field to selected areas in proportion to the absolute value of local concentration gradients. This latter simulation is referred to as the "corrected base run"

Grid differences, A-B, were constructed for each time step over each of the two 24-hr periods of simulation of the base case simulation result (A) minus the corrected result (B) for key chemical species. Normalized percent differences, (A-B) x 100/A, were also calculated. Results are presented here for ROM layer 1, where the largest grid differences were seen. For each day there were 64 x 52 (grid cells) x 48 (time steps), or 159,744 grid differences. Figure 48 presents frequency distributions of these differences for O_3 for each of the two days. Figure 48(a) shows the distribution of residuals (ppb) and Figure 48(b) shows the distribution of normalized residuals (% change from base). The figure shows that between the 5 and 95 percentile levels the absolute grid differences were less than 1.3 ppb and less than 1.7%. Figures 49 and 50 present similar plots for NO_x ($NO+NO_2$) and ROG (carbon-weighted sum of reactive organics), respectively. These figures show that the differences for ROG are also quite small, generally less than 1% through most of the distribution. The results for NO_x show the largest grid differences, with the corrected version producing 8-9% less NO_x than the base run at the 95 percentile level, with 100% differences at the 100 percentile level. (Note that the large negative percent differences at the 0 percentile level are associated with very small concentrations.) The largest NO_x discrepancies are associated with large NO_x point source emissions.

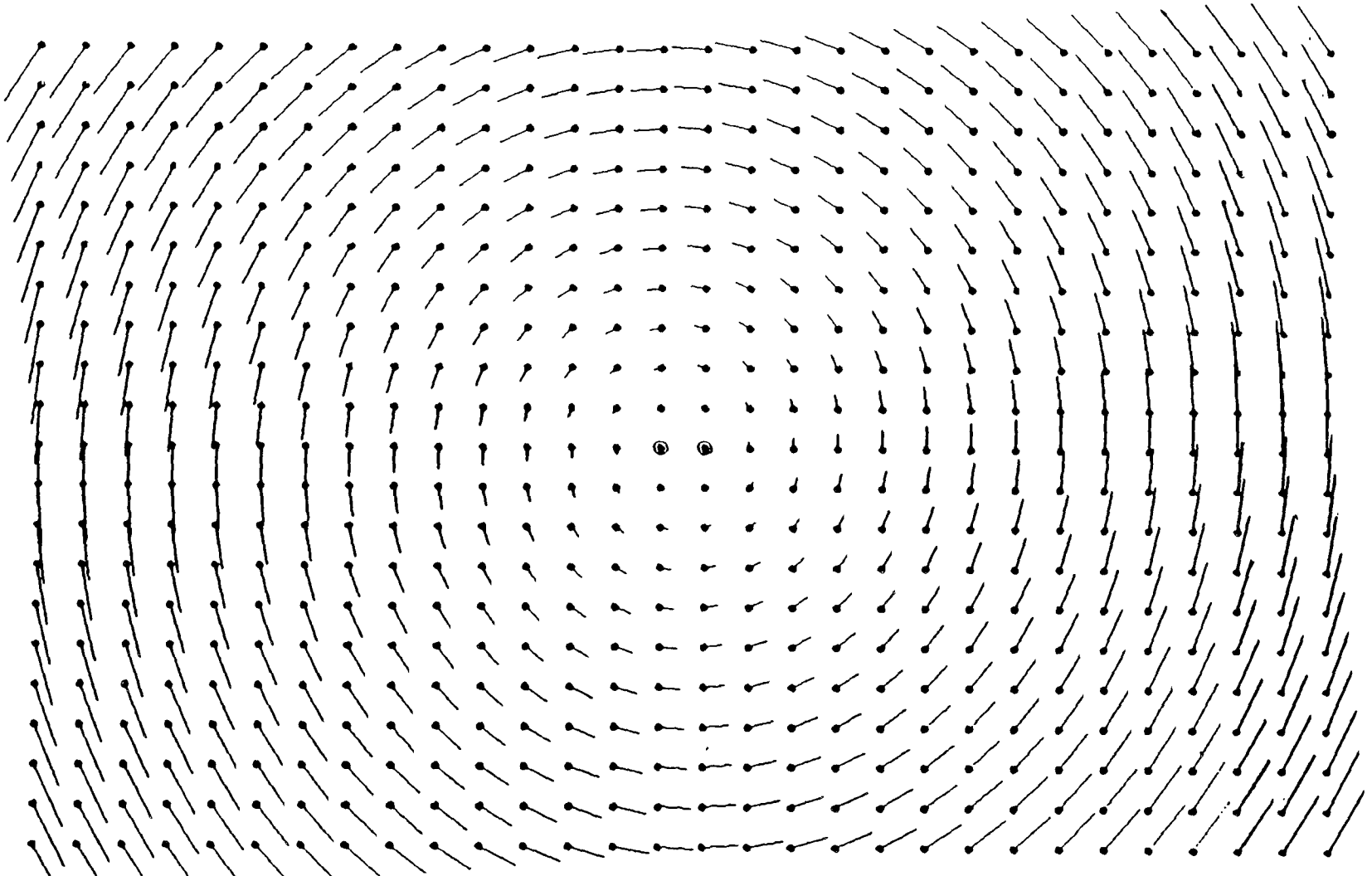

NO INVERSION: 2DUA31:[RUROZONE1.D80194]PF015Z.DAT;1
Windfield for LAYER 1 -- DATE & HOUR 80194:12
Grid stats -- MAX: 26.30 @ row 1, col 60; RMS: 14.83 m/sec.

Figure 29 Anticyclonic rotational wind field used in test cases 1A, 1B, and 1C. The length of the largest vector corresponds to 26.3 m/s.

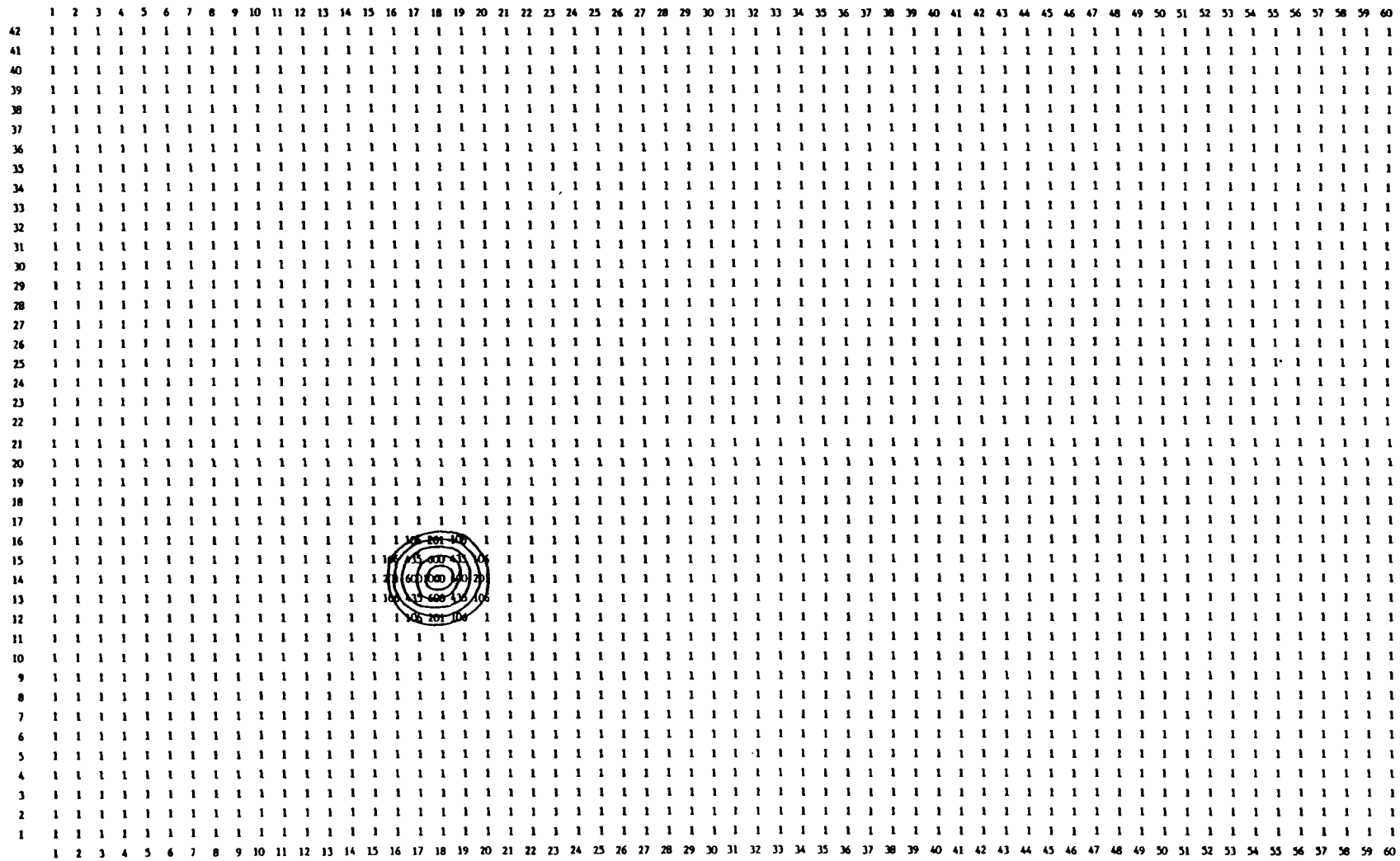

Figure 30. Initial species concentration field in ROM layer 1 for test case 1A. Units are ppm x 1000; contours are drawn at values of 100, 200, 400, 600, 800, 1000.

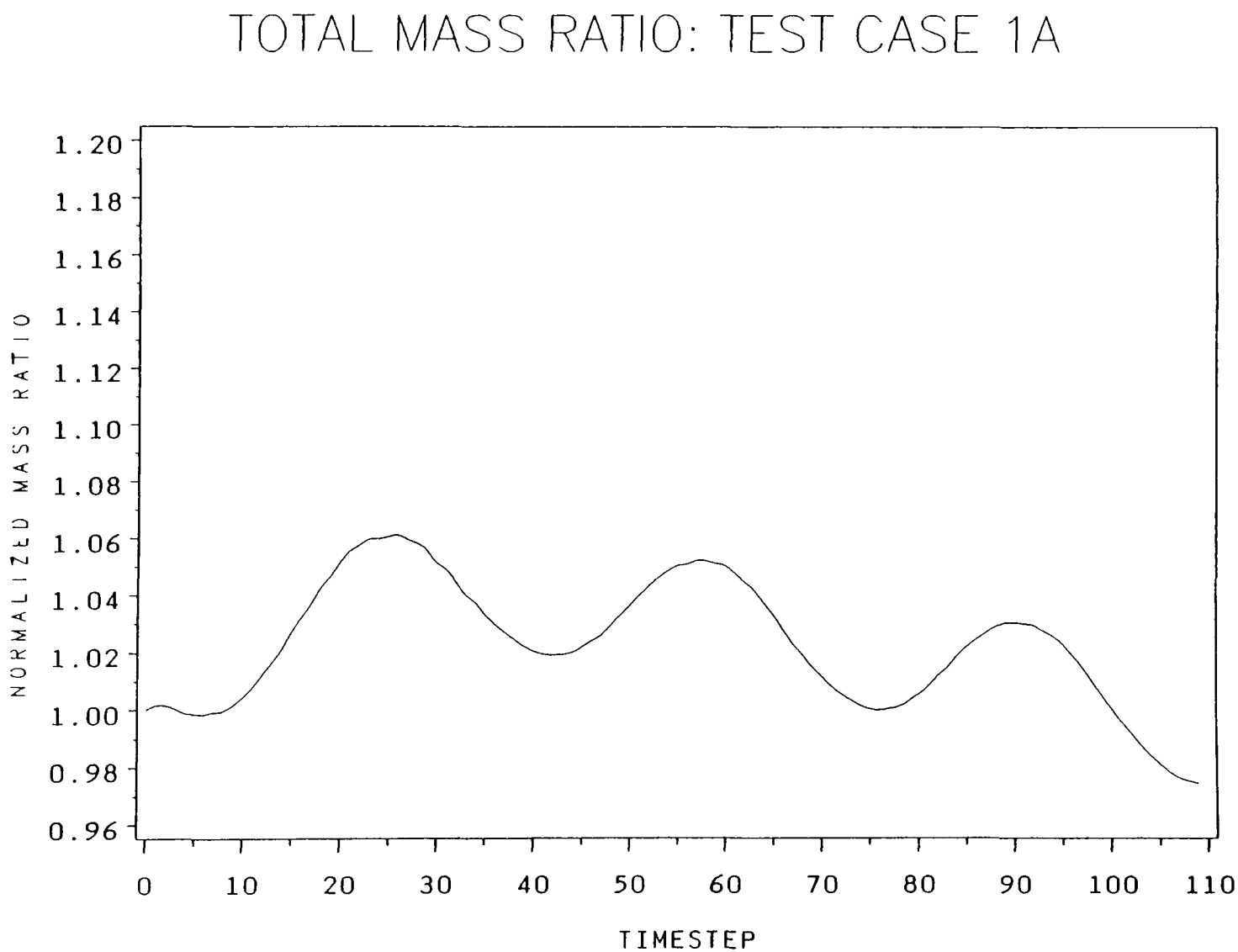

Figure 31. Time series of normalized mass ratio $[M(t)/M(t_0)]$ within the entire ROM domain for test case 1A.

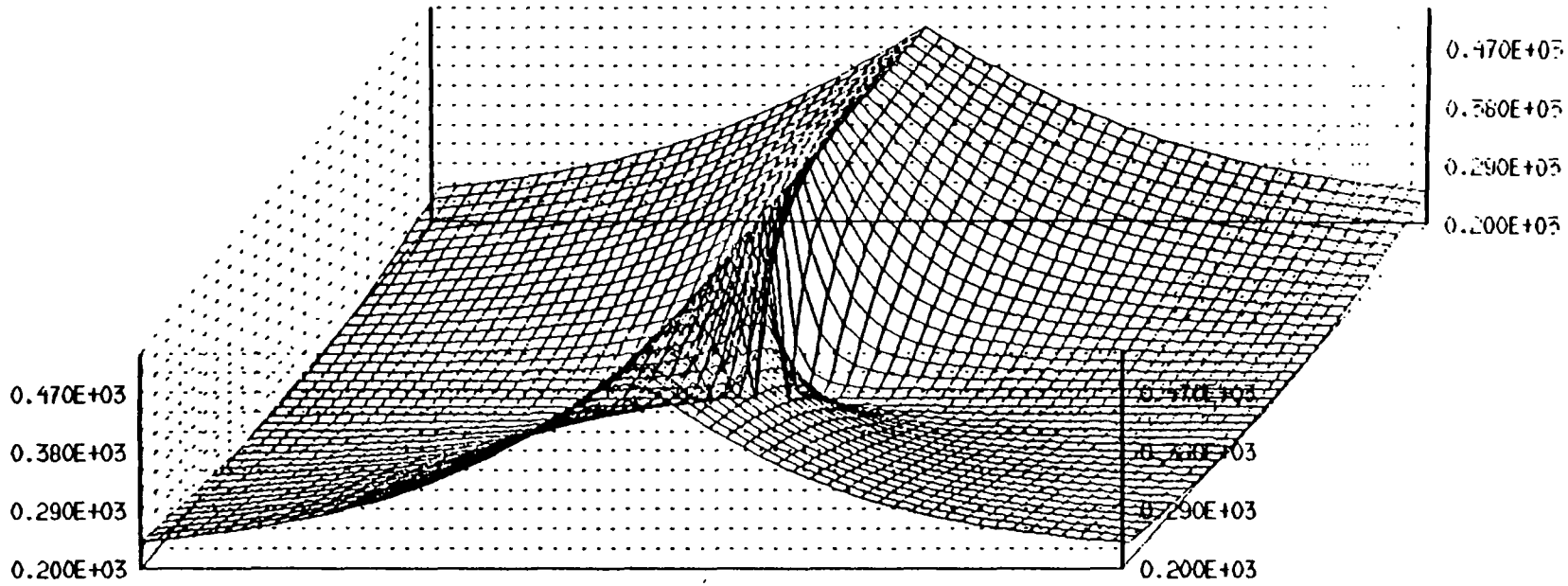

2DUA31:[RUROZONE1.D80194]MF065Y.DAT;1
Data statistics: MAX = 500.0 MEAN = 275.5 SIGMA = 79.57
data for 80194:12 plotted 14-SEP-89,12:23
Parm Z1 m above msl Interface surface elevation

Figure 32. Three-dimensional (x, y, z) schematic of height (m) of top of ROM layer 1 for test case 1B.

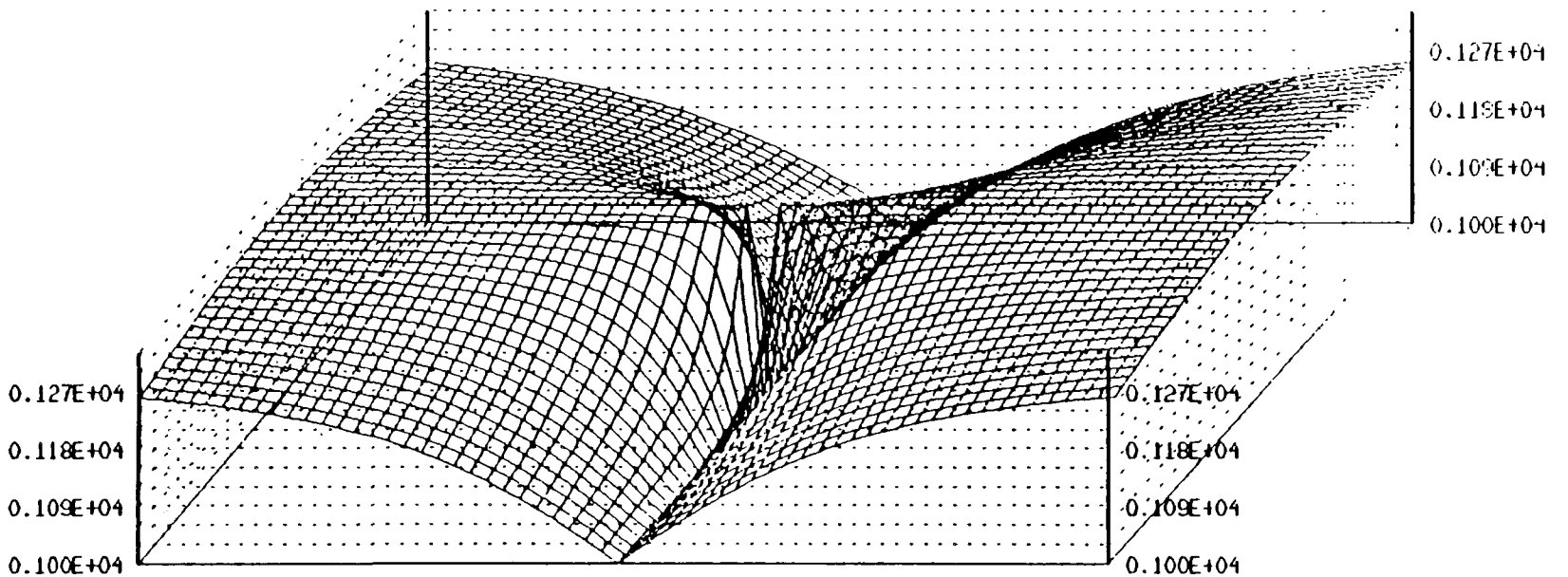

2DUA31:[RUROZONE1.D80194]MF066Y.DAT;1
Data statistics: MAX = 1300. MEAN = 1225. SIGMA = 79.58
data for 80194:12 plotted 14-SEP-89,12:30
Parm Z2 m above msl Interface surface elevation

Figure 33. Three-dimensional (x, y, z) schematic of height (m) of top of ROM layer 2 for test case 1B.

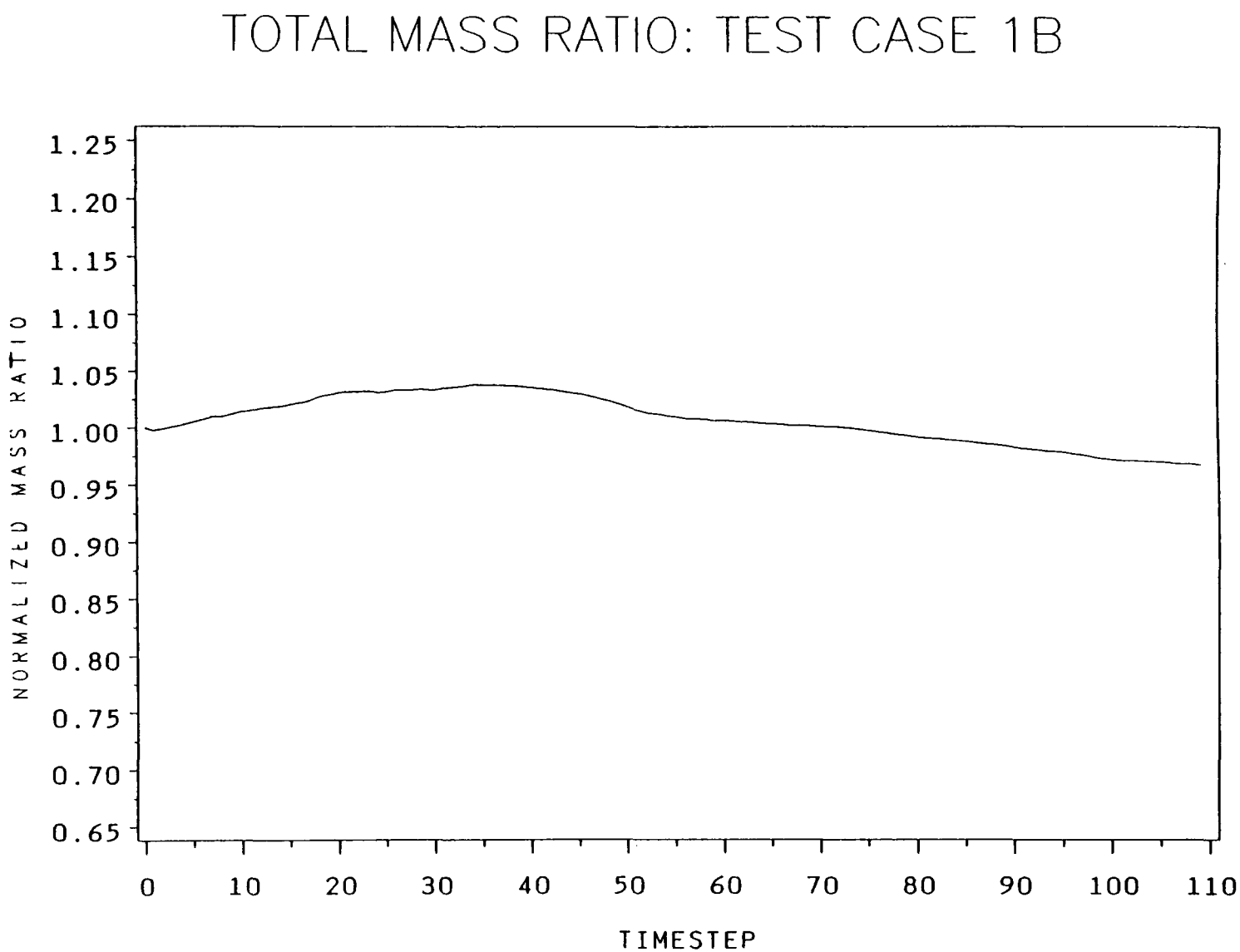

Figure 34. Time series of normalized mass ratio $[M(t)/M(t_0)]$ within the entire ROM domain for test case 1B.

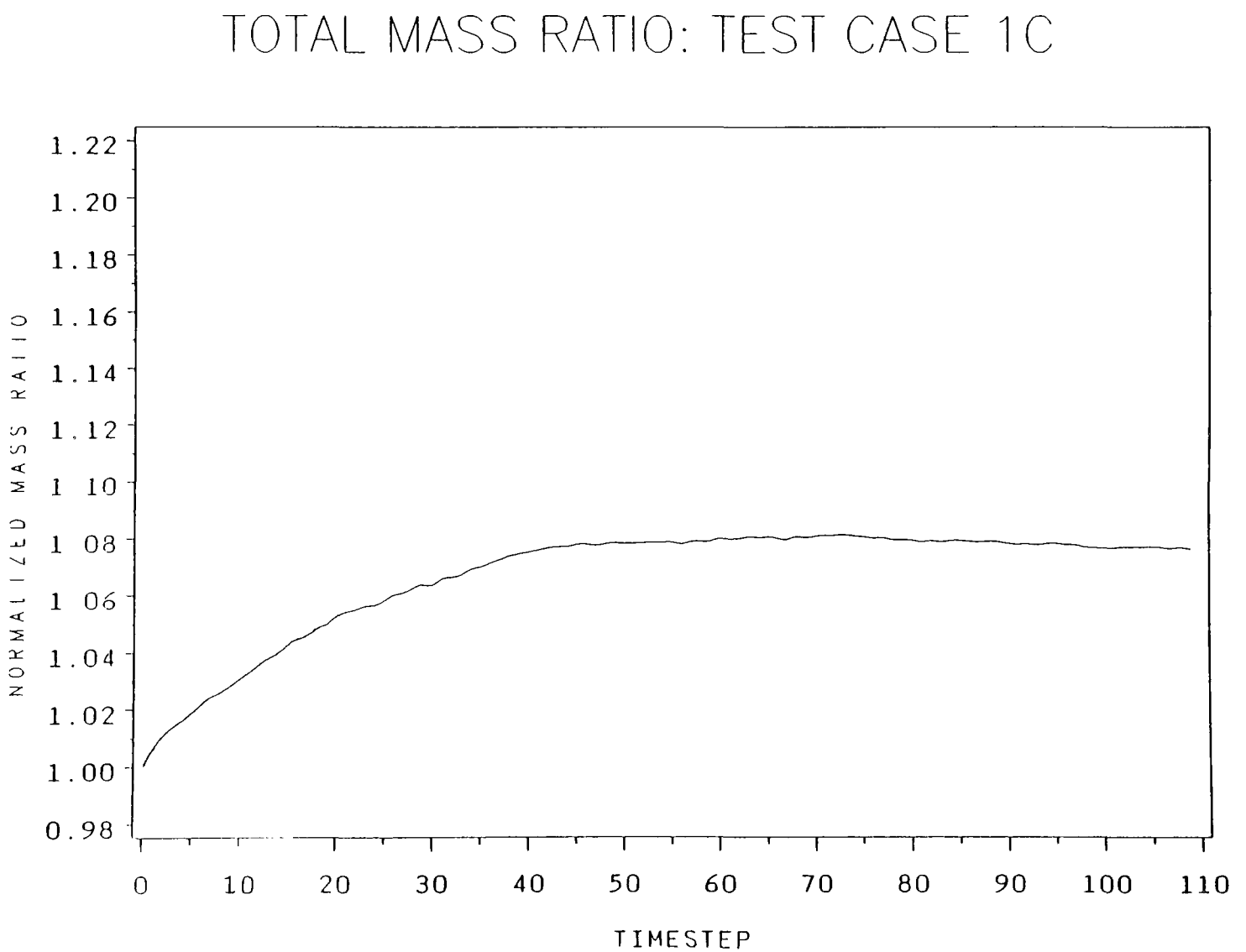

Figure 35 Time series of normalized mass ratio $[M(t)/M(t_0)]$ within the entire ROM domain for test case 1C.

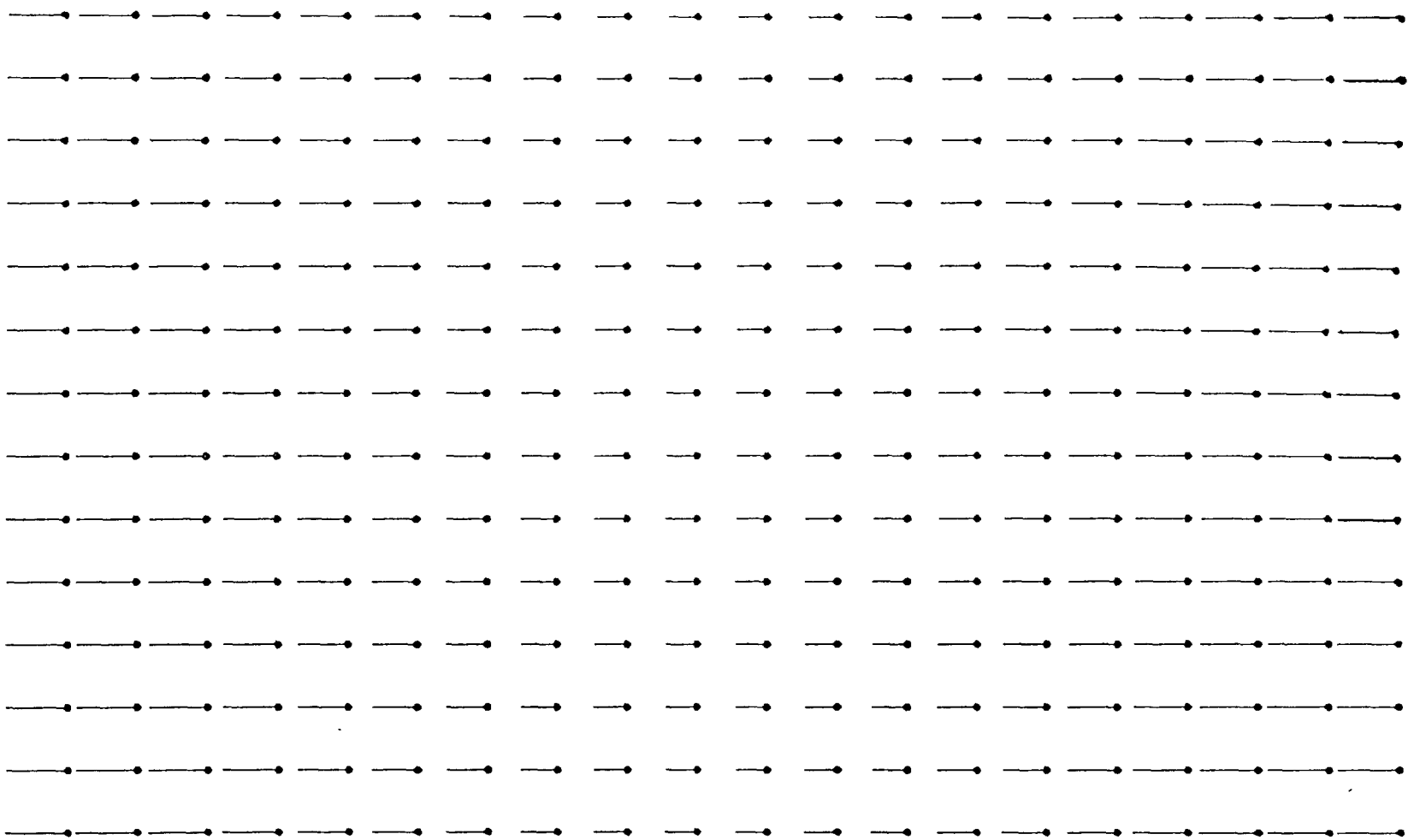

NO INVERSION: 2DUA31:[RUROZONE1.D80194]PF015W.DAT:1
Windfield for LAYER 1 -- DATE & HOUR 80194:12
Grid stats -- MAX: 9.97 @ row 1, col 1; RMS: 7.39 m/sec.

Figure 36. Purely divergent wind field used in test case 2. The length of the longest vector corresponds to 9.97 m/s.

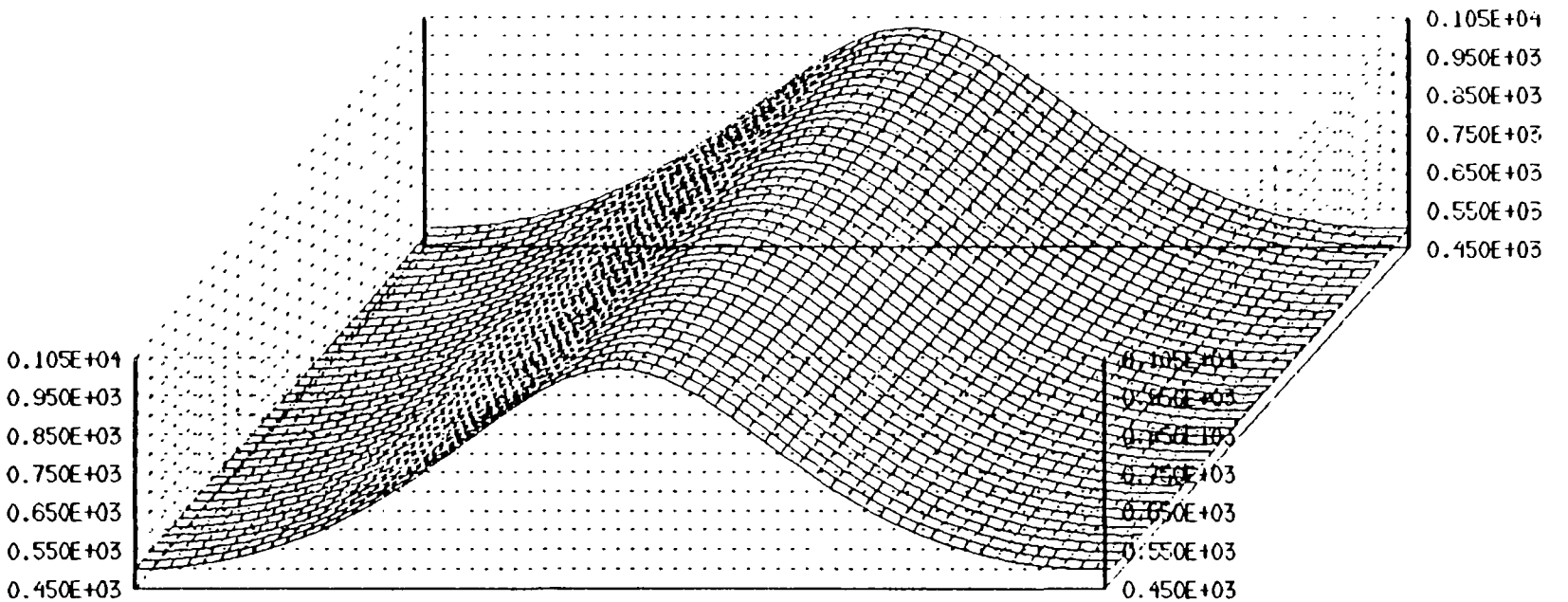

2DUA31:[RUROZONE1.D80194]MF065W.DAT;1
Data statistics: MAX = 1022. MEAN = 707.5 SIGMA = 182.5
data for 80194:12 plotted 8-NOV-89,15:44
Parm Z1 m above msl Interface surface elevation

Figure 37. Three-dimensional (x, y, z) schematic of height (m) of top of ROM layer 1 for test case 2.

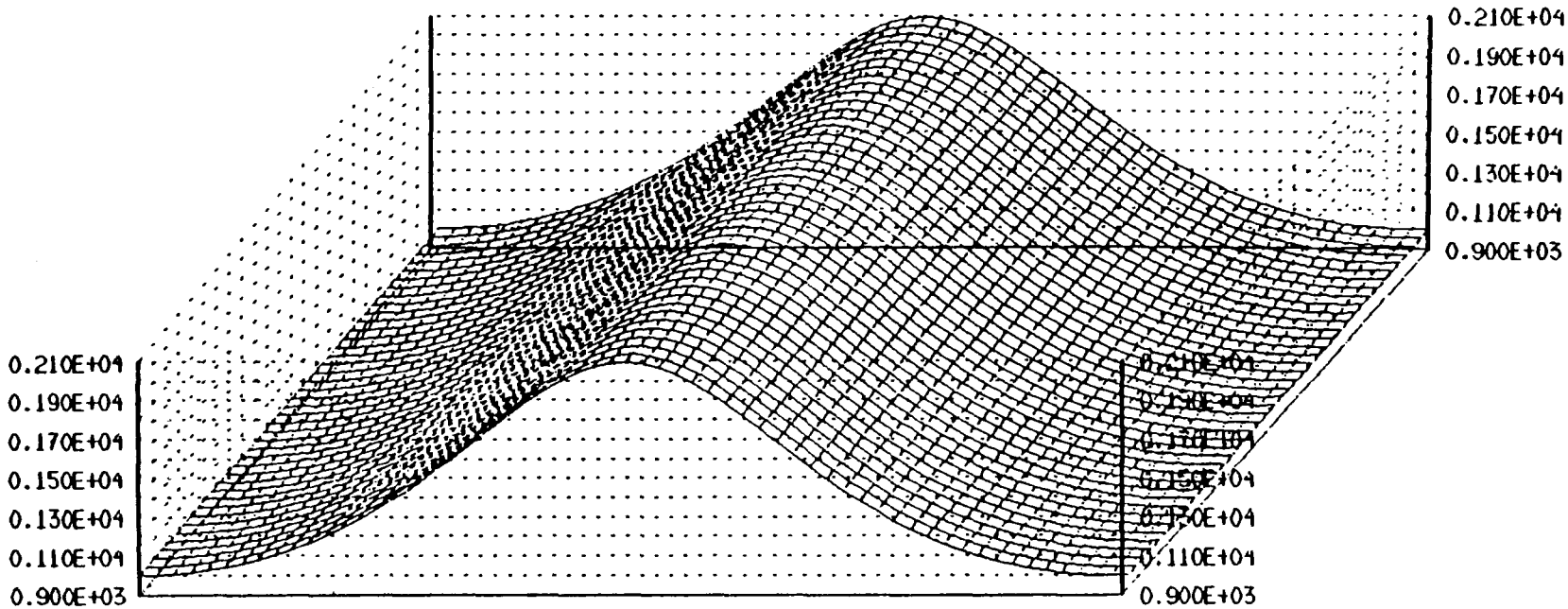

2DUA31:[RUROZONE1.D80194]MF066W.DAT;1
Data statistics: MAX = 2092. MEAN = 1431. SIGMA = 381.6
data for 80194;12 plotted 8-NOV-89.15:45
Parm Z2 m above msl Interface surface elevation

Figure 38. Three-dimensional (x, y, z) schematic of height (m) of top of ROM layer 2 for test case 2.

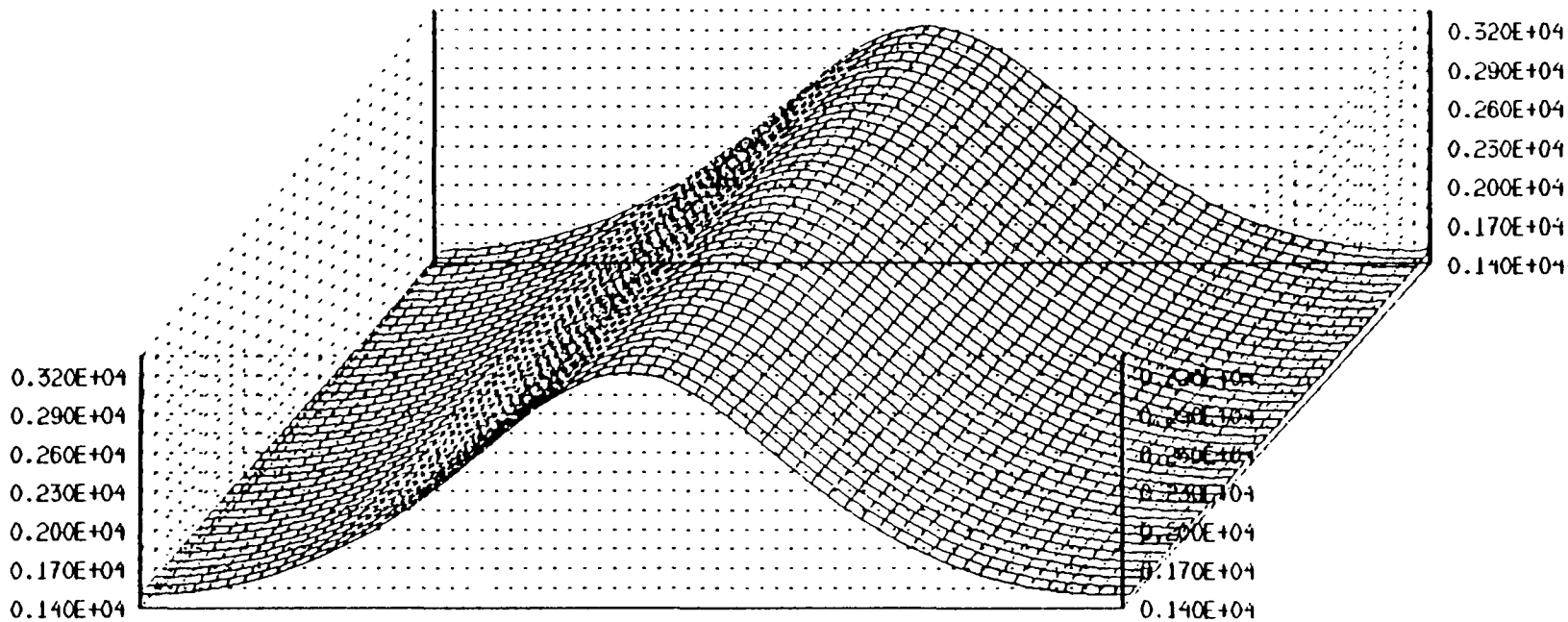

2DUA31:[RUROZONE1.D80194]MF067W.DAT;1
Data statistics: MAX = 3222. MEAN = 2174. SIGMA = 600.7
data for 80194:12 plotted 8-NOV-89,15:47
Parm Z3 m above msl Interface surface elevation

Figure 39. Three-dimensional (x, y, z) schematic of height (m) of top of ROM layer 3 for test case 2.

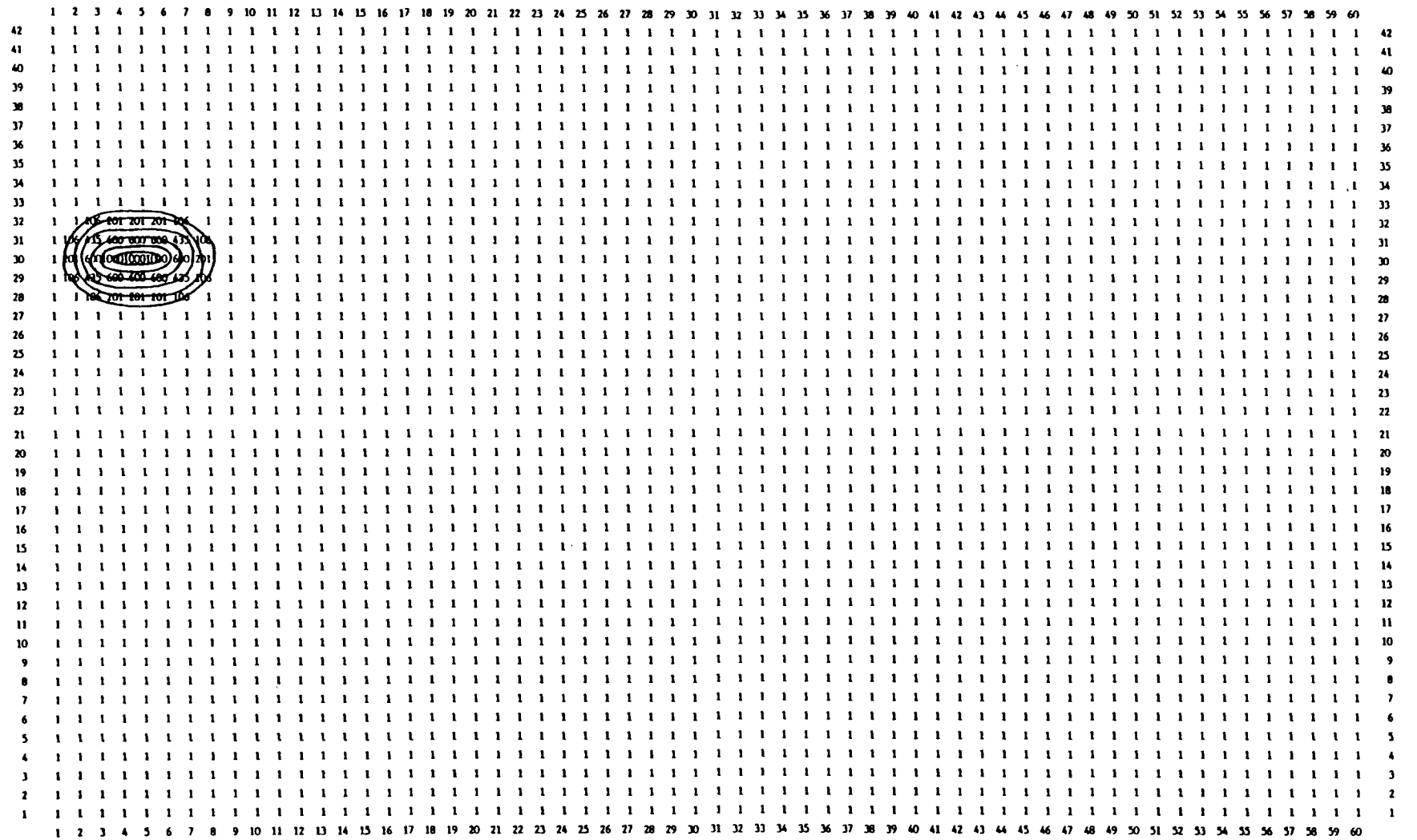

Figure 40. Initial species concentration field in ROM layer 1 for test case 2. Units are ppm x 1000; contours are drawn at values of 100, 200, 400, 600, 800, 1000.

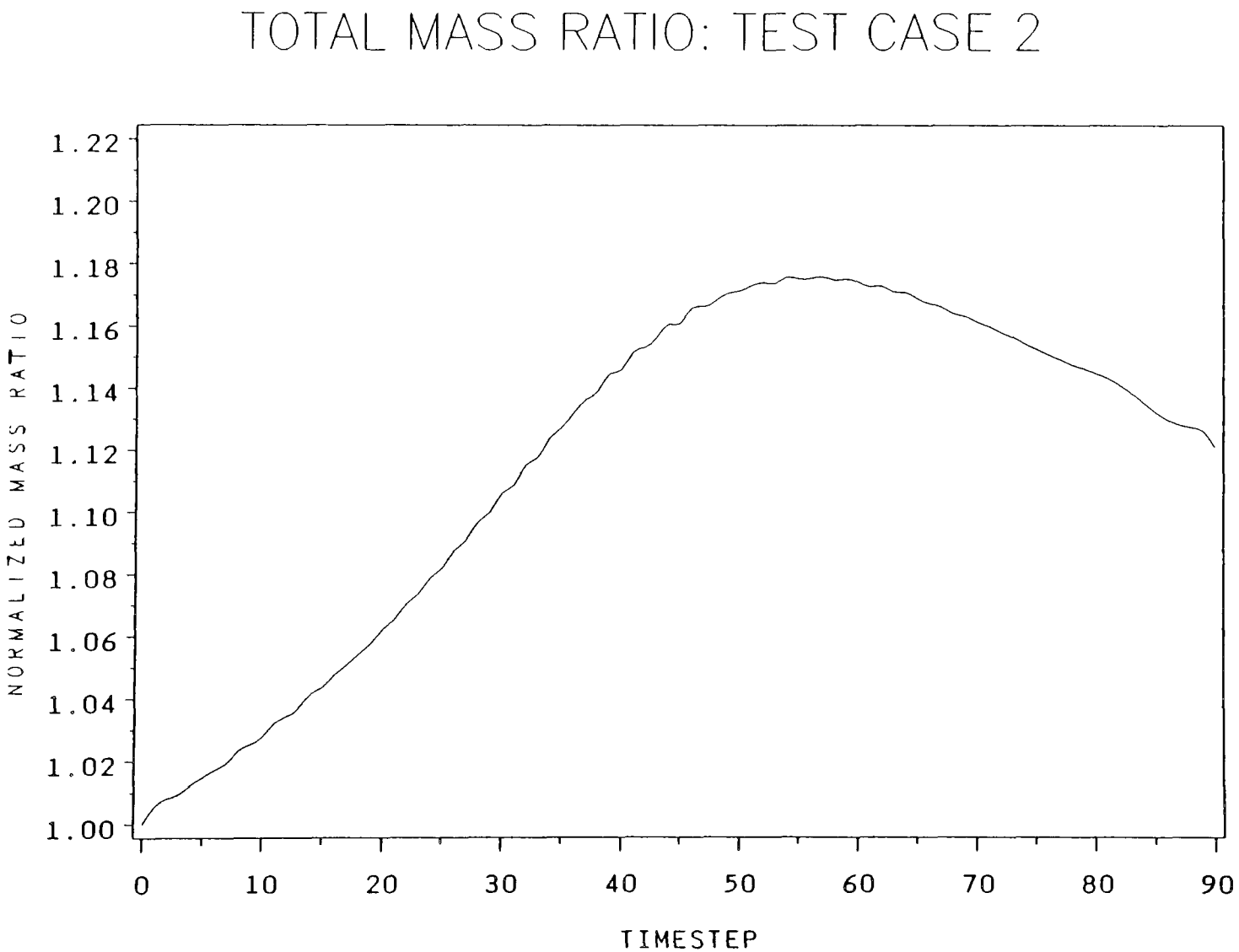

Figure 41. Time series of normalized mass ratio $[M(t)/M(t_0)]$ within the entire ROM domain for test case 2.

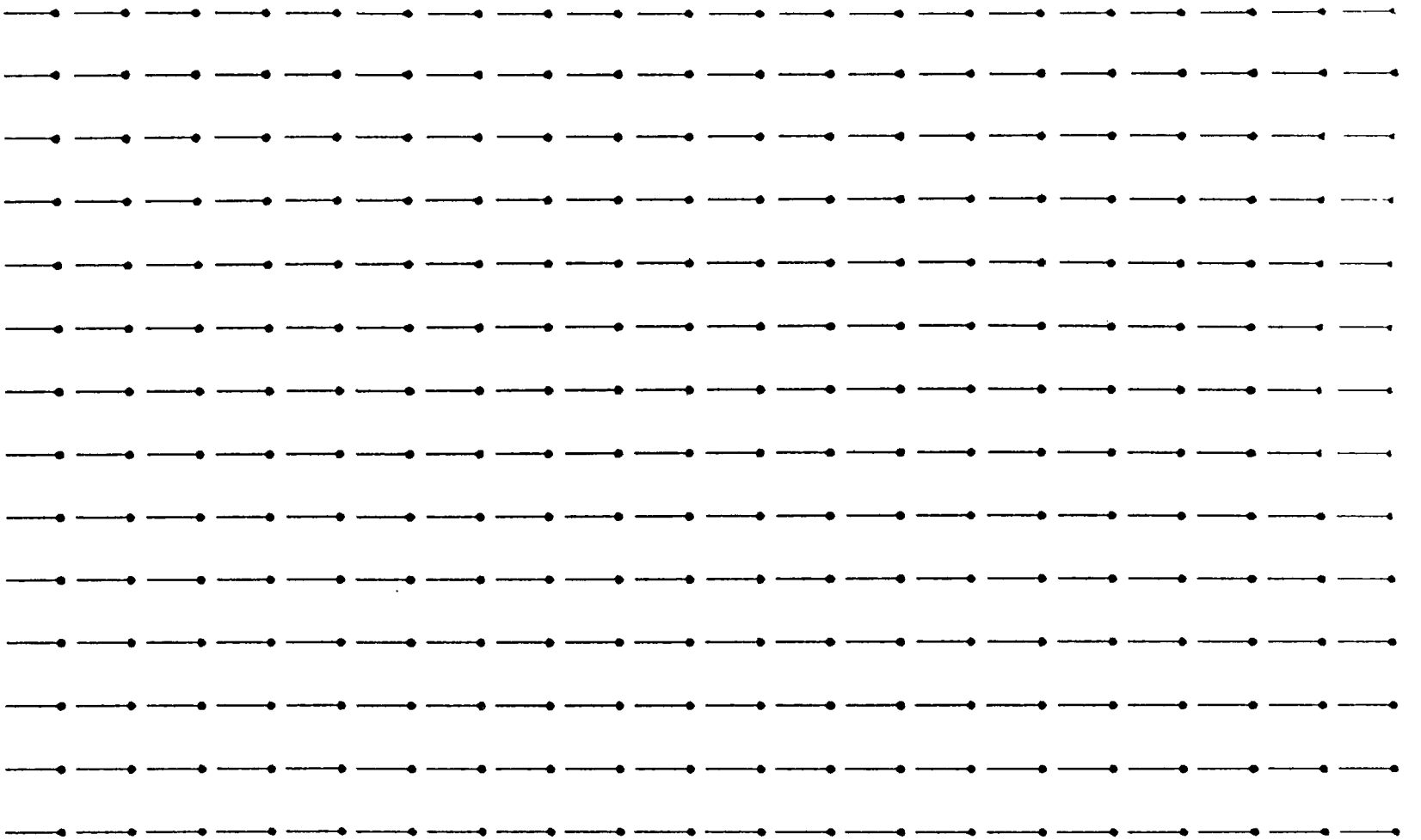

NO INVERSION: 2DUA31:[RUROZONE1.D80194]PF015V.DAT;1
Windfield for LAYER 1 -- DATE & HOUR 80194:12
Grid stats -- MAX: 5.87 @ row 1, col 1; RMS: 5.59 m/sec.

Figure 42. Quasi-constant wind field used in test cases 0, 0A, and 0B. The length of the largest vector corresponds to 5 87 m/s.

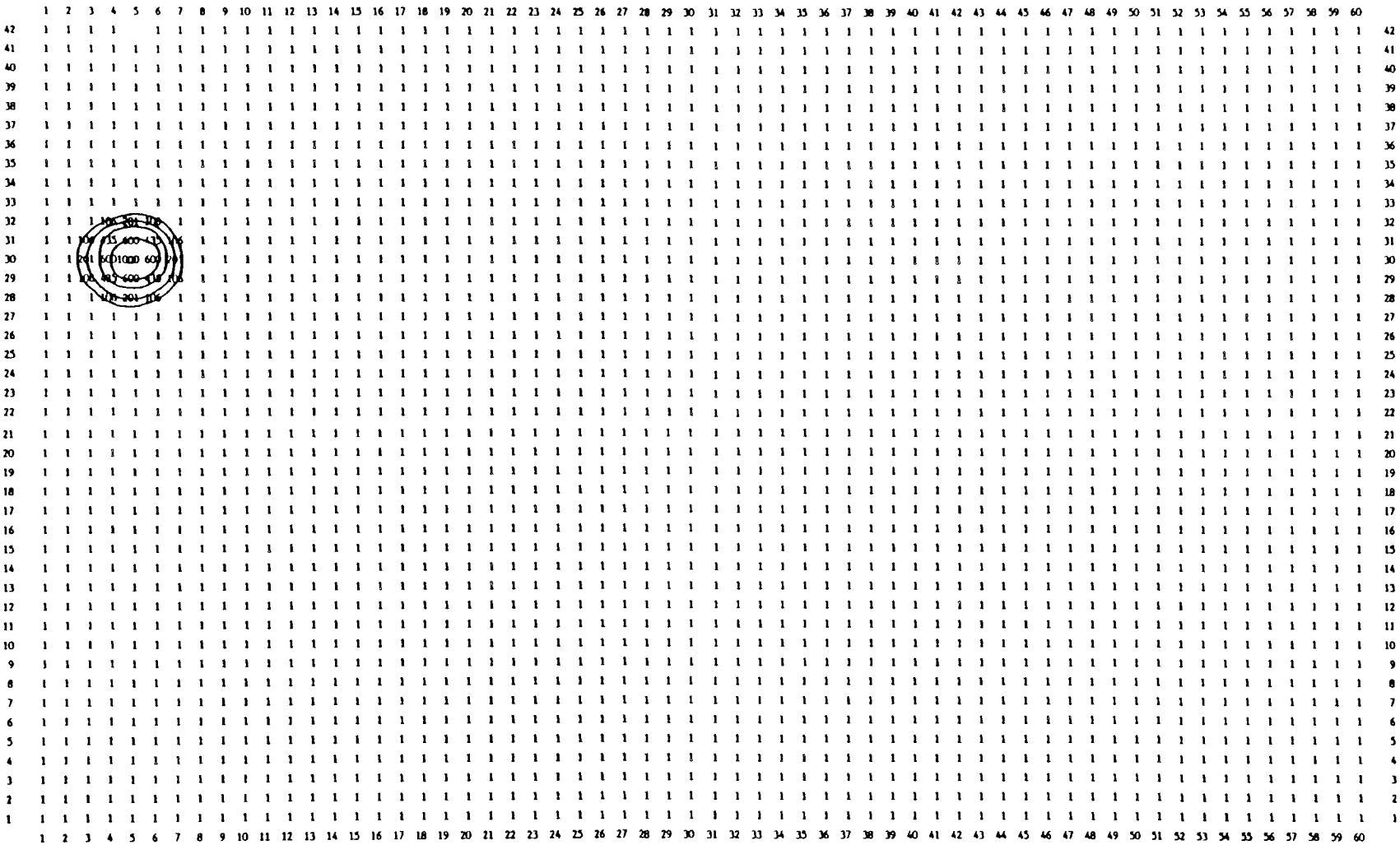

Figure 43. Initial species concentration field in ROM layer 1 for test case 0 Units are ppm x 1000; contours are drawn at values of 100, 200, 400, 600, 800, 1000.

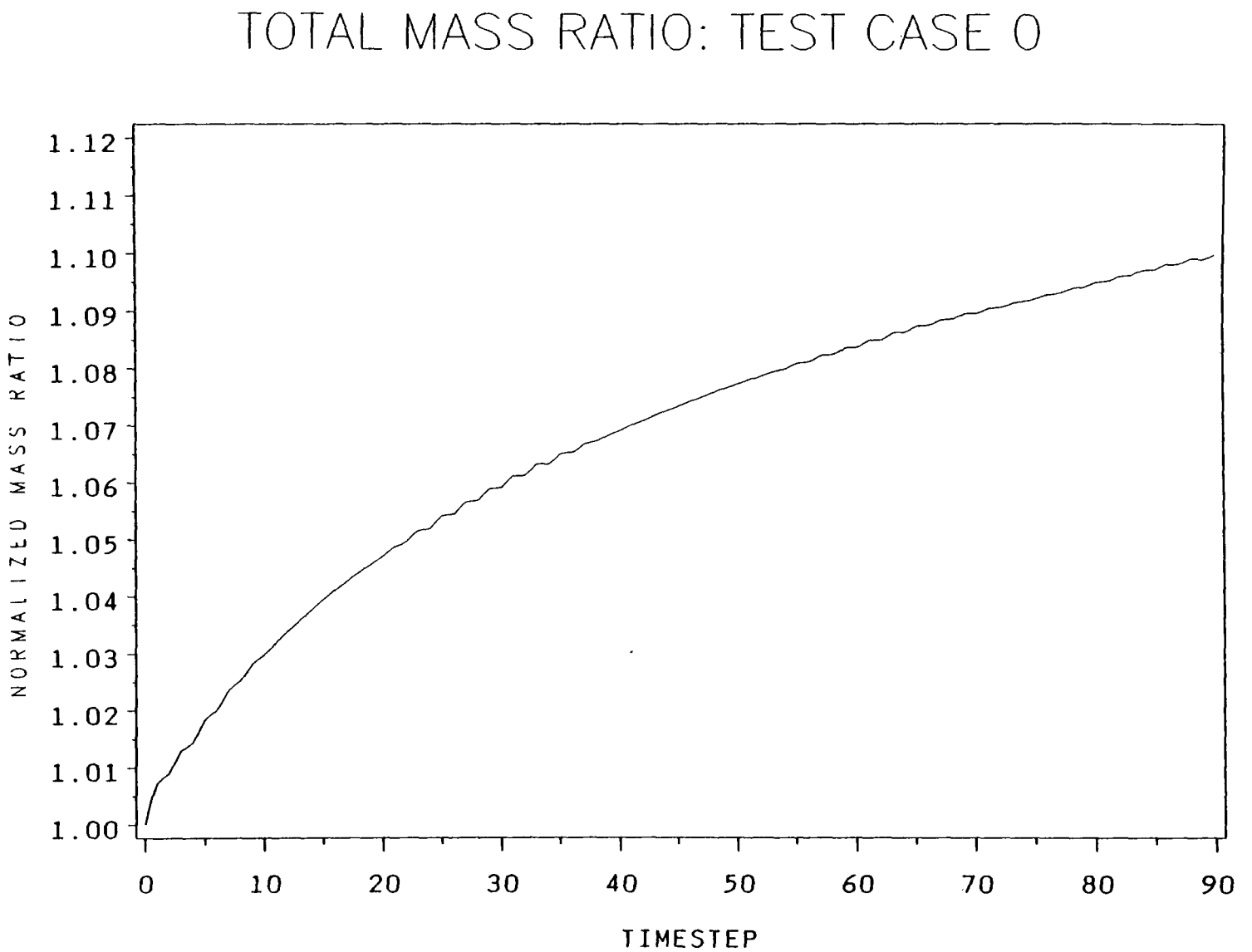

Figure 44. Time series of normalized mass ratio $[M(t)/M(t_0)]$ within the entire ROM domain for test case 0.

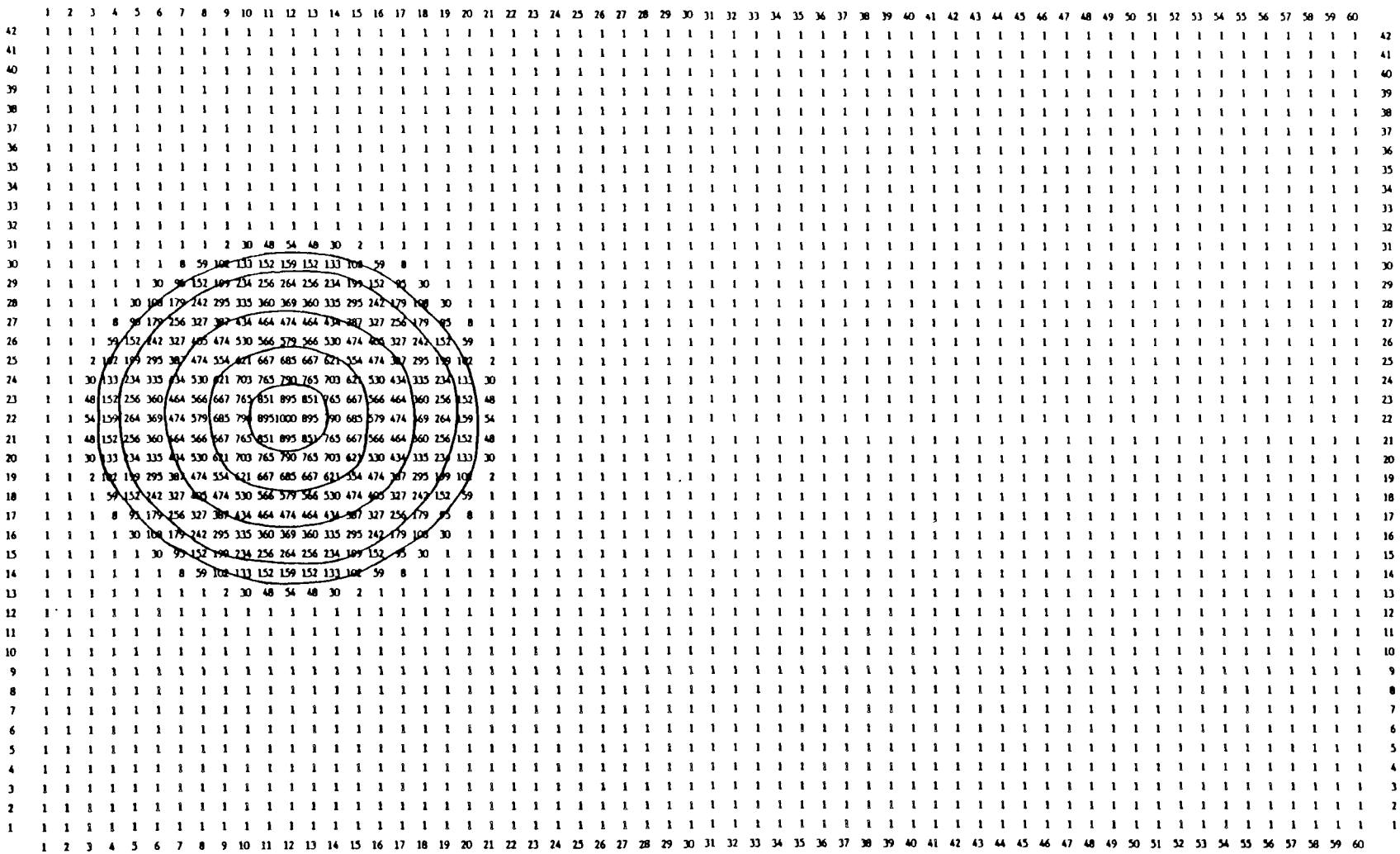

Figure 45 Initial species concentration field in ROM layer 1 for test case 0A. Units are ppm x 1000; contours are drawn at values of 100, 200, 400, 600, 800, 1000.

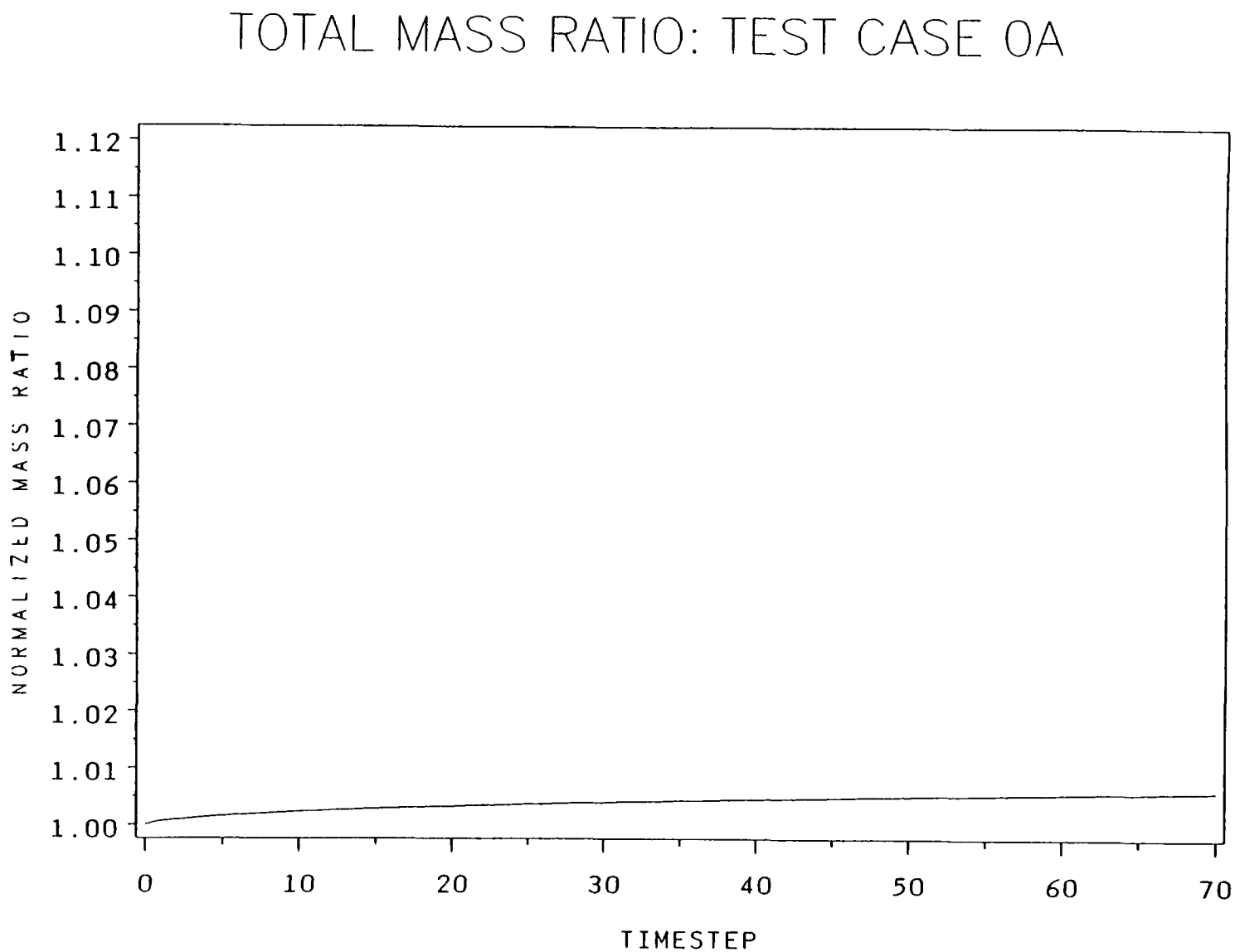

Figure 46. Time series of normalized mass ratio $[M(t)/M(t_0)]$ within the entire ROM domain for test case 0A.

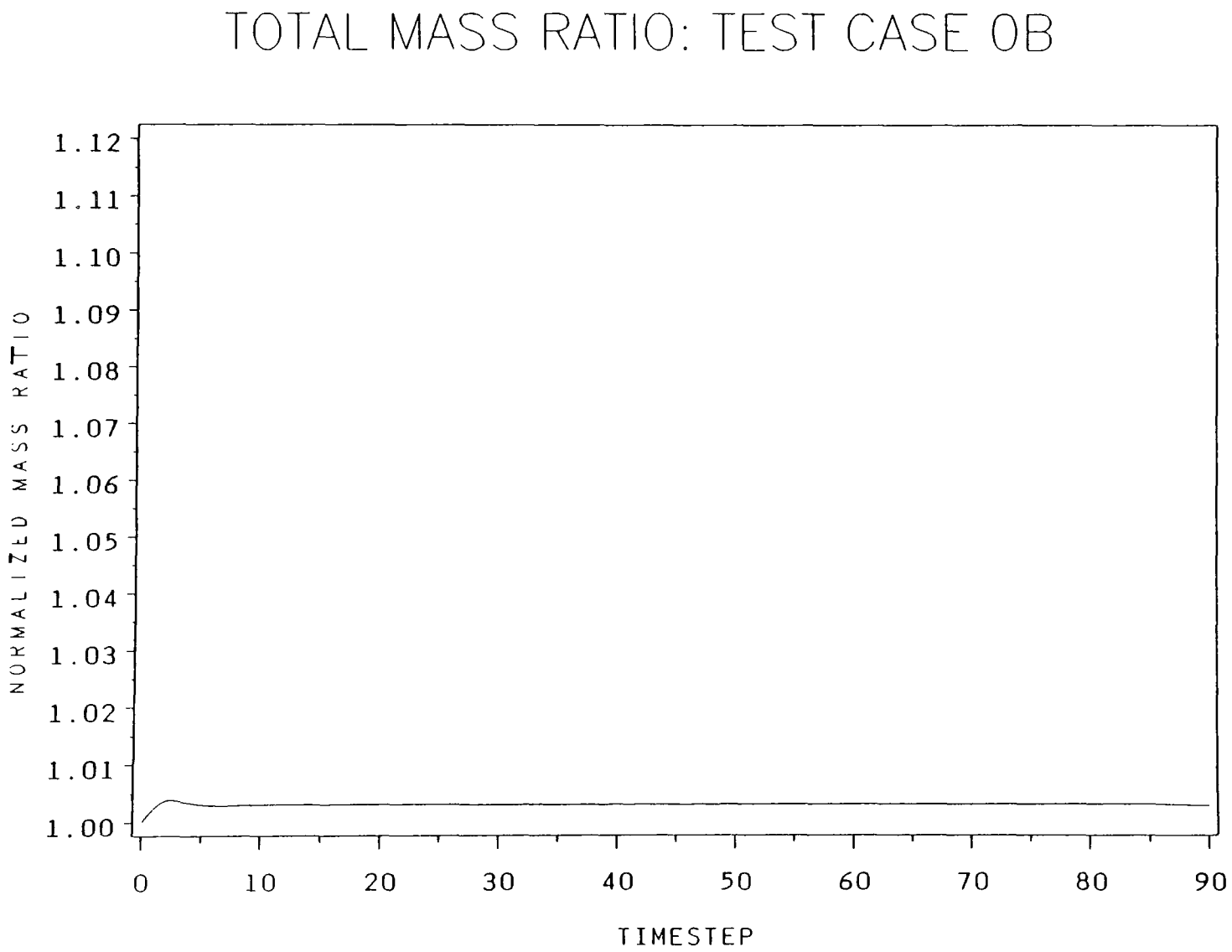

Figure 47 Time series of normalized mass ratio $[M(t)/M(t_0)]$ within the entire ROM domain for test case 0B.

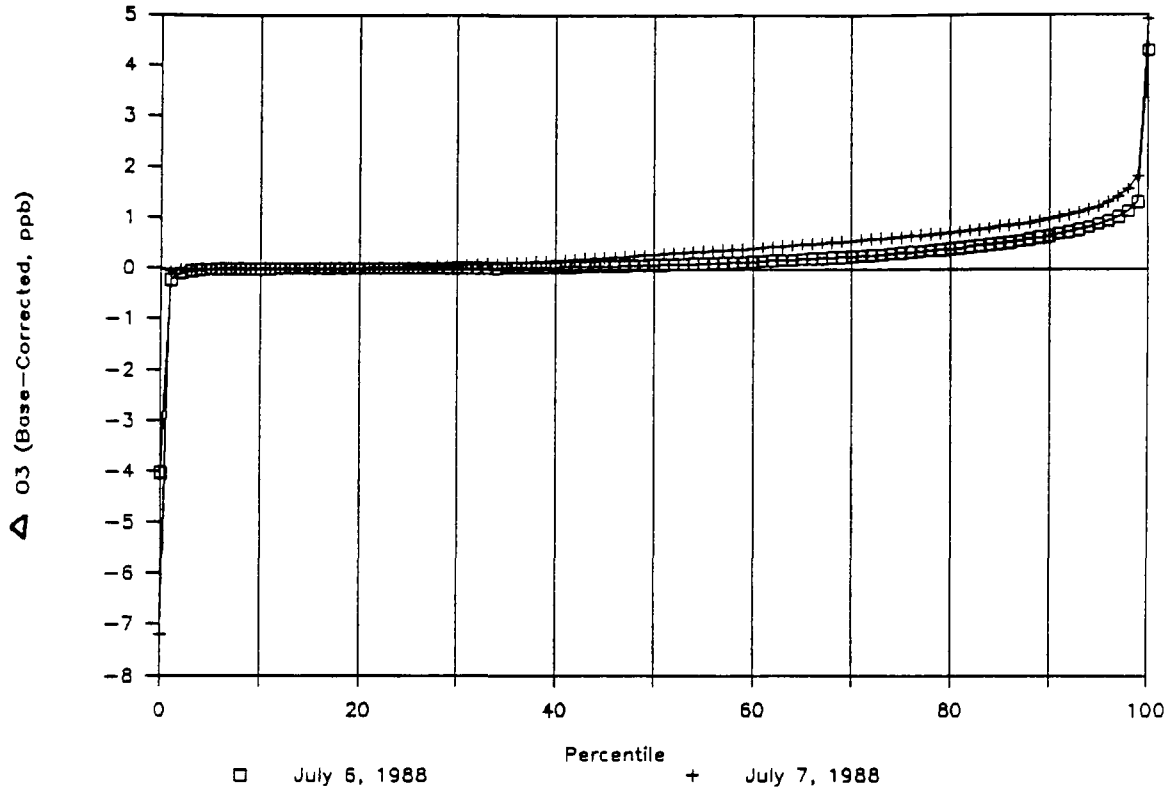

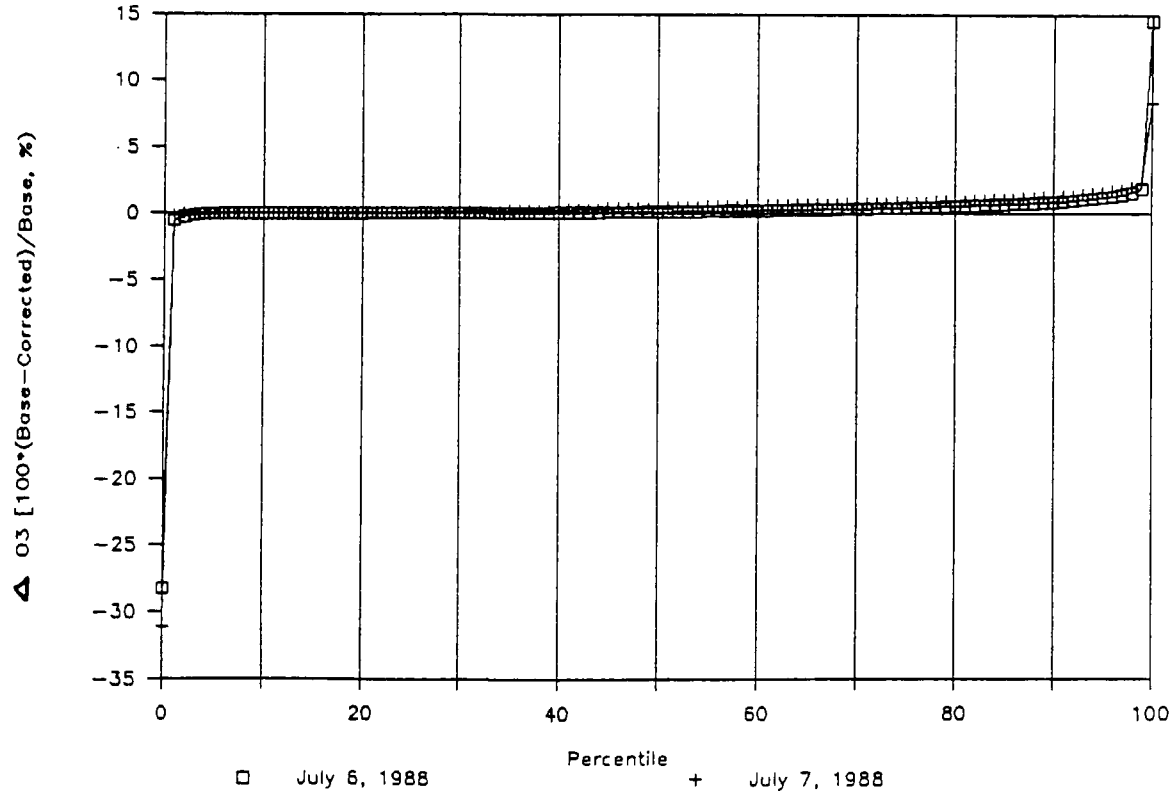

Figure 48. Frequency distribution of paired grid O_3 concentration differences from ROM simulations for a base case (A) and a mass-corrected base case (B) for July 6 and 7, 1988. Top figure (a) shows A-B distribution and bottom figure (b) shows normalized differences, (A-B)*100/A, as percent change from base.

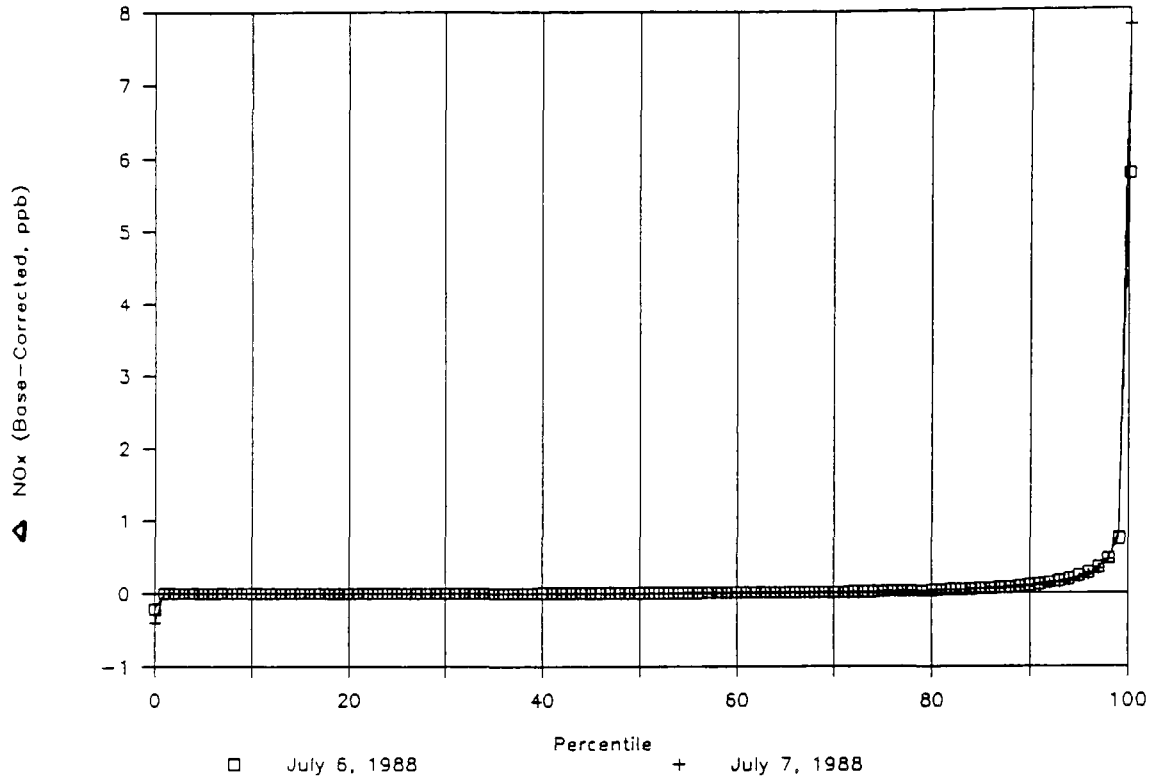

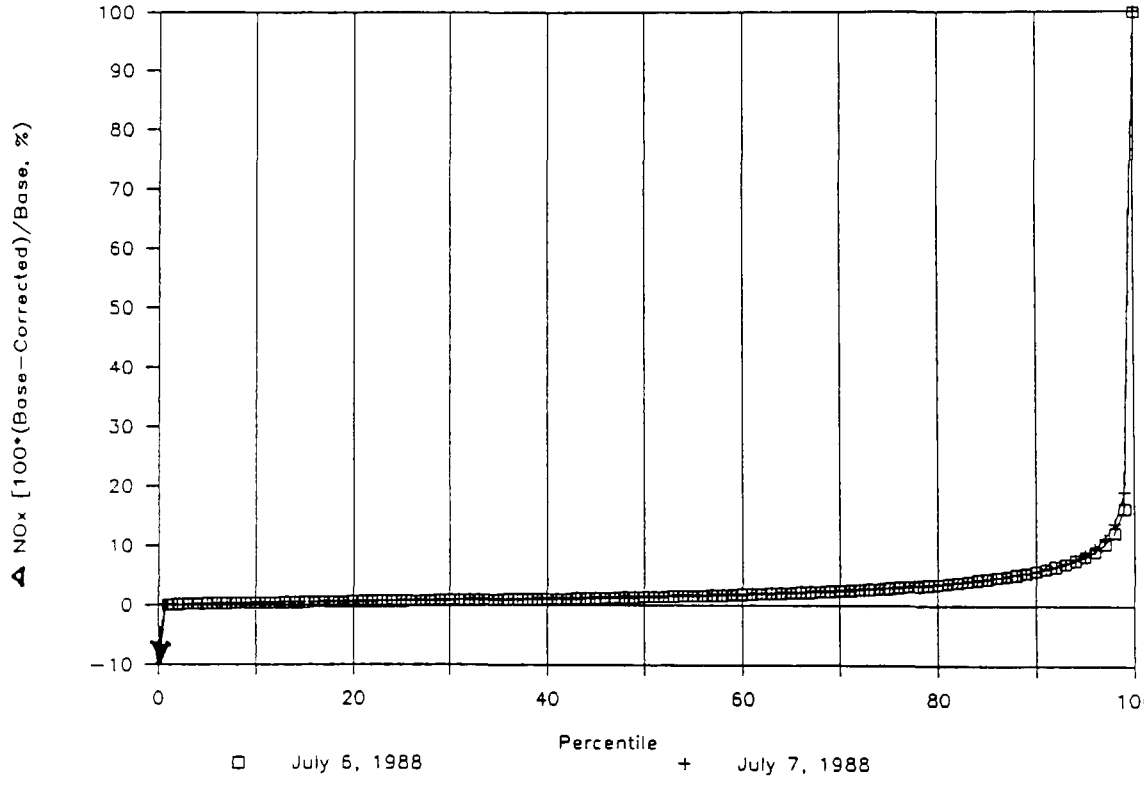

Figure 49 Frequency distribution of paired grid NO_x concentration differences from ROM simulations for a base case (A) and a mass-corrected base case (B) for July 6 and 7, 1988. Top figure (a) shows A-B distribution and bottom figure (b) shows normalized differences, (A-B)*100/A, as percent change from base.

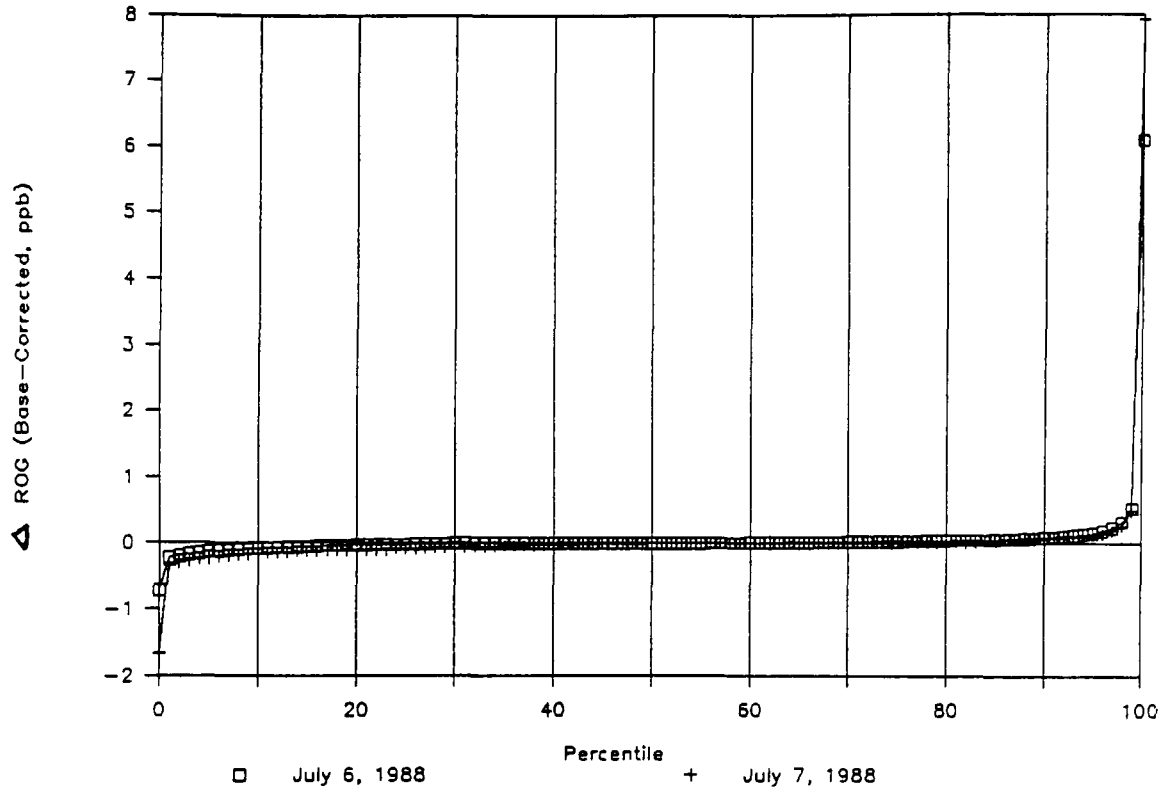

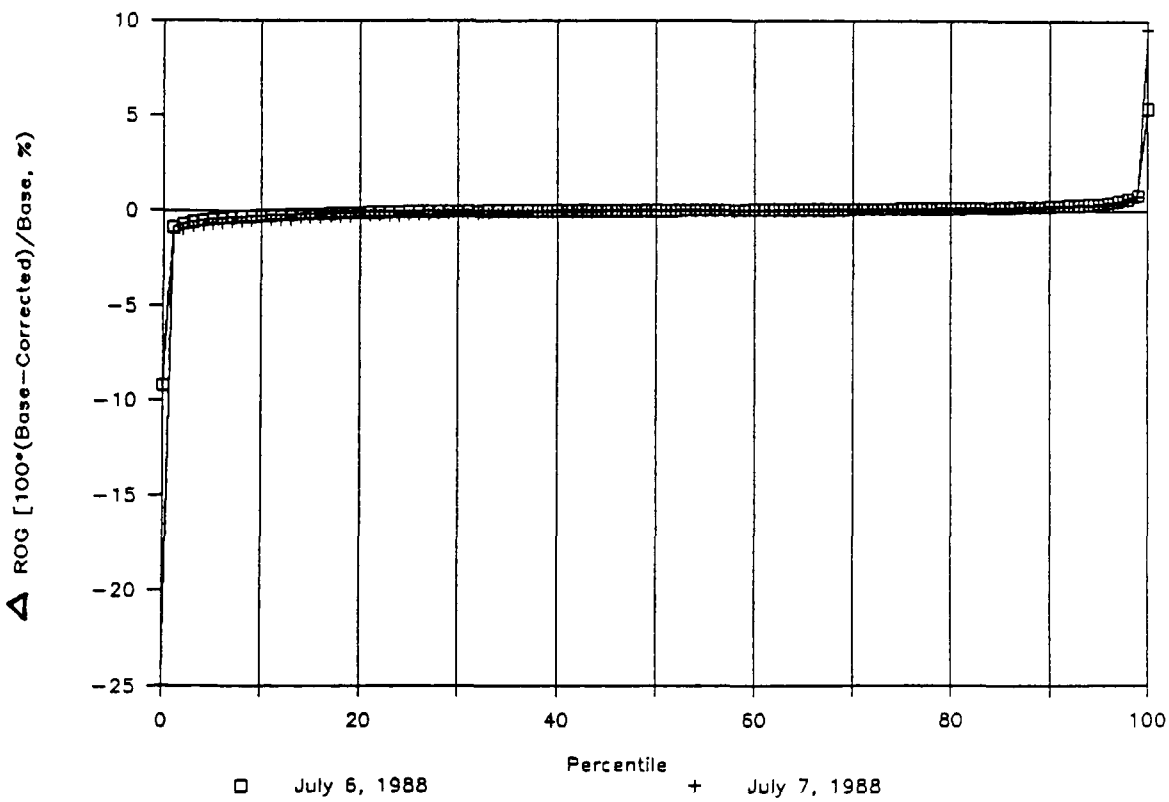

Figure 50. Frequency distribution of paired grid ROG concentration differences from ROM simulations for a base case (A) and a mass-corrected base case (B) for July 6 and 7, 1988. Top figure (a) shows A-B distribution and bottom figure (b) shows normalized differences, (A-B)*100/A, as percent change from base.

SECTION 6

SUMMARY AND RECOMMENDATIONS

Using both an ambient evaluation and a series of diagnostic tests, we evaluated Version 2.1 of the Regional Oxidant Model (ROM2.1). In the ambient evaluation, we assessed ROM2.1's performance for periods of high ozone in July and August of 1985 in the northeastern U.S., using AIRS daytime hourly surface ozone monitoring data. We compared these observations with model estimates in three types of analyses: (1) a comparison of overall statistics to determine whether model estimates exhibited a general bias, (2) a comparison of spatial patterns of maximum concentrations to look for spatial bias in the model estimates, and (3) an assessment of the model's applicability for determining UAM boundary conditions. In the diagnostic tests, we assessed the accuracy of numerical algorithms by evaluating the model's ability to conserve mass; we performed five tests that involved only the horizontal transport algorithm and two that involved both horizontal transport and vertical flux.

In the ambient evaluation portion of the study, we found good overall agreement. For a 26 day simulation, mean concentrations of the modeled and observed daily maximum concentrations agreed to within 1%. Concentrations at the higher ends of the frequency distributions were slightly underestimated; the 95th percentile observed daily maximum concentration was 127 ppb while the estimated concentration was 119 ppb. The tendency to underestimate peak concentrations is to be expected with a coarse grid model such as the ROM because of the spatial averaging that occurs with Eulerian grid computations.

In the Northern Corridor and Southern Corridor geographical groups (groups 1 and 2, respectively), model performance was good, particularly in group 2. The group 1 mean observed and modeled daily maxima agreed to within 11% and the 95th-percentile observed and modeled daily maxima agreed to within 5% (both values were overestimated). For group 2, the mean daily

maxima were within 3% of each other and the 95th-percentile values were within 7% (both values were underestimated). The quantile-quantile plots of observed and modeled daytime hourly concentrations showed the same kinds of tendencies: overestimation in the upper quantiles of group 1 and underestimation in the upper quantiles of group 2, as well as better overall agreement for group 2 than for group 1--only the top 15% of group 1's estimates were within 10% of the observations, while for group 2 the top 70% of the estimates were within 10% of the observations. The medians in the time series plots of daily maxima for these two groups showed analagous underestimate-overestimate tendencies, and these plots also showed that exceedances (values over 120 ppb) were overestimated in group 1 (ten versus eight) and underestimated in group 2 (six versus ten).

Model performance in group 3 (the southwestern part of the domain--southern Virginia, West Virginia, Ohio, and western Pennsylvania), an area removed from the extensive metropolitan area of the Northeast Corridor, was noticeably poorer than the performance for groups 1 and 2. The group 3 mean daily maximum was underestimated by 12% and the 95th-percentile daily maximum was underestimated by 19%. The quantile-quantile plot for group 3 showed that the top 35% of the values were underestimated by more than 10%. The group 3 time series plot showed that 12 out of 14 medians were underestimated, and that exceedances were dramatically underestimated (six versus zero). Underestimates of upper-quantile concentrations in this group perhaps can be attributed to the relatively small-scale urban plumes and uncertainties in estimating naturally-occurring emissions of NO_x and hydrocarbons. However, deficiencies in anthropogenic emissions inventories should not be ignored, and ongoing efforts to improve them should continue.

Groups 4 and 5 (the northern part of the domain, excluding the Northeast Corridor) had observations close to background values, and model estimates generally showed good agreement with observations, especially for the upper values.

Spatial patterns of the three-day maximum concentrations usually showed reasonable model performance. The modeled magnitude and orientation of ozone

plumes in the northern portion of the Northeast Corridor, especially around New York City, compared well with observed plumes. The model also did an excellent job of predicting high ozone levels around coastal sections of Maine. We believe that ROM2.1 performed better than ROM2.0 in these areas because ROM2.1 includes a correction for the westerly bias that occurred in ROM2.0's low-level wind flows. Differences between observed and modeled plumes were most evident during episodes experiencing coastal troughs and squall lines. Underestimates in the Washington, DC, area that were reported in the ROM2.0 evaluation by Schere and Wayland (1989) were seen again in our evaluation. In addition, ROM 2.1 tended to underpredict rural peak concentrations of ozone by about 20 ppb. Few monitoring data are available for evaluating model performance in rural areas, so it is hoped that measurements being taken under the auspices of the National Acid Precipitation and Assessment Program (NAPAP) will aid in future evaluation of ozone concentrations.

The most rigorous portion of this analysis was an evaluation of the model's ability to estimate boundary conditions for UAM application. Although we do not recommend applying the ROM in a deterministic manner, some type of reliable estimation scheme is needed for prescribing boundary conditions when the UAM is to be applied for future-year emission control strategies. Also, model estimates are need because measurements aloft are typically not available for specifying the vertical structure of pollutant concentrations. Furthermore, our analysis showed that using monitoring data for estimating boundary conditions requires a great deal of subjectivity and is fraught with uncertainty.

Overall, ROM2.1 estimates compared quite well with the monitoring data for estimating UAM near-surface boundary conditions in the OMNYMAP domain. The model overestimated the mean concentration for all daytime hours by just 5 ppb (8%) and underestimated the 95th-percentile value by 9 ppb (9%). However, we saw significant day-to-day variability in model performance, ranging from a maximum underestimate of 24% to a maximum overestimate of 49%. A case study performed for July 10, 1985, demonstrated that small-scale meteorological features can cause dramatic effects on model performance,

apparently because such features are not captured in the ROM's overall interpolation of meteorological data. We found that a squall line resulted in a significant overestimate in ozone concentrations along UAM's western boundary (the inflow boundary on that day). We therefore caution UAM users to carefully review ROM estimates and be aware of mesoscale flow conditions. On most days, however, ROM2.1 did a reasonable job estimating UAM boundary conditions.

In the second part of our evaluation, we employed a series of diagnostic tests to assess the model's ability to conserve mass. Table 7 presents a summary of the mass conservation results for seven test cases. For all individual layers and for all layers combined, the table shows the maximum mass increase and maximum mass decrease (if mass decreased) that occurred during the simulation. For test cases 1A and 1B, in which mass flux was allowed between layers, mass changes were expected to occur in individual model layers. For the other tests, however, no change in mass was expected for individual layers. For all tests, there should have been no change in mass for all layers combined (total domain).

The table shows that for most test cases there were serious departures from mass conservation. Only in test case 0A (where the concentration gradients were considerably relaxed) and test case 0B (where negative clipping was suppressed) was the total domain mass effectively conserved. The results for the other five test cases suggest a potential problem with the ROM's numerical transport procedures, despite earlier design tests performed during the ROM's developmental stages (Lamb, 1983) that showed no problems with mass conservation. We have delayed further diagnostic tests, including examining test case 3 with chemical simulation, and further analysis, including preservation of peak concentrations, until the mass conservation problem has been corrected.

A first-order correction algorithm has been developed based on a global assessment of the mass imbalance due to the clipping of negative concentrations. This algorithm was implemented and tested on a two-day ambient simulation with ROM during a high O_3 concentration period. Results

have shown that the differences between the corrected and uncorrected simulation results were almost always less than 1%. Differences seen in the NO_x concentrations were greater than those of the other species, but generally under 10%. These results suggest that the implementation of a mass-correcting scheme in ROM's numerical advection algorithm would be a desirable, although probably not essential feature. We plan to perform further tests to assess the degradation in computation time with the inclusion of the mass correction scheme. With this additional information, we will weigh the improvements in accuracy of the transport solver with the increases in computation time. We will also repeat the diagnostic tests discussed in this section with the global mass-correction algorithm in place and analyze the results in detail. Our analysis has demonstrated the value of this type of diagnostic testing in model evaluation.

Our evaluation has suggested that further improvements to the ROM are warranted. We are working towards improving the specification of layer thicknesses and the computation of naturally-occurring emissions. In future years, we hope that a dynamic meteorological processor can be incorporated that will simulate nonsteady state flows. To continue making advances in model development, additional monitoring data are needed for examining other chemical species (such as NO_x, isoprene, formaldehyde, and HNO_3) and for fully evaluating model performance in rural areas.

TABLE 7. MAXIMUM PERCENTAGE CHANGES IN TOTAL MASS DURING A SIMULATION

ROM LAYER	TEST CASE						
	1A[a]	1B[a]	1C[a]	2	0	0A	0B
1	59.20 -59.00	10.58 -9.75	9.41 -0.39	14.14	9.98	0.60	0.40
2	5.94 -1.23	16.40 -3.73	13.30	17.22	9.98	0.60	0.40
3	72.00 -59.25	1.91 -28.27	9.07	21.60	9.98	0.60	0.40
Total Domain	6.12 -2.55	3.80 -3.39	8.13	17.57	9.98	0.60	0.40

[a] Values shown include maximum positive and maximum negative changes from the initial mass. Other tests only produced positive changes.

REFERENCES

Godowitch, J. and K. Schere. 1989. Plans for the Development of a ROM/UAM Interface. Internal Report, U.S. Enviromental Protection Agency, Office of Research and Development, Research Triangle Park, NC.

Lamb, R. 1983. A Regional Scale (1000 km) Model of Photochemical Air Pollution: Part 1. Theoretical Formulation. EPA-600/3-83-035, U.S. Environmental Protection Agency, Research Triangle Park, NC.

Lamb, R. 1984. A Regional Scale (1000 km) Model of Photochemical Air Pollution: Part II. Input Processor Network Design. EPA-600/3-84-085, U.S. Environmental Protection Agency, Research Triangle Park, NC.

Lamb, R. and S. Hati. 1987. The representation of atmospheric motion in models of regional-scale air pollution. *Journal of Climate and Applied Meteorology*, **26**(7): 837-846.

Lamb, R. and G. Laniak. 1985. A Regional Scale (1000 km) Model of Photochemical Air Pollution: Part III. Tests of the Numerical Algorithms. EPA-600/3-85-037, U.S. Environmental Protection Agency, Research Triangle Park, NC.

McRae, G., W. Goodin, and J. Seinfeld. 1982. Numerical solution of the atmospheric diffusion equation for chemically reacting flows. *Journal of Computational Physics*, **42**(1): 1-42.

Pagnotti, V. 1987. A meso-meteorological feature associated with high ozone concentrations in the northeastern United States. *Journal of Air Pollution Control Association*, **37**(6): 720-722.

SAS Institute Inc. 1985. SAS User's Guide: Basics, Version 5 Edition. SAS Institute Inc., Cary, NC.

Schere, K. and R. Wayland. 1989. EPA Regional Oxidant Model (ROM 2.0): Evaluation on 1980 NEROS Data Bases. EPA-600/x-89-xxx, U.S. Environmental Protection Agency, Research Triangle Park, NC.

U.S. Environmental Protection Agency. 1987. Application of the Urban Airshed Model to the New York Metropolitan Area. EPA-450/4-87-011, Office of Air Quality Planning and Standards, Research Triangle Park, NC.

U.S. Environmental Protection Agency. 1988. Anthropogenic Emissions Data for the 1985 National Acid Precipitation Assessment Program (NAPAP) Inventory. EPA-600/7-99-022, Air and Energy Engineering Research Laboratory, Research Triangle Park, NC.

U.S. Environmental Protection Agency. 1988. Protocol for Regional Ozone Model for Northeast Transport. Office of Air Quality Planning and Standards, Research Triangle Park, NC.

U.S. Environmnetal Protection Agency. 1989. Aerometric Information and Retrieval System (AIRS) User's Guide. Office of Air Quality Planning and Standards, Research Triangle Park, NC.

Vaughan, W. 1985. Transport of Pollutants and PEPES. EPA-600/3-85-033, U.S. Environmental Protection Agency, Research Triangle Park, NC.

Young, J., M. Aissa, T. Boehm, C. Coats, J. Eichinger, D. Grimes, S. Hallyburton, W. Heilman, D. Olerud, S. Roselle, A. Van Meter, R. Wayland, and T. Pierce. 1989. Development of the Regional Oxidant Model Version 2.1. EPA-600/3-89-044, U.S. Environmental Protection Agency, Research Triangle Park, NC.

APPENDIX

STATISTICAL SUMMARIES FOR THE AUGUST 1985 EPISODE

TABLE A-1. Summary statistics of hourly daytime ozone concentrations (ppb) for the August 1985 episode.

Region	n	Mean obs.	Mean model	Std. dev. obs.	Std. dev. model	95th percentile obs.	95th percentile model	Maximum obs.	Maximum model
1	3606	57.7	71.6	33.1	23.4	119.0	114.2	219.0	161.3
2	4095	60.1	64.8	30.0	18.6	110.0	99.2	188.0	129.1
3	3522	48.3	54.0	22.7	12.3	85.0	73.7	135.0	99.6
4	2616	45.6	53.9	21.7	12.9	84.0	76.7	137.0	127.0
5	1566	43.4	55.0	21.5	10.9	81.1	72.6	122.0	116.1

TABLE A-2. Summary statistics of daily maximum ozone (ppb) for the August 1985 episode.

Region	n	Mean obs.	Mean model	Std. dev. obs.	Std. dev. model	95th percentile obs.	95th percentile model	Maximum obs.	Maximum model
1	334	88.3	91.2	37.7	23.3	167.3	141.4	219.0	161.3
2	385	85.4	80.1	27.7	19.1	136.0	112.7	188.0	129.1
3	330	68.1	62.8	19.6	12.2	98.0	82.7	135.0	99.6
4	241	65.4	62.7	20.8	16.1	100.9	96.1	137.0	127.0
5	146	64.2	63.8	20.1	11.2	103.3	81.7	122.0	116.1

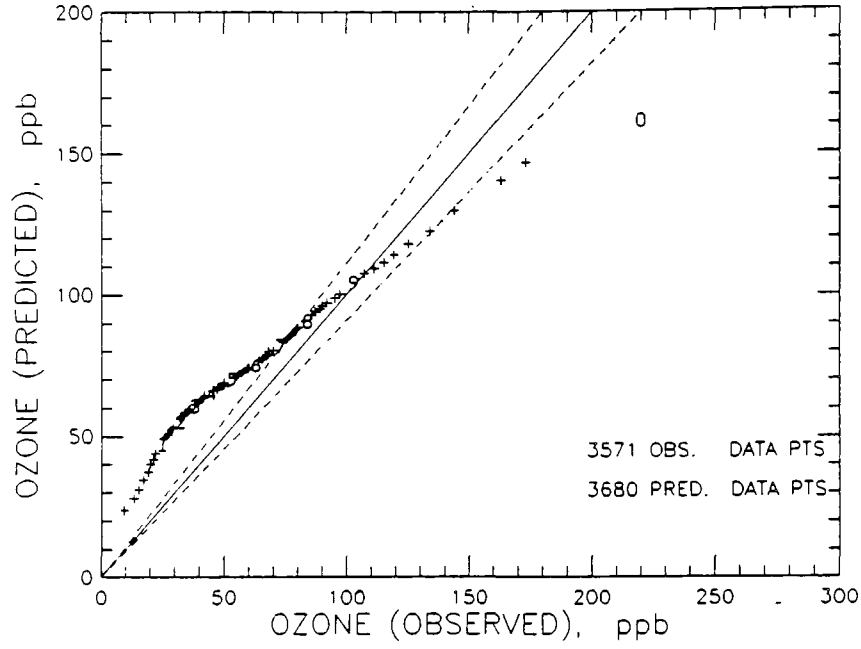

Figure A-1a. Quantile-quantile plot of observed and modeled hourly ozone for the August 1985 episode (Group 1, Northern Corridor).

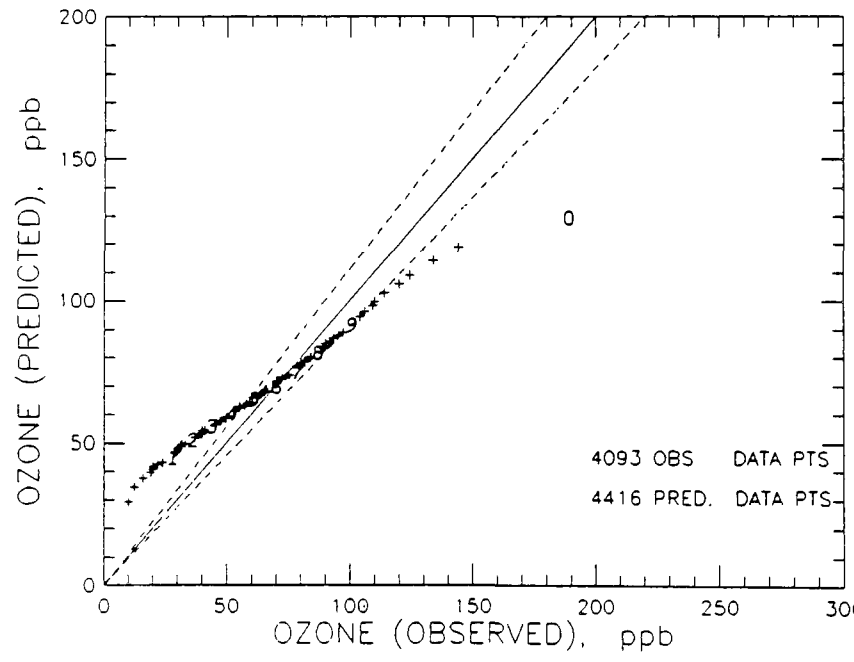

Figure A-1b. Quantile-quantile plot of observed and modeled hourly ozone for the August 1985 episode (Group 2, Southern Corridor).

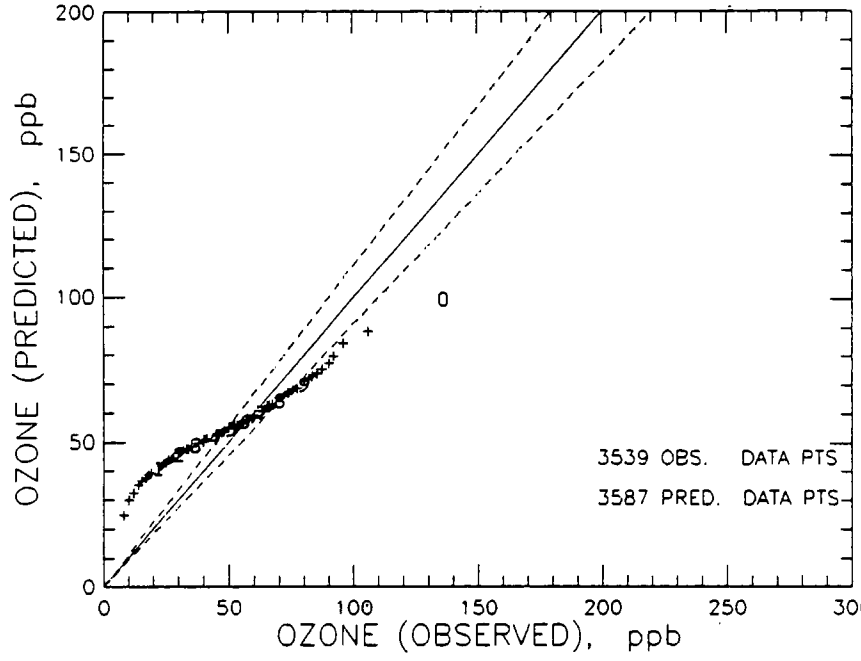

Figure A-1c. Quantile-quantile plot of observed and modeled hourly ozone for the August 1985 episode (Group 3, Ohio Valley-Middle Atlantic).

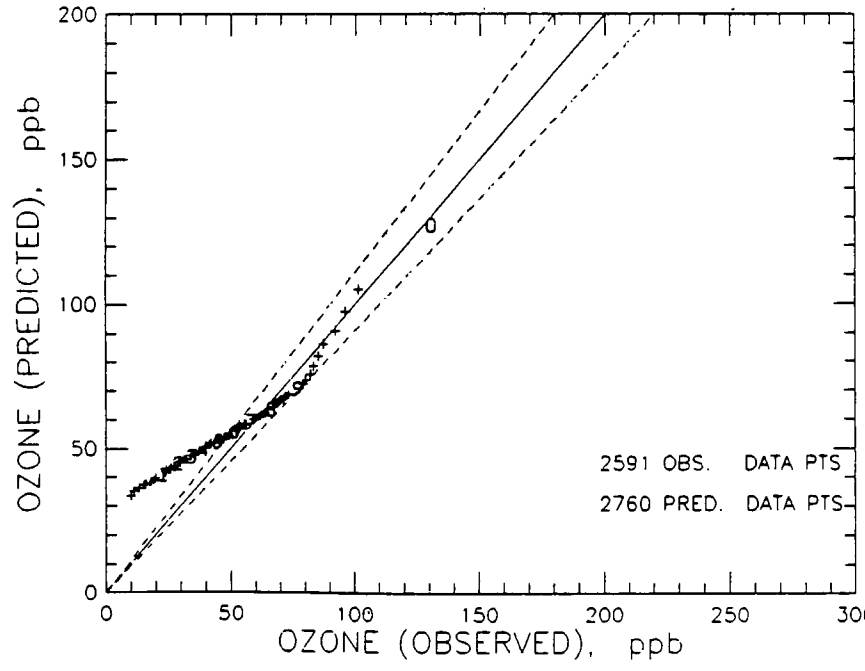

Figure A-1d. Quantile-quantile plot of observed and modeled hourly ozone for the August 1985 episode (Group 4, Interior Northeast).

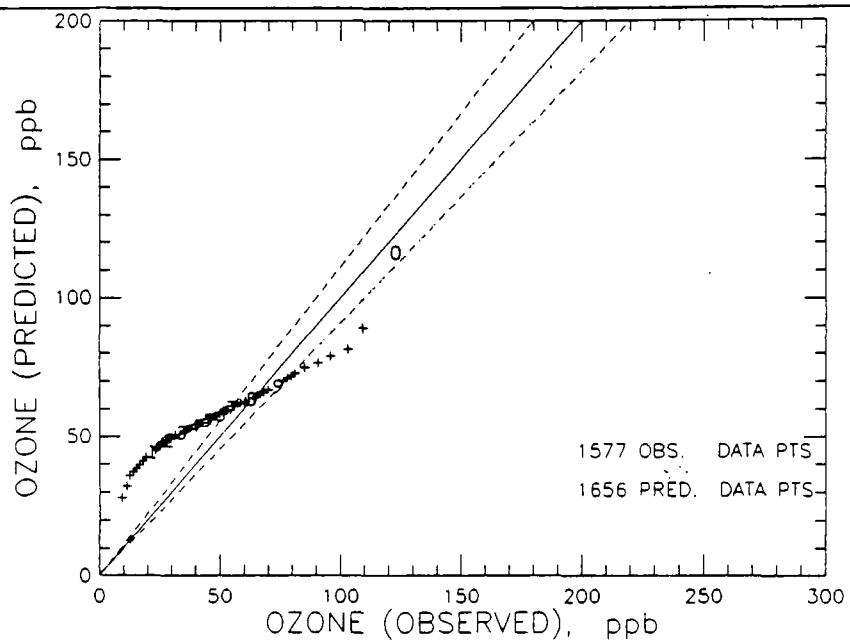

Figure A-1e. Quantile-quantile plot of observed and modeled hourly ozone for the August 1985 episode (Group 5, Great Lakes).

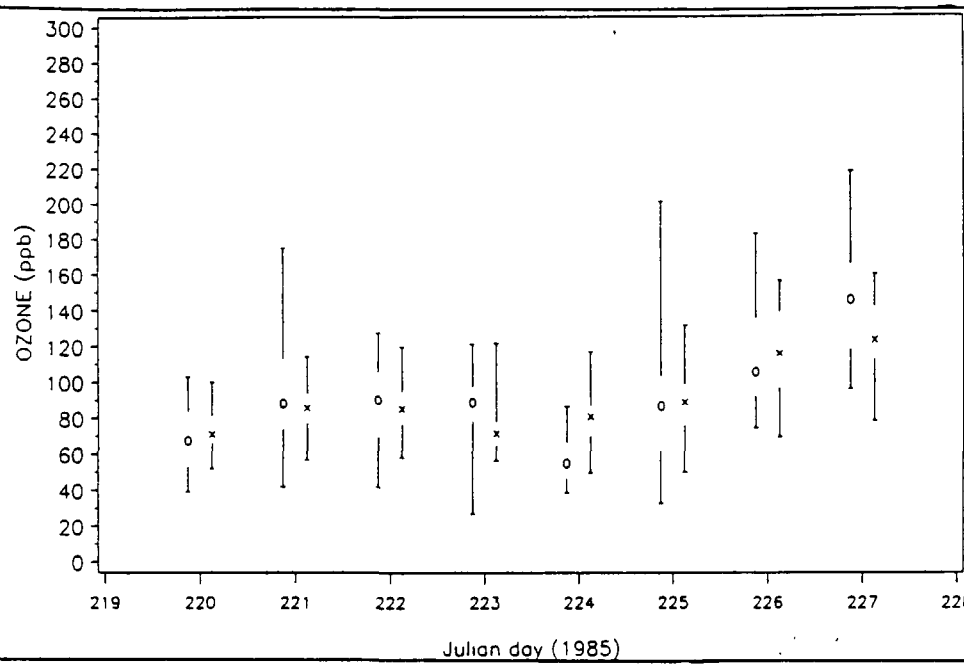

Figure A-2a. Comparison of observed (*o*) and modeled (*x*) maximum ozone for the August 1985 episode (Group 1, Northern Corridor).

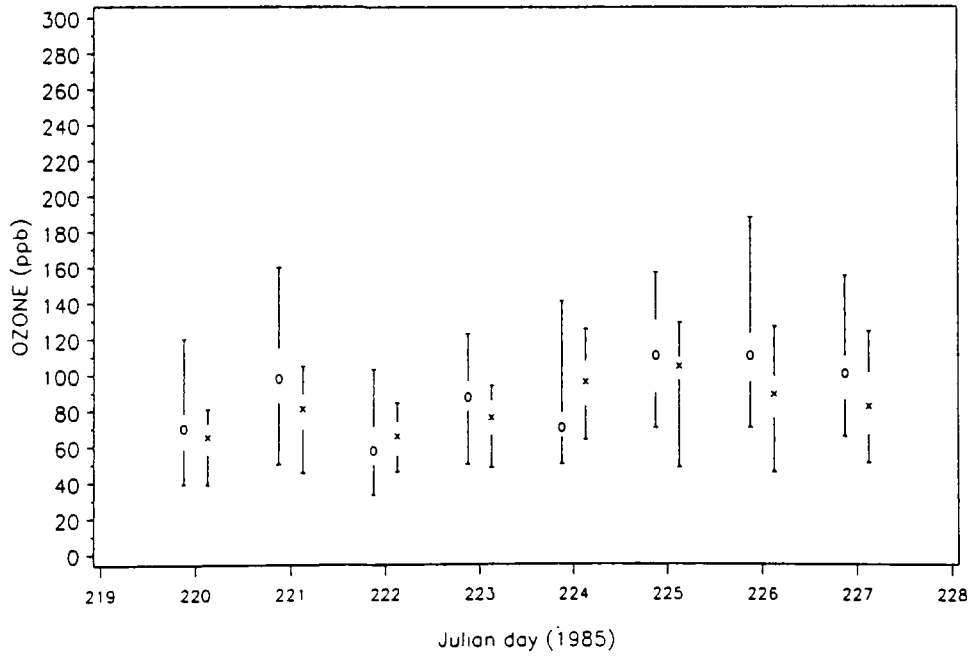

Figure A-2b. Comparison of observed (*o*) and modeled (*x*) maximum ozone for the August 1985 episode (Group 2, Southern Corridor).

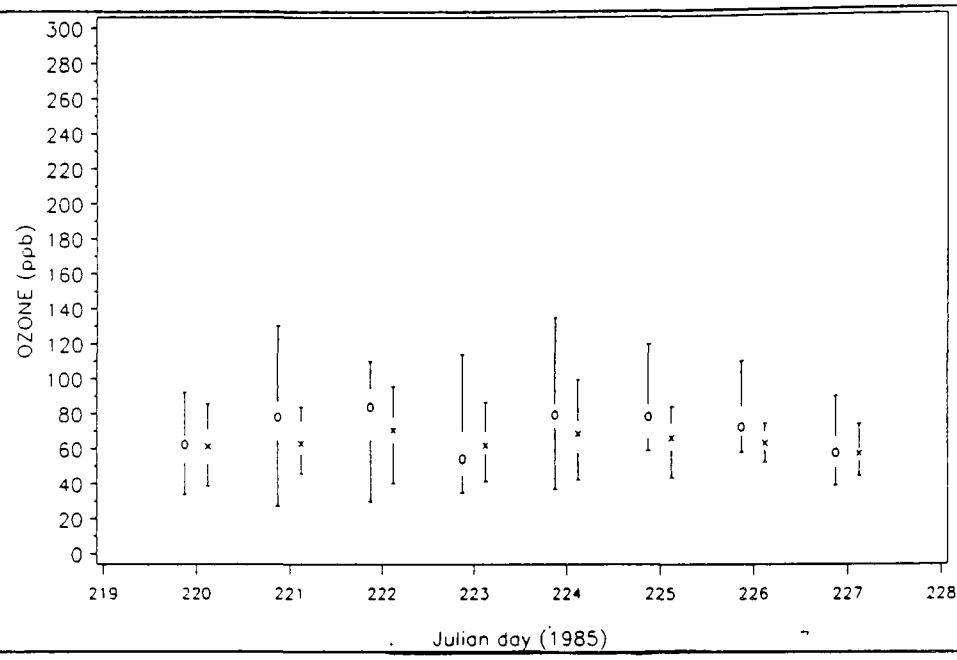

Figure A-2c. Comparison of observed (*o*) and modeled (*x*) maximum ozone for the August 1985 episode (Group 3, Ohio Valley-Middle Atlantic).

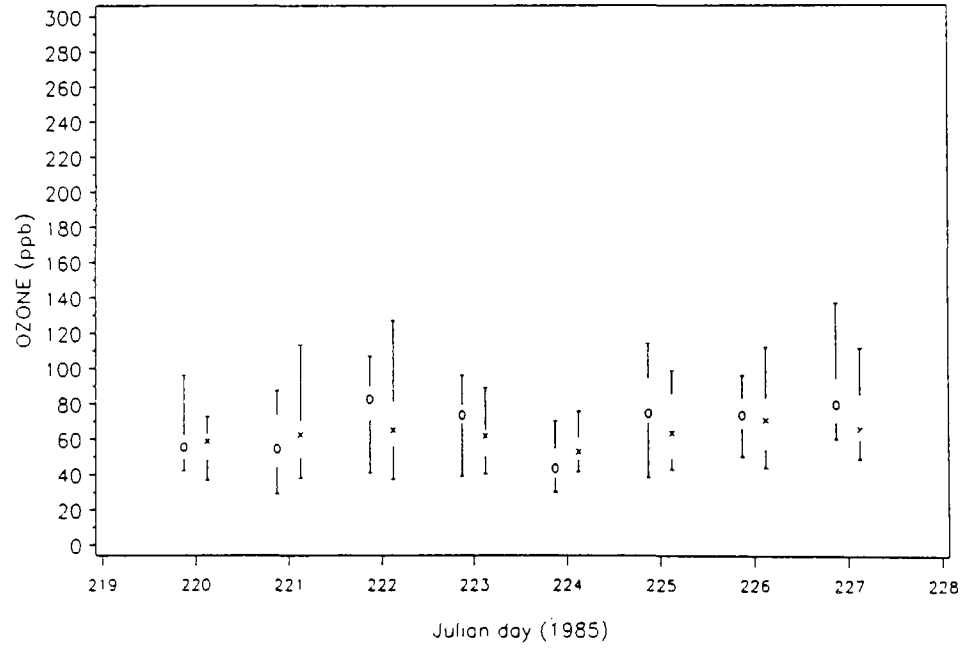

Figure A-2d. Comparison of observed (*o*) and modeled (*x*) maximum ozone for the August 1985 episode (Group 4, Interior Northeast).

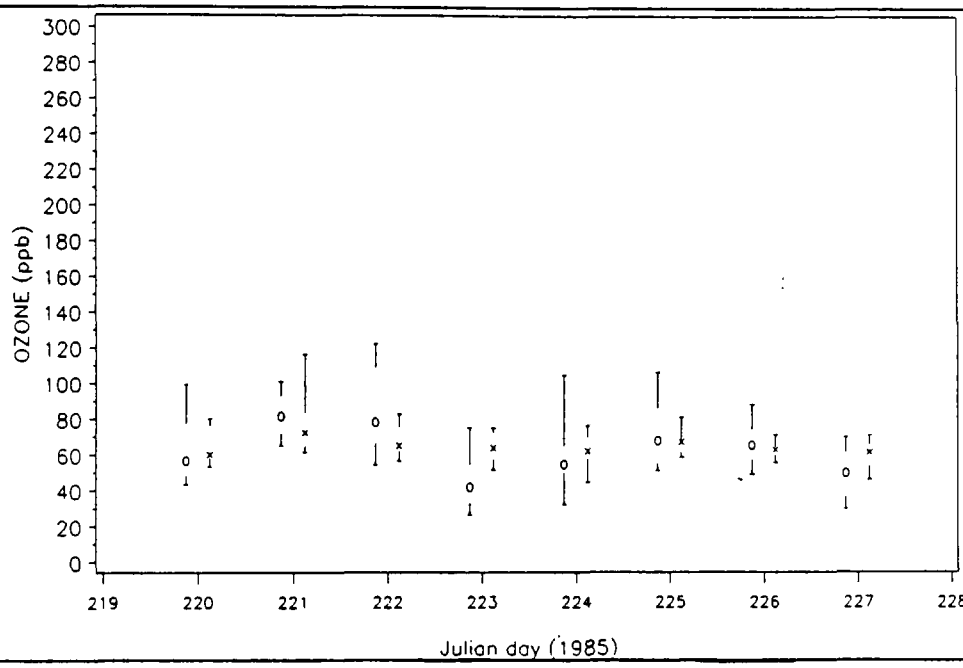

Figure A-2e. Comparison of observed (*o*) and modeled (*x*) maximum ozone for the August 1985 episode (Group 5, Great Lakes).